Chapter 1: Introduction

Cancer: History, Incidence, Causes

Cancer is a disease that has tormented man throughout history. Among the first to document cancer were the ancient Egyptians, whom 5000 years ago wrote detailed accounts of breast cancer.[1, 2] Continuing through the ages, cancer was researched and described by numerous historical figures including Hippocrates, Galen, and Morgagni. It was not until the second half of the 20th century, however, that cancer has been more fully researched and its molecular and cellular basis began to be understood. As a result, many effective treatment regimens have been developed. However, cancer continues to be a major killer.[3, 4] In the U.S., cancer is the second leading cause of death behind heart disease. Each year, approximately 1 million new cases are diagnosed in this country, and roughly 50 percent of those diagnosed will die.

Clearly, cancer is an enormous problem whose solution has remained elusive. Extensive research has determined that cancer is a collection of over two hundred diseases characterized by the uncontrolled growth and proliferation of abnormal cells (cancer cells).[5,6] The development of cancer is commonly referred to as carcinogenesis. It is a complex, multi-step process that involves a series of genetic changes, called mutations, in critical growth regulatory genes. These mutations eventually lead to the development of cancer cells that can reproduce rapidly, invade healthy tissue and spread throughout the body. The eventual result of this process is interference with normal tissue and organ function, leading to the death of the person afflicted.

Cancer can be caused by several sources. Due to the complex nature of cancer development, it is not possible to pinpoint one specific agent as the cause of cancer.[4-6] Rather, it is most likely due to a number of contributing factors. These factors include exposure to certain chemicals, action of viruses, exposure to radiation, and heredity. Collectively, these are known as risk factors. These risk factors are summarized in Table 1.1.

Table 1.1 Risk factors for the development of cancer.

Risk Factor	Mechanism of Action	Example
Chemicals	• Damage DNA, leading to mutations	• Encountered in the manufacture of dyes, chemicals, petroleum products • Associated with tobacco usage, general environmental pollution, diet, some medicines
Radiation	• Damage DNA, leading to mutations	• UV, ionizing radiation, radioactive elements
Viruses	• Not thought to induce cancer • Participate in early stages leading to cancer	• Epstein-Barr virus, human papilloma Virus, hepatitis B virus, HIV
Heredity	• Transmission of a single gene increases likelihood of cancer	• Inherited cancers are commonly diseases of childhood: retinoblastoma, Wilm's tumor • Adult diseases: colon and breast carcinoma
	• Rare hereditary diseases increase likelihood of cancer	• Xenoderma Pigmentosum, Ataxia telangiectasia

Cancer Treatment: Focus on Chemotherapy

At present, surgery and radiation therapies continue to be the mainstays of cancer treatment.[1, 2, 5] Chemotherapy, however, has also proven to be a highly effective treatment method for numerous cancers. Chemotherapy is the use of cytotoxic drugs and hormones

to kill cancerous tumors. It is most commonly used in conjunction with surgery and radiation therapy against rapidly growing cancers that have spread or that are normally disseminated throughout the body. Examples of such cancers include the leukaemias, lymphomas, and Hodgkin's disease. Multiple chemotherapeutic drugs are commonly administered at one time, to take advantage of synergistic effects and to combat the growing problem of resistance. This important type of therapy is referred to as combination chemotherapy.

Chemotherapeutic agents kill cancer by taking advantage of the fact that cancer cells grow and reproduce faster than normal cells.[3, 5] Many useful agents target enzymes and/or substrates related to DNA transcription and synthesis. These drugs therefore exert their toxic and antitumor effects by inhibiting cells that undergo DNA synthesis at some point in their life cycle. The end result is either general cell death leading to necrosis, or the initiation of a controlled series of steps known as programmed cell death (apoptosis).

Survey of Chemotherapeutic Agents

Agents for cancer chemotherapy are often organized into groups according to their origin or mechanism of action.[3, 7, 8] The seven major classes of agents include the alkylating agents, non-classical alkylating agents, antitumor antibiotics, plant alkaloids, antimetabolities, hormonal agents, and miscellaneous agents. The mechanism of action, effectiveness, and relevant examples of each of these classes are shown in Table 1.2.

Problems with Chemotherapy and Their Consequences

Anticancer chemotherapy has numerous problems. Due to the high inherent cytotoxicity of anticancer drugs and their selectivity for fast growing/reproducing cells, significant toxicity can be produced in a variety of normal tissues. As a result, patients commonly experience a host of disagreeable side effects depending upon which tissue/organ or organ system is affected. Perhaps the best known and most widely

Table 1.2 Survey of chemotherapeutic drug classes, including their mechanism of action, example agents, and effectiveness.

Drug Group	Mechanism of Action	Example Drug	Effectiveness of Example Drug
Alkylating Agents	React with DNA	Nitrogen Mustard	Hodgkin's lymphoma
Antimetabolites	Interact with cellular enzymes	Fluorouracil	Breast cancer
Antitumor Antibiotics	Intercalate DNA, formation of free radicals	Doxorubicin	Misc. sarcomas, hematological malignancies, bladder cancer, breast cancer
Plant Alkaloids	Interfere with microtubule function	Vincristine	Acute lymphocytic leukemia, Hodgkin's lymphoma, breast, lung, cervical cancer
Hormonal Agents	Bind to receptors	Prednisone	Breast, prostate cancer
Miscellaneous Agents	Various interactions with cellular DNA, inhibiting replication, transcription	Cisplatin	Testicular, ovarian, bladder cancer, head and neck tumors

experienced are intense nausea and hair loss, which are due to with gastrointestinal and dermatological toxicity.

Another emerging problem area is drug resistance. Cancer cells appear to have an unusual capacity for developing resistance to the effects of anticancer drugs. This is most commonly caused by additional genetic mutation within the cancer cell. However other biochemical mechanisms can contribute, including decreased drug transport, the development of efficient DNA repair mechanisms, and the impairment of drug activation.[3]

The inevitable consequence of toxicity and drug resistance problems has been active research into new anticancer drugs and more effective treatment regimens. An example of such efforts is the discovery and development of cisplatin. Cisplatin, together with doxorubicin and cyclophosphamide, are among the most effective and widely used anticancer drugs known.[9]

Cisplatin: Anticancer Agent Targeting DNA

Initially synthesized by Peyrone in 1844[10], the biological effects of *cis*-diamminedichloroplatinum(II) (cisplatin, Figure 1.1) were accidentally discovered by B. Rosenberg and co-workers in 1965. In these studies, cells of the bacterium Escherichia coli were grown under aerobic conditions, in media enriched with NH_4Cl. When an electrical field was applied through platinum electrodes immersed in the media, the cells grew in long filaments but did not divide.[11,12] Further investigations determined that several compounds producing during electrolysis were responsible for this effect.[13] Preliminary antitumor testing on one of these electrolysis products, *cis*-diamminedichloroplatinum (II), revealed potent activity. Phase I clinical trials began in 1971, and cisplatin quickly proved to be particularly effective against testicular and ovarian cancers.[14, 15] However, severe side effects such as intense nausea, neuropathy, ototoxicity and nephrotoxicity nearly eliminated cisplatin as a viable drug. Special treatment regimens were developed to combat these problems and cisplatin was approved for clinical use in 1979.[16]

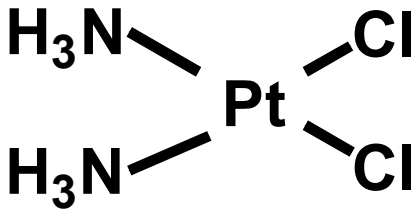

Figure 1.1 *cis*-diamminedichloroplatinum(II) (cisplatin).

Since FDA approval, cisplatin has enjoyed wide clinical use, with the most profound effects observed in combination therapies versus testicular and ovarian cancers. Palliative benefit has also been observed versus small cell lung, bladder, head and neck, and cervical carcinomas. Combination therapies with drugs that interfere with DNA excision repair have shown synergistic effects, and regimens involving concurrent radiation therapy show great promise.[17, 18, 19]

Cisplatin: Mechanism of Action

The clinical effectiveness of cisplatin has spawned considerable study in its mechanism of action. At present, it has been widely accepted that cisplatin produces its cytotoxic effects through an interaction with cellular DNA. This interaction takes the form of a covalent adduct, in which the chloride ligands on cisplatin are lost and replaced by specific DNA bases. These DNA adducts are then thought to mediate cytotoxicity by inhibiting DNA replication and transcription, ultimately leading to programmed cell death (apoptosis). [11, 18-20] However, studies on the geometrical isomer of cisplatin, *trans*-diamminedichloroplatinum (II) (Figure 1.2), indicate that this compound also binds DNA and inhibits DNA replication, but is much less toxic. This observation suggests that the cytotoxicity of cisplatin cannot be explained solely by its ability to cause DNA damage. More complex biochemical mechanisms, among them adduct repair and toxicity, may also contribute.

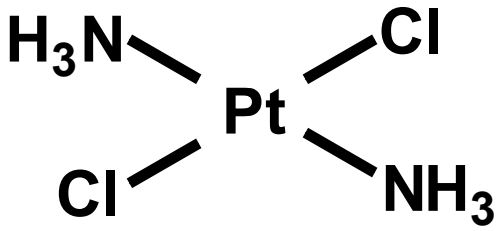

Figure 1.2 *trans*-diamminedichloroplatinum(II) (transplatin).

DNA Structure

DNA (deoxyribonucleic acid) is a polyanion comprised of nucleotide monomers that contain a deoxyribose sugar, a purine or pyrimide base, and an anionic phosphate linker.[20, 21, 25] The purine bases are guanine and cytosine, and the pyrimidine bases are adenine and thymine. Guanine and adenine pair with cytosine and thymine, respectively (otherwise known as *base pairs*). A directional linkage is created through the phosphodiester bond formed between the 5′-phosphate of the first monomer and the 3′-site of the second monomer. The helical, three-dimensional morphology of DNA is a result of one 5′- 3′ strand running parallel to a 3′- 5′ strand. The helix is stabilized by the hydrogen bonding interactions between base pairs and π-stacking interactions between parallel bases perpendicular to the helix axis. The helical arrangement also gives rise to major and minor grooves. The anionic-sugar phosphate groups are close together in the minor groove, creating a region of high charge density. The major groove is much wider and deeper, exposing the base pairs and the N7 position of guanine. A schematic outlining these features is shown in Figures 1.3 and 1.4.

Various double helical structures of DNA can be formed, depending upon the solution conditions.[22] These structures include the A-form, B-form, and Z-form. The B-form (B-DNA) is a right-handed helix that is most stable in low-salt concentrations. In high-salt concentrations the helical axis compresses forming the A-form (A-DNA). The Z-form (Z-DNA) is a left-handed, elongated, zigzag structure helix that favors alternating guanine-cytosine sequences and high concentrations of divalent metal cations.

Cisplatin: DNA Adducts

A key aspect of cisplatin's activity is its aqueous solution chemistry.[17-19] Cisplatin is a neutral, sparingly water-soluble coordination complex with the platinum atom in the 2+ oxidation state. In the clinic, cisplatin is combined with sterile saline and administered intravenously. In the bloodstream, chloride concentrations are high (~100mM) and cisplatin is somewhat unreactive. However, once cisplatin enters the cell

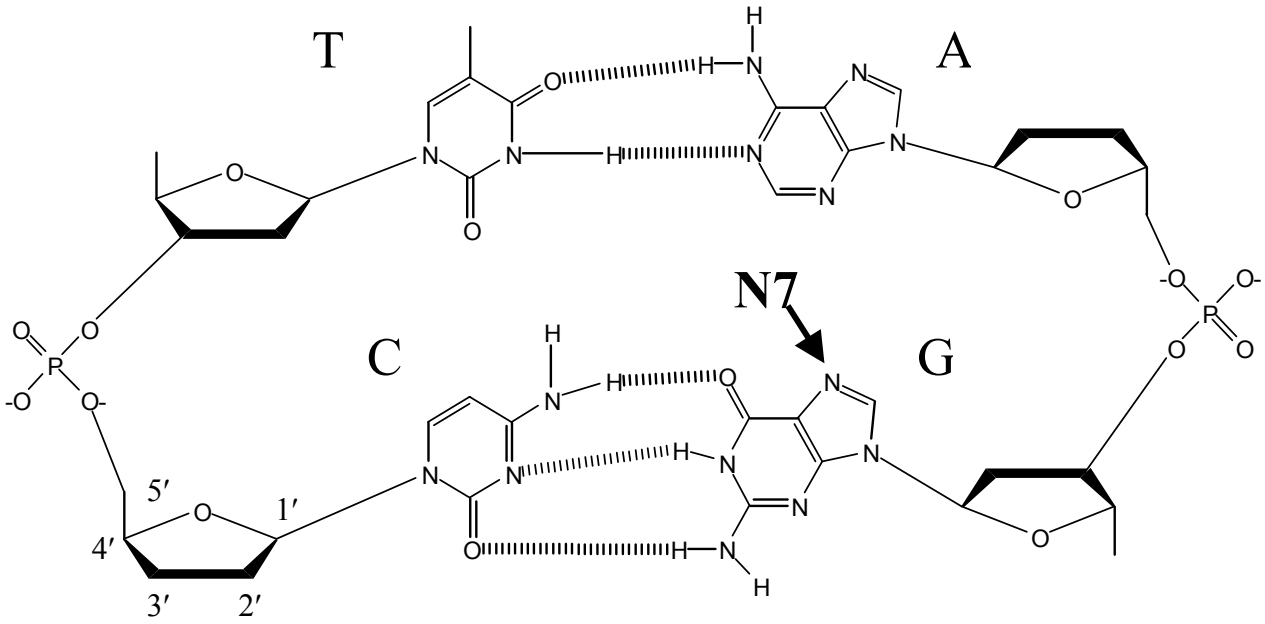

Figure 1.3 Structure of DNA Nucleotides. C = cytosine, G = guanine, A = adenine, T= thymine. N7 position on guanine indicated. Labeling of deoxyribose sugar indicates 3′-5′ directional linkage. Dashed lines indicate hydrogen bonds between paired bases.

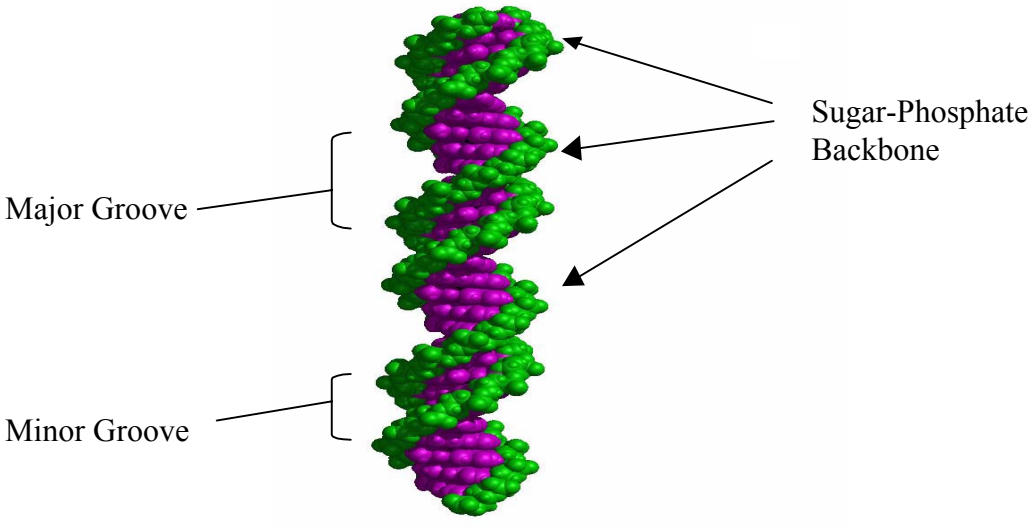

Figure 1.4 Structure of DNA double helix showing major and minor grooves[21].

(by mechanisms presently unknown), the chloride concentration is much lower (~ 4 mM) and hydrolysis of the chloride ligands can take place. The chloride ligands are replaced stepwise by water, forming the positively charged bis-aquo complex. Because water is a better leaving group than chloride, this highly reactive species can then react by ligand substitution with a variety of biological nucleophiles. These nucleophiles include DNA, RNA, proteins and cellular thiols. DNA is believed to be the critical cellular target for cisplatin, based on evidence from studies on DNA-repair deficient cancer cells, which are particularly sensitive to cisplatin. A summary of the entry of cisplatin into the cell and its binding to DNA is shown in Figure 1.5 (derived from ref 17-19).

DNA contains a host of possible binding sites for cisplatin. Early experiments, however, showed that cisplatin forms an association with the bases of DNA. Various X-ray diffraction and NMR studies on the binding of platinum to substituted DNA bases, along with nucleosides and nucleotides, has revealed several possible platinum binding sites. Among these, the N7 position of guanine has been determined to be the most likely target, due to its basicity and location on the surface of the DNA major groove.[20]

In vitro ^{195}Pt NMR studies on the interaction of cisplatin with small, double-stranded DNA fragments (30-50 base pairs) have revealed that DNA binding occurs in two steps. The first, rate-determining step involves the replacement of one chloride atom by water, to form the mono-aquo species. Monofunctional binding to either a single guanine or adenine then occurs. This is followed by loss of the second chloride atom and binding to a nearby purine base to form an intrastrand crosslink, or with a purine base on the complementary DNA strand to form an interstrand crosslink. This second step is kinetically controlled, with a $t_{1/2}$ of 2.1 h.[19, 25] It has been determined that the major *in vitro* cisplatin-DNA adducts are 1,2 intrastrand crosslinks between adjacent guanine bases (dGpG, 60-65%), 1,2 intrastrand crosslinks between adjacent guanine and adenine bases (dApG, 20-25%), and 1,3 intrastrand crosslinks between guanines separated by one nucleotide (dGpXG, ~6%). Additionally, 1,2 interstrand crosslinks between guanines also occur, but at much lower propensity (dGpC/GpC, 1-3%).[18, 19, 23]

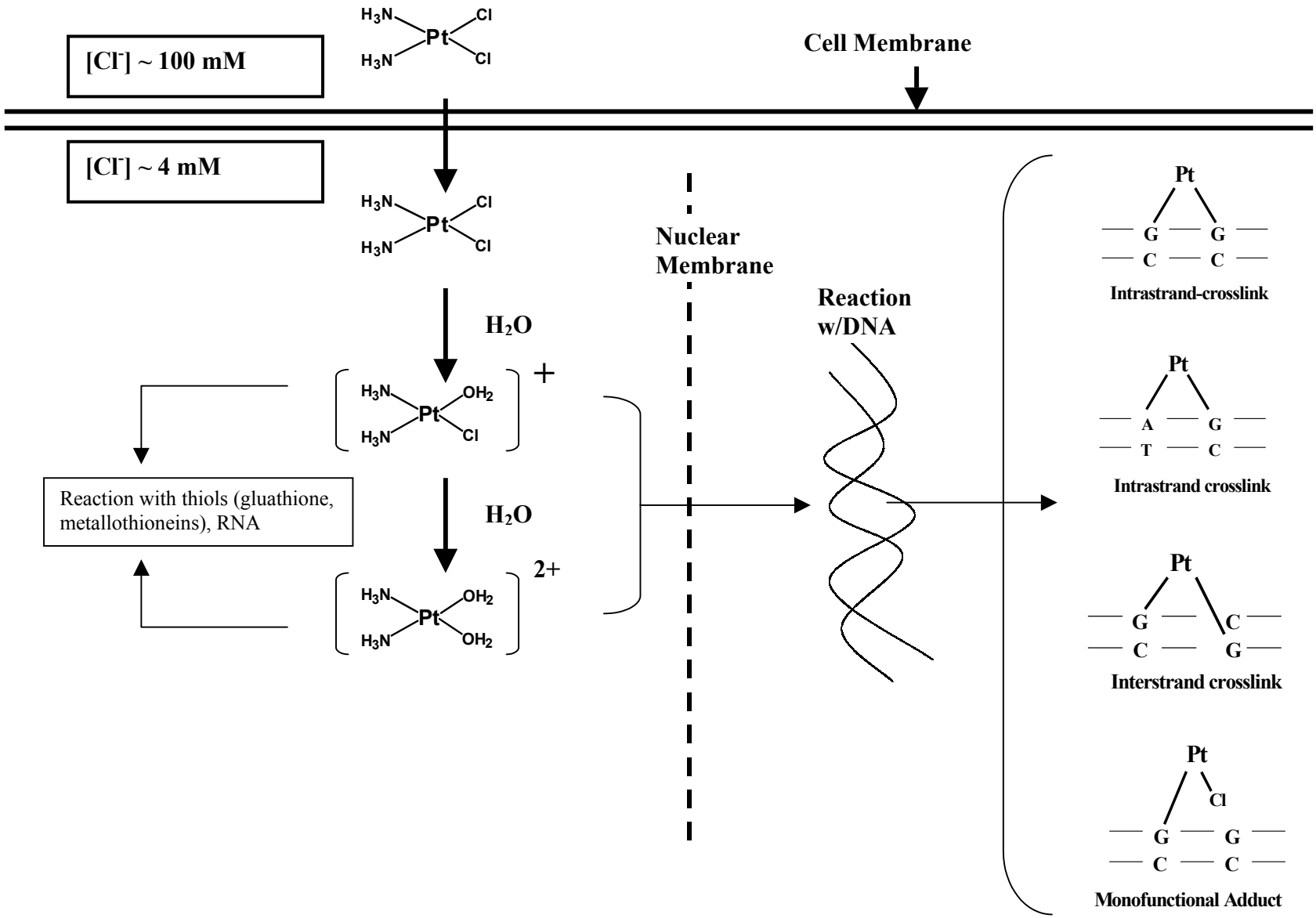

Figure 1.5 Schematic of cisplatin entering the cell and interacting with DNA, RNA and cellular thiols[17-19].

Gel Electrophoresis: Studying Drug-DNA Adducts

A common method used to study the structural effects of drug-DNA binding is gel electrophoresis.[21, 24 - 26] Gel electrophoresis is a technique used in molecular biology to fractionate macromolecules such as nucleic acids and proteins. Separation is achieved on the basis of movement of the macromolecules through a semi-solid gel, under the influence of an electric field. Commonly used gel media for electrophoresis include both agarose and polyacrylamide. The choice of gel medium is dependent on the size of DNA or protein molecule being examined. The function of the gel is to provide physical support for the DNA samples, but it also provides a molecular sieving effect. Fractionation is achieved on the basis of size/molecular mass.

The two major types of electrophoresis conditions are native and denaturing. Native conditions involve nucleic acids and proteins migrating through gels with a retention of secondary structure. Denaturing conditions involve nucleic acids and proteins migrating through gels with little or no secondary structure. For nucleic acids, this means hydrogen bonding is disrupted and the molecule is therefore single-stranded. For proteins, this means the formation of a random coil.

A schematic representing native agarose gel electrophoresis for the separation of nucleic acids is shown in Figure 1.6. A typical experiment begins with the application of a solution of nucleic acids at one end of an agarose gel, which is situated within an electrophoresis apparatus. A voltage is applied to electrodes built into the apparatus, and due to an inherent negative charge as a result of the phosphate groups in the backbone of molecules, the DNA molecules migrate towards the positive electrode (anode). During this journey, the DNA molecules must wind their way through the maze-like matrix of the agarose gel. Since smaller, lighter DNA molecules can more easily negotiate the gel matrix, they travel further and faster than larger, heavier molecules. Because the phosphate groups dictate the charge on the DNA and the number of phosphate groups varies with the length of the DNA, rate of migration is inversely proportional to the

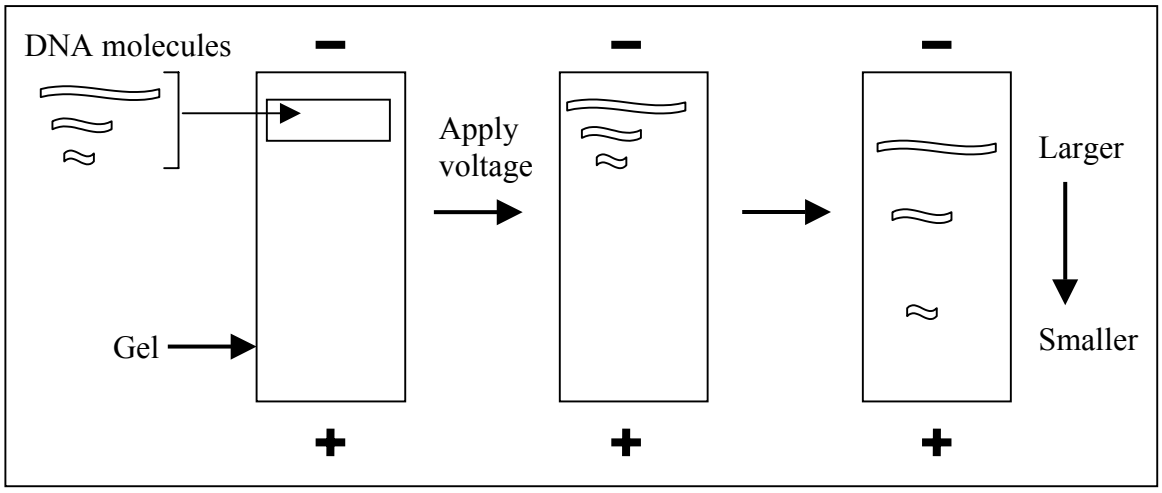

Figure 1.6 Gel Electrophoresis of DNA. Large rectangles represent gels. Ribbon-like structures represent double-stranded DNA (adapted from reference 21).

logarithm of molecular mass. Once the electrophoresis is complete, the gel is commonly stained with ethidium bromide, a fluorescent dye that binds to DNA by intercalation**.** Visualization of DNA is achieved through examination of the gel under UV-light, detecting the ethidium bromide fluorescence.

Native gel electrophoresis has been previously used to detect and study the interaction of cisplatin with DNA. As mentioned above, under electrophoresis the DNA molecule must negotiate the matrix of the agarose gel. The rate at which it migrates is dependent upon the size (molecular weight), charge, and three-dimensional shape of the DNA molecule, along with the applied gel voltage. With the exception of the applied gel voltage, the formation of cisplatin-DNA adducts will certainly alter each of these physical parameters. The result will be different migratory behavior of the cisplatin treated DNA in comparison to untreated DNA.

Analysis of the interaction of cisplatin with plasmid DNA by native gel electrophoresis has shown that cisplatin binds to plasmid DNA, causing a reduction in supercoiling (otherwise known as unwinding).[27, 28] Binding was detected by a comparison of the mobility of the unwound DNA to a control in which no cisplatin was added. Supercoiled plasmid DNA has a compact shape, and a reduction of supercoils

produces a more elongated shape. Therefore, the unwound DNA moved more slowly through the gel, in comparison to the untreated control. The DNA-interaction of other platinum complexes, among them $[Pt(py)_2Cl_2]$ (where py = pyridine), carboplatin, and the bis-platinum series $[\{cis\text{-}PtCl_2(NH_3)_2\}_2NH_2(CH_2)_nNH_2]$ (where n = 4, 5, 6) have also been detected and studied in a similar fashion.[29-32]

In addition to native gel electrophoresis, a number of different methods based on the denaturation of double stranded DNA have been used to detect and characterize interstrand crosslinking activity of platinum complexes. These methods include alkaline elution, alkaline sucrose sedimentation and denaturing gel electrophoresis. The latter method has been particularly useful for defining the extent and sequence specificity of interstrand crosslinks produced by cisplatin and its analogs and has provided evidence for the high efficiency of interstrand crosslinking induced by 1,1/t,t.[44,45]

Effects of Cisplatin-DNA Binding

The binding of cisplatin to DNA significantly distorts the structure of the double helix. Gel electrophoresis studies of the interaction of cisplatin with closed, superhelical plasmid DNAs have shown that cisplatin unwinds the double helix, removing negative supercoils and decreasing electrophoretic mobility. Studies utilizing varying length oligonucleotides by polyacrylamide gel electrophoresis have shown that cisplatin unwinds and bends the helix to varying degrees, dictated by the type of adduct formed.[33-35] Studies by Marzilli and co-workers have also identified a hairpin-like distortion associated with cisplatin-DNA intrastrand adducts.[36]

These structural distortions are known to give rise to biological effects that may hold the key to the antitumor activity of cisplatin. In order for a cell to replicate, certain enzymes known as DNA polymerases must interact with DNA. It has been shown that cisplatin blocks these interactions and thereby interferes with the replication process.[37] In addition, a group of proteins that recognize distortions in DNA conformation have been shown to bind to cisplatin-DNA lesions. These proteins are known as damage

recognition proteins (DRPs) and evidently recognize only cisplatin G-G and A-G adducts.[38] At present, it is believed that these proteins may play a vital role in the antitumor activity of cisplatin, by shielding cisplatin-DNA lesions from normal repair mechanisms. The end result would be the continued presence of the DNA distortion and thus inhibition of replication.

Problems with Cisplatin

Like any anticancer drug, the clinical use of cisplatin has been limited by toxicity.[18, 19] Accumulation of cisplatin commonly occurs in the kidney, resulting in tubular damage. This damage can be minimized by saline hydration and diuresis, along with the administration of nucleophillic thiols and thiol ethers. These treatments allows for the administration of higher cisplatin doses, but at this point other toxic side effects begin to accumulate. These include bone marrow depression, neurotoxicity, ototoxicity, and gastrointestinal toxicity (nausea and vomiting).

In addition to toxicity, the clinical use of cisplatin is becoming limited due to the ability of cancer cells to develop resistance to this drug. A variety of mechanisms have been proposed, and it is most likely that all contribute to some extent.[39] As in the case with other cancer chemotherapeutic agents, these mechanisms include reduced transport across cell membranes, reaction of sulfhydryl peptides such as glutathionine with cisplatin resulting in deactivation, and enhanced repair of cisplatin-DNA adducts.[40- 43]

Cisplatin Analog Research

Excellent clinical effectiveness, toxicity problems and cancer-cell resistance have all contributed to the prolific field of cisplatin analog research. The main idea behind these investigations has been to develop platinum complexes that have a better therapeutic index than cisplatin by reducing side effects and/or increasing potency. To date, two cisplatin analogs have been developed that achieve this purpose, carboplatin

and oxaliplatin, which are shown in Figure 1.7. Carboplatin (diammine(cyclobutane-dicarboxylato)platinum(II), Paraplatin) is a highly effective antitumor agent that entered into clinical use in 1981. It has a similar clinical profile as cisplatin but with much lower toxicity. This has been attributed to slower hydrolysis of the cyclobutane-dicarboxylato ligand in comparison to the *cis*-chlorides on cisplatin.[19, 20] Oxaliplatin is a 1,2 diaminocyclohexane based-platinum complex currently approved for use in France. It has shown excellent response in 5-fluorouracil combination regimens against advanced colorectal and ovarian cancers.

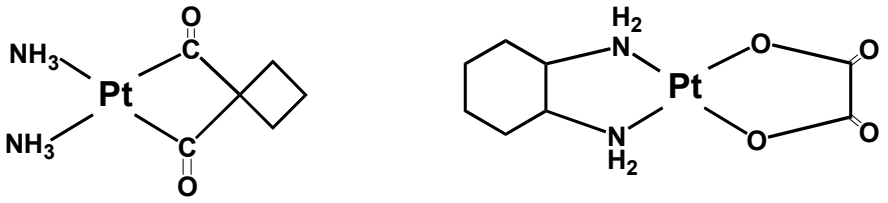

Carboplatin Oxaliplatin

Figure 1.7 Chemical structures of cisplatin analogs presently used in the clinic.

Other notable areas of cisplatin analog research include orally-active platinum(IV)-based drugs, a surging reinterest in *trans*-platinum complexes, and platinum-terpyridine complexes.[9, 44-46] Platinum-multimetallic systems are also of interest. N. Farrell and co-workers have synthesized a series of bis-platinum complexes of the general formula [{*cis*-$PtCl_2(NH_3)$ }$_2${μ-$H_2N(CH_2)_nNH_2$}] (where n= 3,4,5). These complexes have been shown to bind DNA, forming primarily interstrand crosslinks in much higher proportions than cisplatin.[29, 30] The compound [{*trans*-$PtCl(NH_3)_2$}$_2${μ-H_2N $(CH_2)_4$ NH_2}]Cl_2 (1,1/t,t, Figure 1.8) shows even more efficient interstrand crosslinking, as well as significant cytotoxic and antitumor activity.[31, 47-50] Moving onto ever-larger platinum systems, Farrell and co-workers have recently developed a novel trinuclear 4+ charged platinum compound ([{*trans*-

$PtCl(NH_3)_2\}_2$ μ-{*trans*- $Pt(NH_3)_2$ (H_2N $(CH_2)_6$ $NH_2)_2$ }]$(NO_3)_4$, BBR 3464) that binds to DNA primarily through long-range 1,4 interstrand crosslinks. The structure of BBR 3464 is shown in Figure 1.9. Preclinical activity studies in cisplatin sensitive and resistant murine L1210 cell lines have shown promise.[51-53] Currently, this complex is in Phase I clinical trials in the UK.

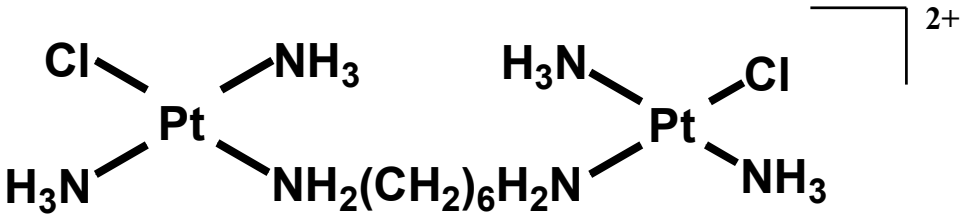

Figure 1.8 Structure of [{*trans*-$PtCl(NH_3)_2\}_2$ {μ-$H_2N(CH_2)_6NH_2$}]Cl_2 (1,1/t,t).

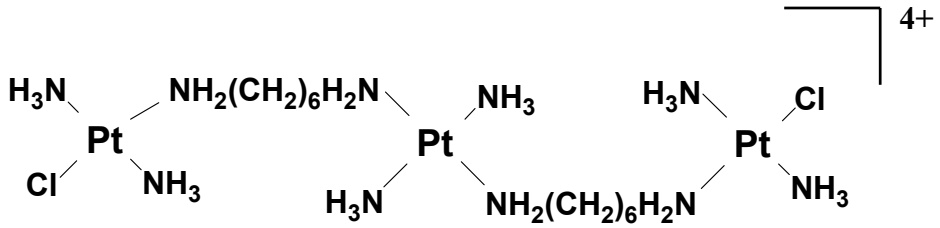

Figure 1.9 Structure of BBR 3464.

Other Metal-Based Anticancer Agents

In addition to platinum, numerous other metal complexes hold promise as anticancer agents. These include various complexes of the early transition metals along with gold, tin, and gallium.[54-57] Due to the success of cisplatin considerable interest

remains in complexes of the platinum group metals.[58] Presently, various complexes of rhodium, iridium, ruthenium and paladium are under development for use in cancer chemotherapy.[59, 60]

DNA Intercalators

Intercalation as a mode of DNA binding was first proposed by Lehman in 1961.[61] It is defined as a non-covalent association in which a planar, heteroaromatic molecule slides between the base pairs of DNA.[62, 63] The physical effects of this interaction on the DNA helix are profound. The DNA base pairs and helical backbone become unwound, resulting in helical unwinding and an increase in helix length and rigidity. Overlap between DNA helix and intercalator exists at the unwinding site, rigidly holding the intercalator and orienting it perpendicular to the helical axis. By virtue of this tight "sandwiching" between the DNA bases, the intercalator is electronically stabilized by π - π stacking and dipole-dipole interations.[64-66]

DNA binding by intercalation has been demonstrated for a wide variety of drugs, carcinogens and dyes.[66- 69] Intercalating drugs can cause mutations in DNA, and several (doxorubicin, daunomycin, adriamycin) are used as drugs in the clinic.[70] Due to their potent activity, the development of DNA-intercalating drugs continues to be at the forefront of medicine. Examples of some common intercalating drugs and dyes are shown in Figure 1.10.

DNA intercalating agents need not be solely organic in nature. Numerous metal-based compounds can bind to DNA by intercalation . Among the best studied of these is (2-hydroxyethanethiolato)(2,2′: 6′, 2′′ -terpyridine)platinum(II) ($[Pt(terpy)(HET)]^{+1}$, which occupies a unique place in the study of intercalation.[71- 79] Single crystal X-ray diffraction studies by Lippard and co-workers clearly showed that this platinum complex inserts between DNA base pairs.[80, 81] The intercalating ligand 2,2′: 6′, 2′′ -terpyridine is shown in Figure 1.11. In addition, examination of polycrystalline DNA fibers containing

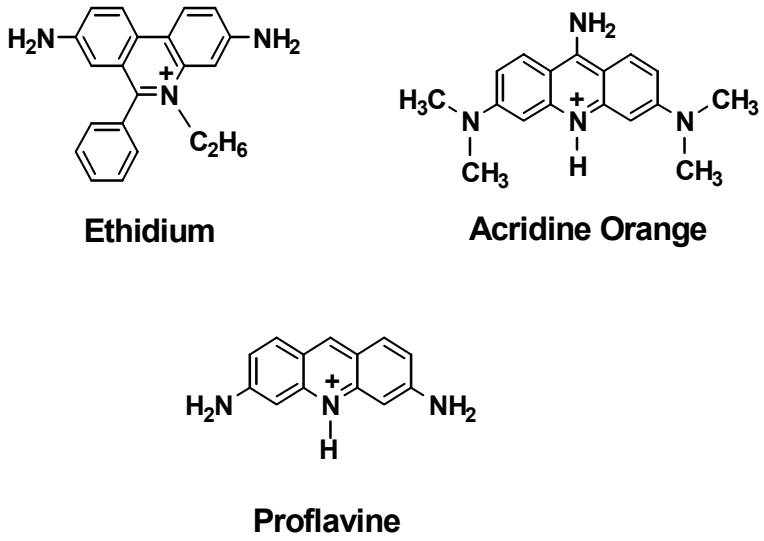

Figure 1.10 Structures of DNA intercalating dyes.

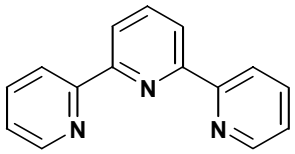

Figure 1.11 Structure of 2,2′: 6′, 2′′ -terpyridine (terpy).

intercalated $Pt(terpy)(HET)]^{+1}$ by fiber X-ray diffraction methods helped establish the nearest-neighbor exclusion principle. This principle states that intercalated molecules occupy every other inter-base pair site at saturation.[68] Other metal-based intercalators of interest include methidiumpropyl-Fe(II)EDTA, $[Cu(phen)_2]$, and metallophorphyrins.[82, 83]

Ru(II) Based DNA Intercalators

Ru(II)-polypyridyl complexes have been intensely studied as DNA-intercalators. The purpose of such investigations has been to develop nucleic acid probes, novel therapeutics, and diagnostic agents that target double-stranded DNA.[84] The suitability of Ru(II) polypyridyl complexes as DNA-binding agents arises from their stability, redox chemistry and light absorbing properties. Polypyridyl ligands such as 2,2′-bipyridine and 1,10-phenanthroline are bidentate, forming strong bonds to Ru(II) systems. Also, these ligands have vacant π orbitals that can accept electron density from the Ru(II) atom. This type of π backbonding supplements the σ bonding arising from the donation of the lone pair of electrons from the ligand to the metal. This results is a metal complex with good chemical stability. In addition, d^6 octahedral ruthenium tris-polypyridyl complexes are coordinatively saturated, inert to substitution, and most are water-soluble.[85, 86] Another reason for the suitability of Ru(II) complexes as DNA-binding agents is that these compounds have good light absorbing properties. Ru(II) polypyridyl complexes absorb strongly throughout much of the ultraviolet and visible spectrum and often display efficient long-lived emissions. These properties provide useful handles for monitoring the interactions of these complexes with nucleic acids.

When a tris-chelated ruthenium complexe absorbs a photon of light, it enters into an excited state. Absorption of light results in the promotion of an electron from a filled orbital to an unfilled one. The electronic transitions desribed above involve molecular orbitals. The nature of the orbitals involved in the absorption of light are commonly described using the linear combination of atomic orbitals (LCAO) approach. In this approach, each molecular orbital is a combination of one or more atomic orbitals. Figure 1.12 shows the application of this approach for a octahedral d^6 metal complex.[87] The orbitals with patterned boxes denote filled orbitals, whereas blank orbitals represent unfilled orbitals. For a d^6 octahedral metal complex, the filled metal-based $d\pi$ orbitals and the unfilled ligand-based π^* orbitals are the most imporant. These orbitals represent the highest occupied molecular orbitals (HOMO) and lowest occupied molecular orbitals

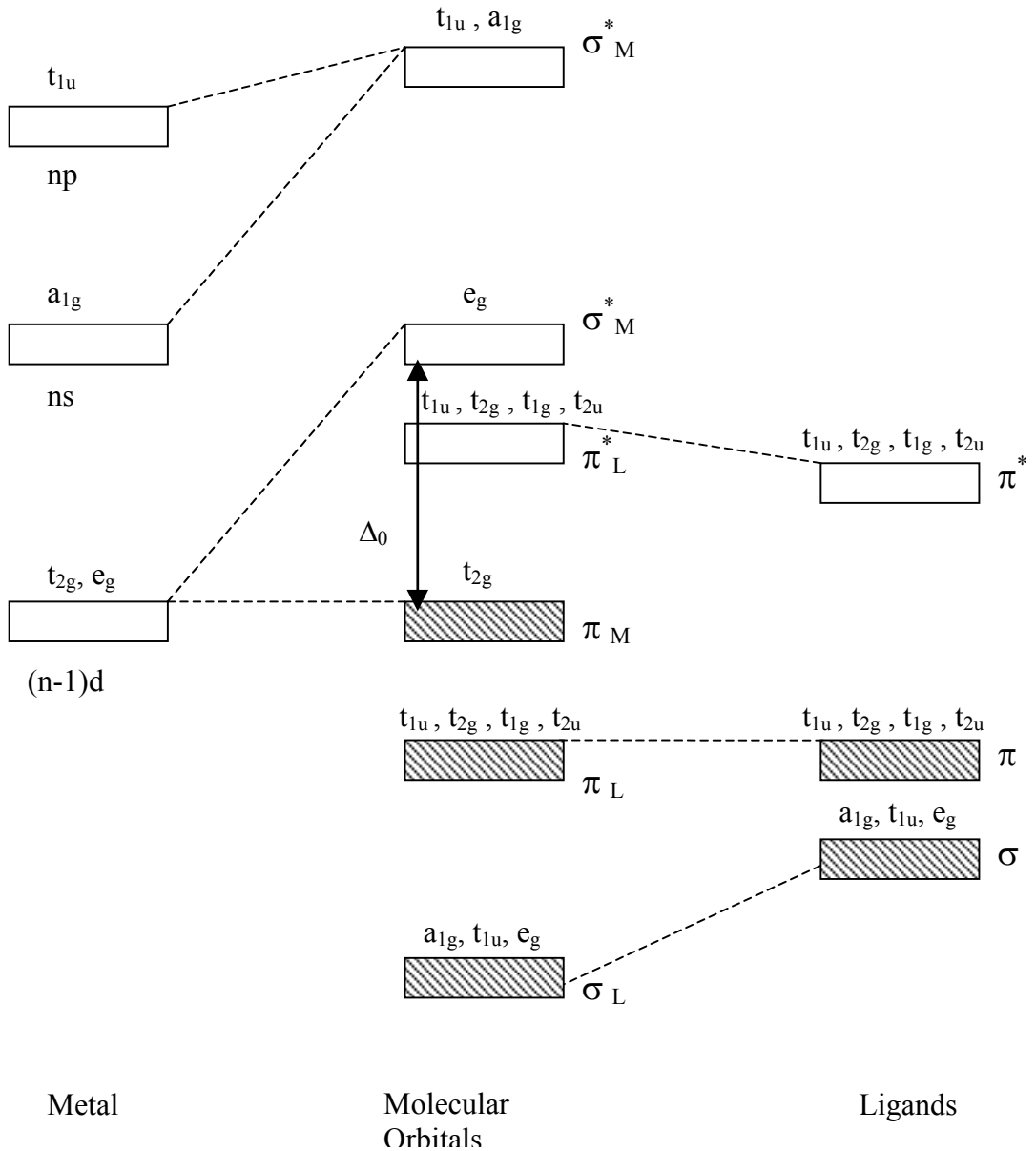

Figure 1.12 Block molecular orbital diagram for a d^6 octahedral complex with π bonding. Shaded blocks denote filled molecular orbitals. Blocks with multiple symmetry labels (i.e., t_{1u}, t_{2u}, t_{1g}, t_{2g}) represent groups of orbitals at different energies.[87]

(LUMO). The attributes and energy of these two orbitals are vitally important to understanding the light absorbing properties of Ru(II) polypyridyls, since these orbitals are involved in the lowest energy electronic transition and excited state.[88]

The major electronic transitions that occur for ruthenium octahedral d^6 complexes incorporating polypyridyl ligands are shown in Figure 1.13. These include ligand $n \rightarrow \pi^*$ and $\pi \rightarrow \pi^*$ transitions, metal to ligand charge transfer transitions (MLCT) and ligand field transitions (LF). The intensity of these transitions is subject to spin and Laporte selection rules. Typically, transitions that are both spin and Laporte allowed (ligand $\pi \rightarrow \pi^*$ and MLCT transitions) have large molar extinction coefficients (10^3-10^5 M^{-1} cm^{-1}). Transitions that are only spin allowed (ligand field, LF) tend to have much lower (e.g., <1000 M^{-1} cm^{-1}) molar extinction coefficients.[88]

The most important of these electronic transitions in relation to DNA binding is the metal-to-ligand charge transfer transition (MLCT) in the visibile spectrum. This transition is very intense, distinct from DNA absorptions, and well characterized in the literature. In addition, this transition is sensitive to enviroment, making it a useful spectroscopic handle to monitor the interactions of these complexes with nucleic acids.

An exceedingly well-studied Ru(II) light absorber is $[Ru(bpy)_3]^{+2}$.[89] This complex is photostable, displays luminescence in solution at room temperature, has a moderate excited state lifetime, and is able to undergo excited-state electron and energy-transfer processes. This unique combination of properties has lead to the study of this compound for solar energy conversion schemes.[90] The capabilities of this complex have been expanded through the preparation of numerous derivatives, in which those incoporating polypyridyl bridging ligands have been of particular interest. Such complexes are capable of binding an additional metal centers to form thermally stable polymetallic complexes.

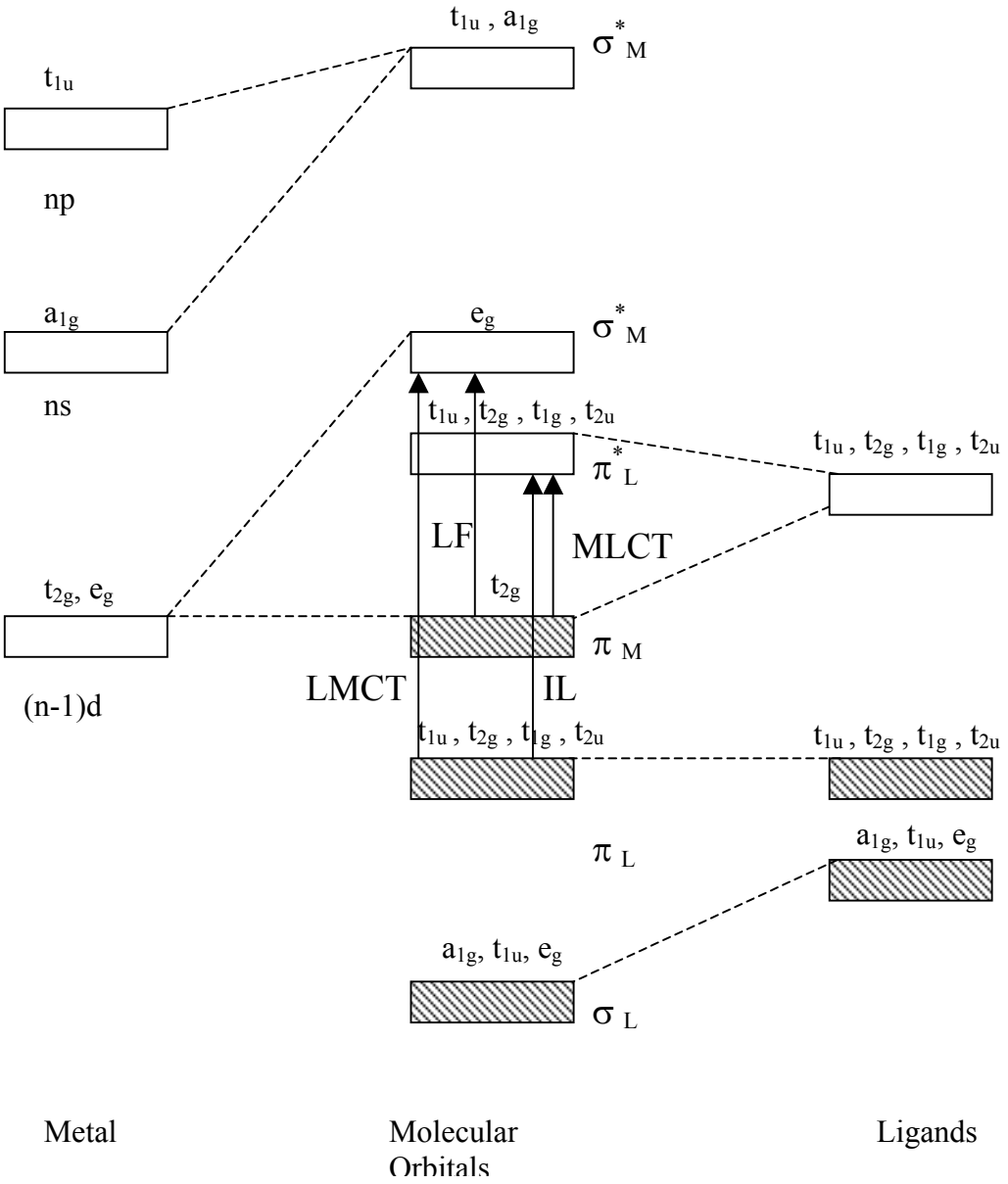

Figure 1.13 Major electronic transitions for octahedral transition metal complexes. Shaded blocks denote filled molecular orbitals. Blocks with multiple symmetry labels (i.e., t_{1u}, t_{2g}, t_{1g}, t_{2u}) represent groups of orbitals at different energies. MLCT indicates metal to ligand charge transfer transition. LF indicates ligand field transition. IL indicates inter-ligand transition. LMCT indicates ligand to metal charge transfer transition.[87]

The optical and redox properties of ruthenium bridging ligand complexes have been well studied.[91- 101] All absorb strongly in the UV and visible regions of the electromagnetic spectrum. The lowest energy transition is an intense MLCT (metal-to-ligand charge-transfer) band in the visible region, assigned as Ru ($d\pi$) $\rightarrow$ polyazine (π^*) in nature. Internal ligand $\pi \rightarrow \pi^*$ and $n \rightarrow \pi^*$ transitions are also observed for these systems. These complexes typically display one emission band associated with the Ru$\rightarrow$ BL MLCT excited state. The emission shifts to lower energy with bridging ligands having lower energy π^* orbitals. Tris-chelated ruthenium bridging ligand complexes display a single one-electron reversible oxidation corresponding to the $Ru^{II/ III}$ couple. Three one-electron reversible reductions also occur, corresponding to sequential reduction of the bridging and terminal ligands. Absorption and electrochemical data for a series of ruthenium tris-chelated polypyridyl complexes is shown in Table 1.3.

$[Ru(phen)_3]^{2+}$: Chiral DNA Intercalator

One highly studied Ru(II) polypyridyl compound in regard to DNA binding is $[Ru(phen)_3]^{2+}$ (where phen = 1,10-phenanthroline). In a 1983 study using circular dichroism, Yamagishi was able to show that Λ- and Δ- $[Ru(phen)_3]^{2+}$ form an association with the DNA helix.[102] Following up on this study, a series of investigations by Barton and co-workers utilizing a wide variety of spectroscopic, photophysical and biophysical techniques have suggested that Λ- and Δ-$[Ru(phen)_3]^{2+}$ bind to DNA by two non-covalent modes.[103-105] These include (1) a groove-bound mode stablized by hydrophobic interactions of the ligands with the minor groove and (2) intercalation in the major groove.[106] In addition, Barton and co-workers demonstrated that the the Δ-isomer perferentially binds and recognizes right-handed helices.[88,107]

These intriguing results have elicited considerable debate on the binding mechanism of this complex. A number of studies by other researchers have suggested that $[Ru(phen)_3]^{2+}$ binds DNA through only a partially intercalative mode, or through a

Table 1.3 Absorption spectroscopy and electrochemical data for a series of Ru(II) tris-chelated polypyridyl complexes, where bpy = 2,2′- bipyridine, phen = 1,10-phenanthroline, dpq = 2,3-bis(2-pyridyl)quinoxaline, dpb = 2,3-bis(2-pyridyl)benzoquinoxaline. Reported reductions indicate sequential ligand based reductions, $L^{0/-}$. Potentials are reported in volts vs. SCE.

Complex	Absorption λ_{max} (nm)	Oxidations, (V)	Reductions, (V)			Ref
		$E_{1/2}$, $Ru^{II/III}$	$E_{1/2}(1)$	$E_{1/2}(2)$	$E_{1/2}(3)$	
$[Ru(bpy)_3]^{2+}$	450	1.26	-1.35	-1.53	-1.78	a
$[Ru(phen)_3]^{2+}$	447	1.31	-1.34	-1.47	c	a
$[(bpy)_2Ru(dpp)]^{2+}$	464(sh) 441 470 430	1.33	-1.06	-1.48	c	a
$[(phen)_2Ru(dpp)]^{2+}$	465(sh) 434	1.39	-1.07	-1.35	c	a
$[(bpy)_2Ru(dpq)]^{2+}$	517 426(sh) 391(sh) 350(sh)	1.47	-0.72	-1.40	-1.62	a,b
$[(phen)_2Ru(dpq)]^{2+}$	601 420(sh) 398 380(sh)	1.42	-0.79	-.1.50	c	a
$[(bpy)_2Ru(dpb)]^{2+}$	550 390	1.48	-0.62	-1.26	-1.60	b

[a] Adapted from reference 181.
[b] Electrochemical data adapted from reference 100.
[c] Not reported.

non-intercalative mode within the DNA minor groove.[108- 110] A more "developed" view of the actual DNA-binding characeristics of this compound is found in an exhaustive investigation by Satyanarayana and co-workers.[111] In these studies, the DNA binding of $[Ru(phen)_3]^{2+}$ was compared against well-established intercalators. The results of these studies question both the data previously obtained and the validity of many of the techniques previously used to suggest that $[Ru(phen)_3]^{2+}$ binds to DNA through classical intercalation. Rather, the authors propose that Λ- and Δ- $[Ru(phen)_3]^{2+}$ are "non-classical" DNA intercalators, binding weakly to DNA by a predominantly electrostatic mode. Modest stereoselectivity of DNA binding is still present however, with the Δ- isomer binding somewhat better to B-DNA.

$[(bpy)_2Ru(dppz)]^{2+}$ and $[(phen)_2Ru(dppz)]^{2+}$: "Molecular Light Switches for DNA"

In a series of studies by Barton and co-workers, the most critical factor governing DNA binding affinity for Ru(II) complexes was determined to be the shape of the metal complex and how this shape matches the DNA helix.[112] Drawing upon these conclusions, Barton and co-workers have examined the interaction of $[(bpy)_2Ru(dppz)]^{2+}$ and $[(phen)_2Ru(dppz)]^{2+}$ (where bpy = 2,2′-bipyridine, phen = 1,10-phenanthroline, dppz = dipyrido[3,2-*a*: 2′, 3′-*c*]phenazine) with double-stranded DNA. The structures of these complexes are shown in Figures 1.14 and 1.15. These complexes are especially suitable for possible DNA interactions studies due to their intense MLCT transitions in the visible and the extended planar character of the dppz ligand.[113-115]

It has been determined that $[(bpy)_2Ru(dppz)]^{2+}$ and $[(phen)_2Ru(dppz)]^{2+}$ bind DNA by intercalation, with affinities in the range of $10^7\ M^{-1}$.[84, 116-121] These complexes also display intriguing luminescence behavior. Both complexes luminesce in nonaqueous solvents, but show little luminesence in water. This luminescence arises from the Ru→ dppz CT excited state. Absence of luminescence in water has been attributed to the interaction of water with the phenazine nitrogens, quenching the luminescence.

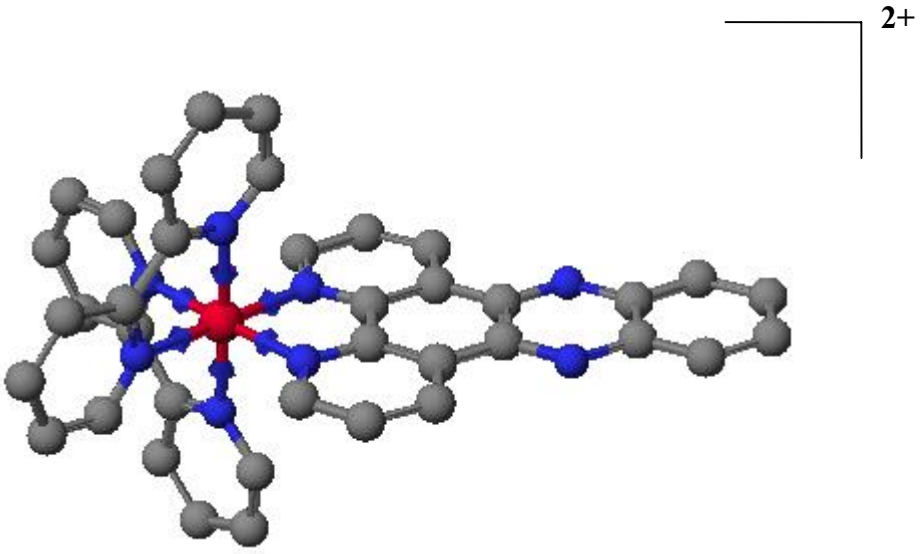

Figure 1.14 Structure of $[(bpy)_2Ru(dppz)]^{2+}$ where bpy = 2,2′- bipyridine, dppz = dipyrido[3,2-*a*: 2′, 3′-*c*]phenazine. Red = Ru(II), blue = N. H omitted for clarity.

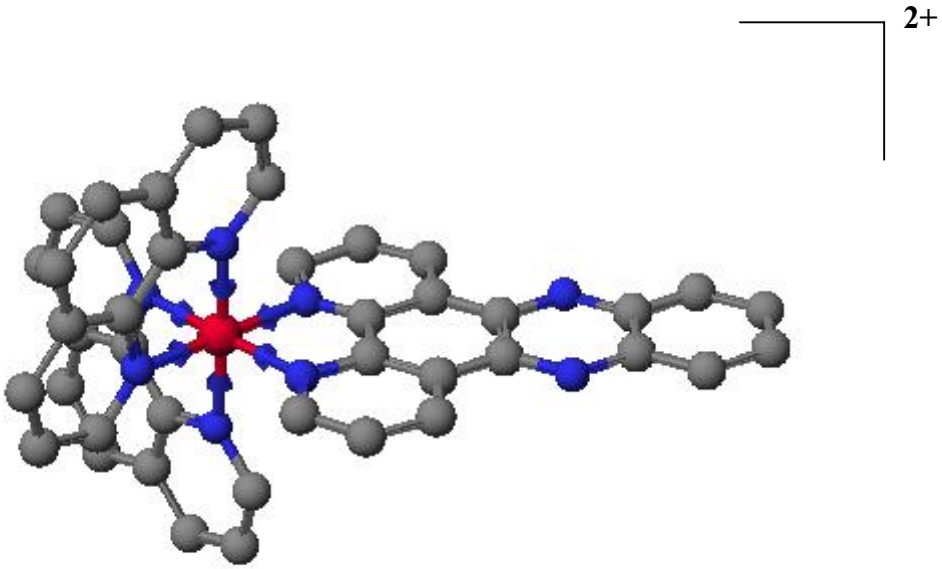

Figure 1.15 Structure of $[(phen)_2Ru(dppz)]^{2+}$, where bpy = 2,2′- bipyridine, phen = 1,10-phenanthroline, dppz = dipyrido[3,2-*a*: 2′, 3′-*c*]phenazine. Red = Ru(II), blue = N. H omitted for clarity.

However, at room temperature and in aqueous solution, intense luminescence is observed in the presence of DNA. This has been attributed to the intercalation of the dppz ligand into the DNA helix, protecting the phenazine nitrogens from an interaction with water, thereby allowing luminescence to occur. This interesting behavior has lead to the label "molecular light switch," since these compounds display no detectable luminescene in water but luminesce brightly in the presence of DNA.[117, 118, 122]

The study of the DNA interactions of Ru(II) complexes continues to be a rich area of research. Whereas $[Ru(phen)_3]^{2+}$ and $[(L)_2Ru(dppz)]^{2+}$ (where L = 2,2′-bipyridine and 1,10-phenanthroline) are perhaps the best known, numerous other Ru(II)-polypyridyl complexes have been shown to bind to DNA by intercalation.[123-127] Several osmium (II) complexes also display intercalative binding to DNA.[128- 130]

Ru(II) Bimetallic Complexes as DNA Intercalators

The synthesis of polyazine bridging ligands has led to the development of a new class of metal complexes: multimetallic complexes.[91-100, 131-135] Through the correct synthetic application of terminal and bridging ligands, multimetallic complexes can be readily prepared. Numerous examples of these types of complexes utilizing platinum-group metals are present in the literature, and many have been investigated for photochemical and electrochemical applications.[136-148]

Bimetallic complexes of Ru(II) can also interact with DNA. Murphy and co-workers reported that the Ru(II) bimetallic complex $[(NH_3)_4Ru(dpb)Ru(NH_3)_4]^{4+}$ (where dpb = 2,3-bis(2-pyridyl)benzoquinoxaline) intercalates into the DNA helix, with a binding constant of $10^5\ M^{-1}$.[149] As with the Ru(II)-dppz derivatives previously mentioned, the extended planarity of the dpb ligand is critical for the intercalation process. Norden and co-workers have reported the interaction of a novel Ru(II) bimetallic complex, $[L_2Ru\{dppz(11\text{-}11')dppz\}RuL_2]$ (where L = 1,10-phenanthroline, 2,2′-bipyridyl, dppz = dipyrido[3,2-*a*: 2′, 3′-*c*]phenazine, Figure 1.16) with DNA.[150] Having two chiral centers, this complex exists in four enantiomeric forms. Using a variety of techniques including

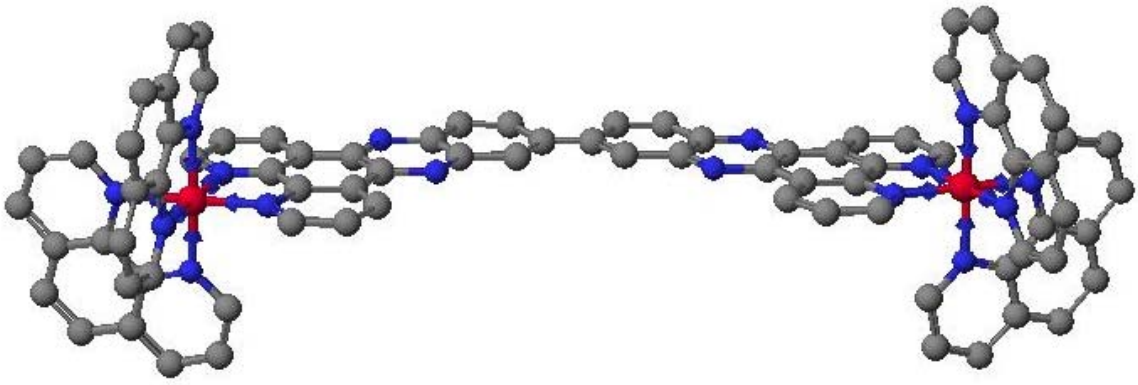

Figure 1.16 Structure of [$L_2Ru\{dppz\ (11\text{-}11')dppz\}RuL_2$] (where L = 1,10-phenanthroline, 2,2′-bipyridyl, dppz = dipyrido[3,2-*a*: 2′, 3′-*c*]phenazine). Red = Ru(II), Blue = N. H omitted for clarity.

circular dichroism and absorption studies, this complex was determined to have a high affinity for DNA ($K \approx 10^{12}\ dm^{-1}mol^{-1}$). The binding mode was suggested to be a groove-bound, non-classical intercalative mode. In addition, a slight stereospecificity was observed for the phenanthroline ΛΛ derivatives.

Project Description

The goal of this research is to design and establish a new class of supermolecules coupling ruthenium and platinum that display covalent binding to DNA. This required the development of synthetic methods for these novel multimetallic complexes. A study of their physical and spectroscopic properties was also essential in order to probe and in the future alter properties of this new class of supermolecules. As discussed in the preceding chapter, cisplatin is a highly effective anticancer agent with a broad spectrum of clinical activity. However, this compound is known to cause severe toxic side effects. Innate and acquired resistance to cisplatin are also major clinical issues. Therefore, research into cisplatin analogs that limit side effects and circumvent resistance is an active and exceedingly important field of research.

The approach used in this work was to bring together two important classes of known DNA binding agents, combining them into one structural motif. Ruthenium

polyazine complexes incorporating ligands with extended, planar aromatic regions may be readily prepared and a few have been shown to bind to DNA by intercalation. The framework of these complexes may be extended by incorporating polyazine bridging ligands within the ruthenium coordination sphere. Addition of a suitable metal center is then possible through the vacant coordination site on the bridging ligand. The *cis*-$Pt^{II}Cl_2$ active site of cisplatin could therefore be added to this framework. The end result would be a complex with possible bifunctional DNA-binding character, i.e., binding to DNA through intercalation and/or crosslinking.

In this study, four complexes were synthesized that incorporate these features, $[(bpy)_2Ru(BL)PtCl_2](CF_3SO_3)_2$ and $[(phen)_2Ru(BL)PtCl_2](CF_3SO_3)_2$ (where bpy = 2,2′-bipyridine, phen = 1,10-phenanthroline, BL = 2,3-bis(2-pyridyl)quinoxaline (dpq) and 2,3-bis(2-pyridyl)benzoquinoxaline (dpb)). All four complexes contain the *cis*-$Pt^{II}Cl_2$ active site of cisplatin, and a ruthenium unit that contains planar polyazine ligands. Ruthenium complexes incorporating the 1,10-phenanthroline ligand have been shown to bind to DNA by intercalation, as with the ruthenium bimetallic complex $[(NH_3)_4Ru(dpb)Ru(NH_3)_4]^{4+}$.[103-107, 111, 149] These four new ruthenium-platinum bimetallic complexes are shown in Figures 1.17 – 1.18, with the terminal and bridging ligands used to construct these complexes shown in Figure 1.19.

A polyazine-bridged ruthenium-platinum bimetallic complex offers several advantages not currently present in platinum-based drugs. Being a neutral complex, cisplatin has limited water-solubility. The addition of a Ru^{II} center adds an additional 2+ charge to the bimetallic complex, allowing for increased water-solubility. The ruthenium monometallics are also excellent chromophores, thereby providing a possible spectroscopic handle for examining the binding of these complexes to DNA. The molecular framework of this type of molecule may also be readily changed through

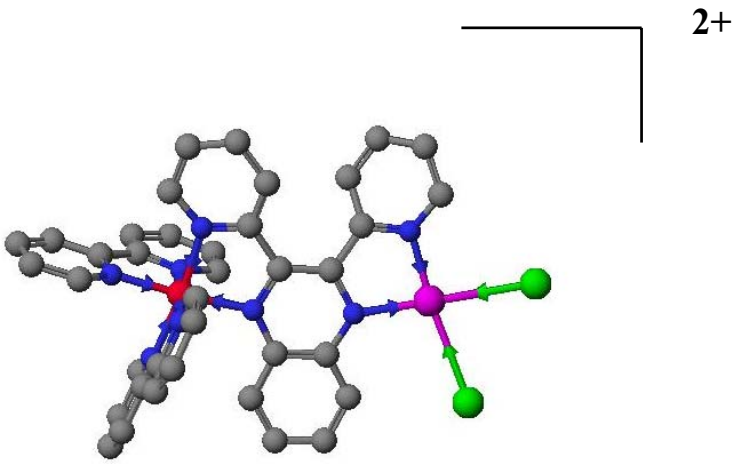

$[(bpy)_2Ru(dpq)PtCl_2](CF_3SO_3)_2$

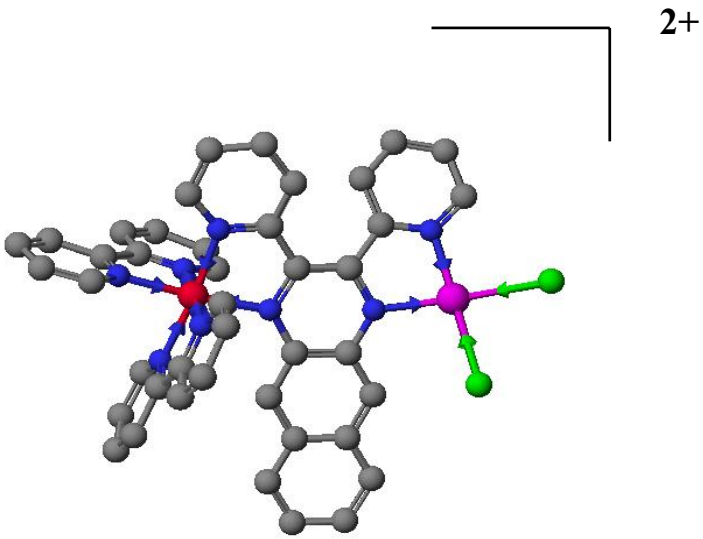

$[(bpy)_2Ru(dpb)PtCl_2](CF_3SO_3)_2$

Figure 1.17 Structures of $[(bpy)_2Ru(dpq)PtCl_2](CF_3SO_3)_2$ and $[(bpy)_2Ru(dpb)PtCl_2](CF_3SO_3)_2$, where bpy = 2,2′-bipyridine, dpq = 2,3-bis(2-pyridyl)quinoxaline, dpb = 2,3-bis(2-pyridyl)benzoquinoxaline. Red = Ru(II), blue = N, violet = Pt(II), green = Cl. H omitted for clarity.

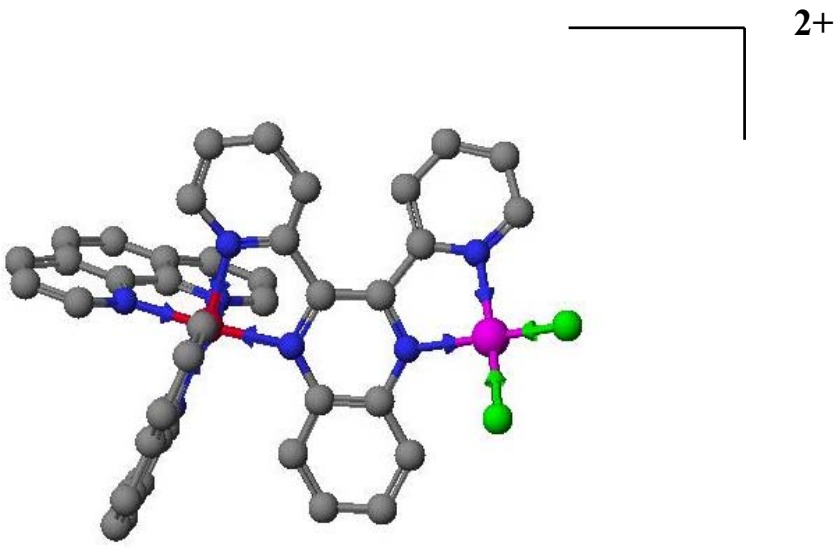

$[(phen)_2Ru(dpq)PtCl_2](CF_3SO_3)_2$

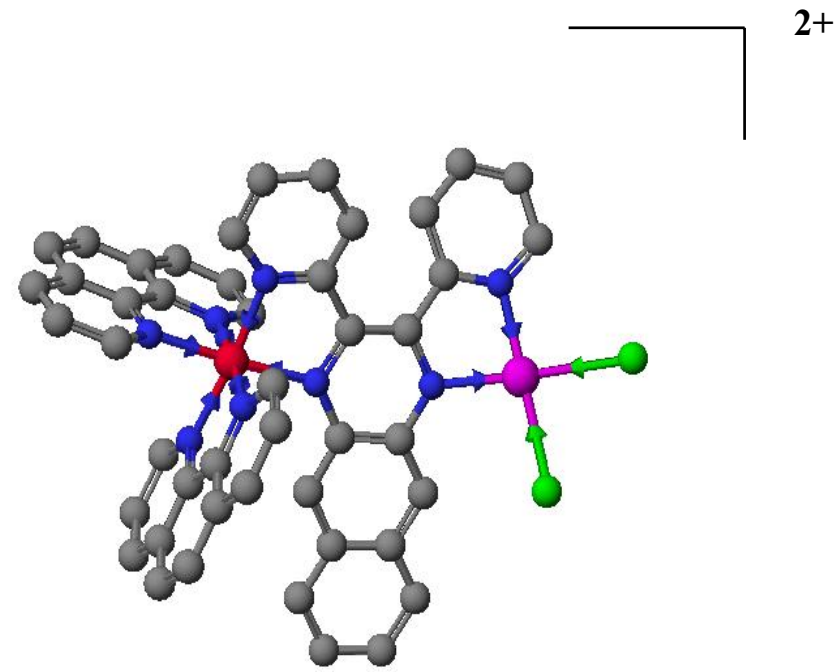

$[(phen)_2Ru(dpb)PtCl_2](CF_3SO_3)_2$

Figure 1.18 Structures of $[(phen)_2Ru(dpq)PtCl_2](CF_3SO_3)_2$ and $[(phen)_2Ru(dpb)PtCl_2](CF_3SO_3)_2$, where phen = 1,10-phenanthroline, dpq = 2,3-bis(2-pyridyl)quinoxaline, dpb 2,3-bis(2-pyridyl)benzoquinoxaline. Red = Ru(II), blue = N, violet = Pt(II), green = Cl. H omitted for clarity.

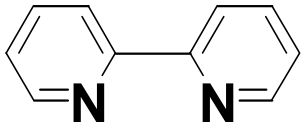

bpy

phen

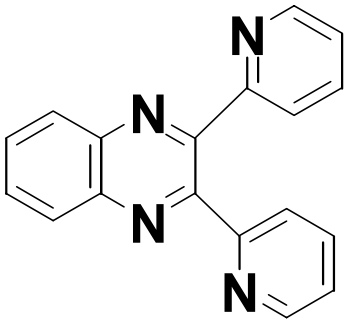

dpq

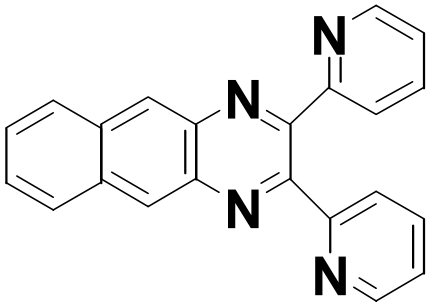

dpb

Figure 1.19 Terminal and bridging ligands used to construct Ru-Pt complexes. bpy = 2,2′-bipyridine, phen = 1,10-phenanthroline, dpq = 2,3-bis(2-pyridyl)quinoxaline, dpb = 2,3-bis(2-pyridyl)benzoquinoxaline.

incorporation of different terminal and/or bridging ligands around the ruthenium center, as well as attachment of other moieties. The study of a group of complexes with a varying molecular framework may provide important clues for elucidating the structure-activity relationships of this new class of supermolecules.

Another goal of this work was to develop simple, reproducible, *in vitro* DNA binding assays to determine if the supermolecules bind DNA. An *in vitro* reaction with DNA followed by analysis by gel electrophoresis offers many advantages for the detection of DNA binding activity. Binding of these complexes to DNA will change the molecular weight, charge and three-dimensional shape of the DNA. These effects are easily observed in an electrophoretic gel, in comparison to untreated DNA control and complexes with known DNA binding affinities. Choice of electrophoresis conditions (i.e., native or denaturing) may also allow a more complete analysis of the mode of DNA crosslinking exhibited by the supermolecules. Analysis of the electrophoresis results (gel densitometry, calculating R_f values) may provide an additional means of characterizing DNA adduct formation, allowing comparisons of DNA binding ability among metal compounds. Finally, modeling the migration of metal-bound DNA through an electrophoresis gel (according to molecular weight effects and assuming 100% metal binding) and comparing this data with experimentally measured migration distances may provide some insight as to the cause of any observed gel effects.

Chapter 2: Experimental

Materials, Synthetic Studies. $RuCl_3 \bullet 3H_2O$ and K_2PtCl_4 were obtained from Johnson-Matthey and used as received. Dimethylsulfoxide and adsorption alumina were obtained from Fisher and used without further purification. All remaining chemicals were obtained from Aldrich Chemical Company and used as received, unless otherwise noted. The supporting electrolyte for electrochemical studies was tetrabutylammonium hexafluorophosphate, prepared by the metathesis of tetrabutylammonium bromide with potassium hexafluorophosphate, recrystallized twice from 100% ethanol, dried under vacuum, and stored in a vacuum dessicator. $[(bpy)_2RuCl_2]$ was prepared as previously described.[151]

Materials, DNA Interaction Studies. Molecular biology grade chemicals used for DNA interaction studies were purchased from Fisher and used as received. Cis-diamminedicloroplatinum(II) (cisplatin) was purchased from Aldrich and used as received. The compound 1,1/t,t was a gift from Dr. N. Farrell, Virginia Commonwealth University. Lyophilized calf thymus DNA (type XV, activated) was obtained from Sigma. Bacteriophage Lambda DNA was obtained from Promega. The plasmid, pBluescript KS+, was obtained from Stratagene and all materials used in amplification and purification were purchased from Fisher. Electrophoresis-grade Low EEO agarose, tris (hydroxymethyl)-aminomethane (Tris), boric acid, ethidium bromide and phenol hydroxyquinoline were also obtained from Fisher. A phenol/0.1% hydroxyquinoline solution was prepared as described previously.[25] EcoRI and HindIII restriction endonucleases (including enzyme buffers) were purchased from Promega. Distilled-dionized water (ddH_2O) was obtained from the Virginia Tech Biology Department, where dionization was conducted on a MilliQ 10 system.

FAB-Mass Spectrometry. FAB mass spectral analysis was conducted on a Fisons VG Quattro triple-stage quadrupole mass spectrophotometer using *m*-nitrobenzyl alcohol as the matrix.

Electrochemistry. A Bioanalytical Systems 100W electrochemical analyzer was used to record the cyclic and Oster young Square Wave voltammograms. The supporting electrolyte was 0.1 M Bu_4NPF_6 and all measurements were taken in Burdick and Jackson UV-grade acetonitrile. The electrode system consists of a 1.9-mm diameter platinum disk working electrode, a platinum wire auxiliary electrode, and a Ag/AgCl reference electrode (0.29V vs. NHE). The Ag/AgCl reference electrode was calibrated versus the $FeCp_2/FeCp_2^+$ couple, which is taken to be 0.665 V vs NHE in 0.1 M TBAH.[152]

Electronic Absorption Spectroscopy. Electronic absorption spectra were obtained using a Hewlett Packard 8452 diode array spectrophotometer with a 2 nm resolution and a range from 190 to 820 nm, interfaced to an IBM compatible PC. Samples were prepared using Burdick and Jackson UV grade acetonitrile, and the cuvette was 1 cm in pathlength with quartz windows. Samples used for the calculation of ε were prepared gravimetrically.

Emission Spectrometry. Emission spectra were obtained using a Perkin-Elmer Model LS 50 B luminescence spectrometer linked to an IBM-compatible PC. Samples were prepared using ddH_2O (distilled-deionized) and the cuvette was 1 cm pathlength with quartz windows.

Metal-DNA Reactions. DNA-metal reactions were performed using 1.5 ml microcentrifuge tubes, and all volume transfers were accomplished utilizing Eppendorf Reference Pipetters. Centrifugation was accomplished using a MSE Micro Centaur centrifuge, and incubations were performed in a Blue M Stabil-Therm Dry Type Bacteriological Incubator.

Gel Electrophoresis. Native gel electrophoresis was carried out in Owl Scientific Model B1A-BP minigel rigs (30 ml gel volume, 300 ml buffer volume). Electrophoresis buffer was recirculated using VWR Scientific Model 54856-075 medium-flow pumps. Applied voltage was provided by an Owl Scientific Model OSP-15 variable voltage power supply. All gels were loaded using Fisher-Brand gel loading tips. Agarose-ddH_2O

solutions were heated using a GE Model JES632WN microwave oven. To ensure consistency between experiments, electrophoresis time was monitored using a VWR 4 channel digital timer. Agitation during ethidium bromide staining was provided by a Blue M model 745 Bacteriological Incubator (agitation only, no heating).

Gel Imaging. Completed electrophoresis gels (native and denaturing) were photographed using a Fisher Biotech FB-PDC-54 Camera, utilizing Polaroid Type 667 instant film. UV-illumination was provided by a Fisher Scientific FBI-88 Transilluminator. The resulting Polaroid prints were then scanned at 150 dpi using an Apple ColorOne 600/27-flatbed scanner linked to a Power MacIntosh 8500/120.

Gel Densitometry. The ethidium bromide fluorescence of each metal-DNA reaction band was quantitated by using the AlphaImager 2000™ gel documentation system. This system consists of a UV-transilluminator, light cabinet, and camera, all linked to an IBM compatible PC computer.

2,3-bis(2-pyridyl)quinoxaline. 2,3-bis(2-pyridyl)quinoxaline was prepared by a modification of the previously published method of Goodwin and Lions.[153] 2,2'-pyridyl (4.24 g, 20.0 mmol) and 1,2-phenylenediammine (2.16 g, 20.0 mmol) were heated at reflux in 50 ml 95% EtOH for 3 h. The reaction was then cooled to room temperature, and the crude product was collected by vacuum filtration. Purification was accomplished by recrystallization in hot ethanol (~75 ml) to yield the colorless dpq ligand. Purity was checked by the absence of a C=O peak at ~1700 cm^{-1} in the IR spectrum. Yield: 4.3 g, 15 mmol, 75%.

2,3-bis(2-pyridyl)benzoquinoxaline. 2,3-bis(2-pyridyl)benzoquinoxaline was prepared by a modification of the preparation for dpq where 2,3-diamminonapthalene was substituted for *o*-phenylenediammine. 2,2'-pyridyl (3.4 g, 16 mmol) and 2,3-diamminonapthalene (2.6 g, 16 mmol) were heated at reflux in 125 ml of 95% EtOH for 5 h. The reaction was then allowed to slowly cool to room temperature and the crude product was collected by vacuum filtration. Purification was afforded in 3 steps, with the

first step involving a single recrystallization from 100% EtOH (~150 ml). The second step involved purification by alumina column chromatography, using 100% dichloromethane as the eluent. The first band was brown in color and was assumed to be unreacted starting material. The second, yellow band was the product and was collected. The solvent was removed from the product by rotary evaporation. The third step involved a final single recrystallization from 100% EtOH to yield the yellow dpb ligand. Purity was checked by the absence of a C=O peak at ~1700 cm^{-1} in the IR spectrum. Yield: 3.5 g, 11 mmol, 66%.

$[(bpy)_2Ru(dpq)](CF_3SO_3)_2$. In order to provide adequate water solubility for the DNA-interaction studies, all metal complexes were prepared as triflate salts. The synthesis of $[(bpy)_2Ru(dpq)](CF_3SO_3)_2$ was a modification of a previously published procedure.[93] In this procedure, $[(bpy)_2Ru(dpq)](PF_6)_2$ is the final product but an additional step involving the reaction of $[(bpy)_2RuCl_2]$ with $AgCF_3SO_3$ in acetone was added to produce the triflate salt. $[(bpy)_2RuCl_2]$ (0.250 g, 0.51 mmol) and $AgCF_3SO_3$ (0.260 g, 1.02 mmol) were stirred in 50 ml acetone for 1 h at RT. Solid AgCl that was formed was removed by vacuum filtration, and dpq (0.14 g, 0.51 mmol) was added to the filtrate. This solution was heated at reflux for 5 h, and the solvent was then removed by rotary evaporation. Purification was achieved by alumina column chromatography, using 2:1 toluene/acetonitrile as the initial eluent, followed by a change to 1:2 toluene/acetonitrile. The dark-red fraction that was the first to elute was collected and the solvent was removed by rotary evaporation. The dark-red product then dissolved in minimal acetonitrile, flash precipitated in 150 ml diethyl ether, and collected by vacuum filtration. Yield: 0.26 g, 0.27 mmol, 52%. $E_{1/2}$ (V vs. Ag/AgCl): +1.50, -0.75, -1.39, -1.60. λ_{max}^{abs} = 518 nm.

$[(bpy)_2Ru(dpb)](CF_3SO_3)_2$. The synthesis of $[(bpy)_2Ru(dpb)](CF_3SO_3)_2$ was a modification of the preparation of $[(bpy)_2Ru(dpq)](CF_3SO_3)_2$, in which the dpb ligand was substituted for dpq. $[(bpy)_2RuCl_2]$ (0.25 g, 0.51 mmol) and $AgCF_3SO_3$ (0.26 g, 1.0 mmol) were stirred in 50 ml acetone for 1 h at RT. Solid AgCl that formed was removed by vacuum filtration, and dpb (0.17 g, 0.51 mmol) was added to the filtrate. This solution was

heated at reflux for 5 h, and the solvent was then removed by rotary evaporation. Purification was achieved by alumina column chromatography, using 2:1 toluene/acetonitrile as the initial eluent, followed by a change to 1: 2 toluene/acetonitrile. The first, yellow band to elute was unreacted dpb. The second, dark-red band was the product and was collected. The solvent was then removed by rotary evaporation. The dark-red product was dissolved in minimal acetonitrile, flash precipitated in 150 ml diethyl ether, and collected by vacuum filtration. Yield: 0.32 g, 0.30 mmol, 59%. $E_{1/2}$ (V vs. Ag/AgCl): +1.49, -0.60, -1.25, -1.58. λ_{max}^{abs} = 550 nm.

$[(phen)_2RuCl_2]$. The synthesis of $[(phen)_2RuCl_2]$ was a modification of a previously published procedure.[142] $RuCl_3 \bullet 3H_2O$ (2.0 g, 5.7 mmol), 1,10 phenanthroline (2.7 g, 15 mmol) and LiCl (1.60 g, 232 mmol) were heated at reflux in 30 ml DMF for 8 h. The reaction mixture was then cooled to RT, 60 ml reagent grade acetone was added, and the resulting solution cooled at 0 °C overnight. The product was then collected by vacuum filtration, washed three times with 25 ml portions of cold dH_2O, followed by three 25 ml portions of diethyl ether. The resulting greenish-black product was then dried overnight under vacuum. Yield 1.6 g, 2.9 mmol, 52%.

$[(phen)_2Ru\ (dpq)](CF_3SO_3)_2$. $[(phen)_2RuCl_2]$ (0.20 g, 0.36 mmol) and $AgCF_3SO_3$ (0.20 g, 0.79 mmol) were stirred in 50 ml acetone for 1h at RT. The solid AgCl that formed was removed by vacuum filtration, and dpq (0.11 g, 0.39 mmol) was added to the filtrate. This solution was heated at reflux for 8 h, and the solvent was then removed by rotary evaporation. Purification was achieved by alumina column chromatography, using 1:1 toluene/acetonitrile as the eluent. The first, dark-red band was the product and was collected. The solvent was then removed by rotary evaporation. The dark-red product was then dissolved in minimal acetonitrile, flash precipitated in 150 ml diethyl ether, and collected by vacuum filtration. Yield: 0.18 g, 0.17 mmol, 48%. $E_{1/2}$ (V vs. Ag/AgCl): +1.49, -0.73, -1.39, -1.60. λ_{max}^{abs} = 518 nm.

$[(phen)_2Ru\ (dpb)](CF_3SO_3)_2$. The synthesis of $[(phen)_2Ru\ (dpb)](CF_3SO_3)_2$ was a modification of the preparation for $[(phen)_2Ru\ (dpq)](CF_3SO_3)_2$, in which the dpb ligand

was substituted for dpq. [$(phen)_2RuCl_2$] (0.20 g, 0.36 mmol) and $AgCF_3SO_3$ (0.201 g, 0.79 mmol) were stirred in 50 ml acetone for 1h at RT. Solid AgCl that formed was removed by vacuum filtration, and dpb (0.088 g, 0.26 mmol) was added to the filtrate. This solution was heated at reflux for 8 h, and the solvent was then removed by rotary evaporation. Purification was achieved by alumina column chromatography, using 1:1 toluene/acetonitrile as the eluent. The first, yellow band was unreacted dpb. The second, dark-red band was the product and was collected. The solvent was then removed by rotary evaporation. The dark-red product was then dissolved in minimal acetonitrile, flash precipitated in 150 ml diethyl ether, and collected by vacuum filtration. Yield 0.15 g, 0.14 mmol, 52%. $E_{1/2}$ (V vs. Ag/AgCl): +1.51, -0.58, -1.25, -1.57. λ_{max}^{abs} =550 nm.

[$Pt(dmso)_2Cl_2$]. The synthesis of $Pt(dmso)_2Cl_2$) (dmso = dimethyl sulfoxide) was according to a modification of a previously published procedure.[154- 156] K_2PtCl_4 (1.3 g, 3.0 mmol) and dmso (0.70 g, 9.0 mmol) were combined in 10 ml of dH_2O. This mixture was allowed to sit at RT overnight, after which medium yellow crystals formed. These crystals were collected by vacuum filtration, and washed three times with 90 ml portions of dH_2O, ethanol, and diethyl ether. Yield: 0.84 g, 2.0 mmol, 66%.

Note on Syntheses of Ru,Pt Bimetallic Complexes. During the synthetic development of the Ru-Pt bimetallic complexes, it was determined that all Ru-Pt bimetallic compounds were unstable on alumina adsorption. Therefore, a synthesis had to be designed such that no chromatographic purification was required. The following synthetic procedures reflect this.

[$(bpy)_2Ru(dpq)PtCl_2$](CF_3SO_3)$_2$. [$(bpy)_2Ru(dpq)$](CF_3SO_3)$_2$ (0.100 g, 0.100 mmol) and $Pt(dmso)_2Cl_2$ (0.054 g, 0.13 mmol) were heated at reflux` in 40 ml 100% EtOH for 3 h. The solution was then filtered hot, and the resulting dark blue precipitate was washed with six 30 ml portions of hot 100% EtOH. The first washing was a faint red color (denoting possible unreacted starting material), which disappeared by the fourth washing. Two additional washings were accomplished in order to assure complete removal of any unreacted starting material. This was followed by three washings with 30

ml portions of diethyl ether. Yield: 0.067 g, 0.053 mmol, 53%. $E_{1/2}$ (V vs. Ag/AgCl): +1.72, -0.20, -0.82, -1.72. λ_{max}^{abs} 584 nm. The MS data for this system, presented in Table 2.1 (full spectrum shown in Appendix E-1), confirms the identity of the product.

$[(bpy)_2Ru(dpb)PtCl_2](CF_3SO_3)_2$. The synthesis of $[(bpy)_2Ru(dpb)PtCl_2](CF_3SO_3)_2$ was a modification of the preparation of $[(bpy)_2Ru(dpq)PtCl_2](CF_3SO_3)_2$, in which $[(bpy)_2Ru(dpb)](CF_3SO_3)_2$ was substituted for $[(bpy)_2Ru(dpq)](CF_3SO_3)_2$. $[(bpy)_2Ru(dpb)](CF_3SO_3)_2$ (0.075 g, 0.072 mmol) and $Pt(dmso)_2Cl_2$ (0.038 g, 0.090 mmol) were heated at reflux in 40 ml 100% EtOH for 3 h. The solution was then filtered hot, and the resulting dark green precipitate was washed with six 30 ml portions of hot 100% EtOH. The first washing was again a faint red color (denoting possible unreacted starting material), which disappeared by the fourth washing. Two additional washings were accomplished in order to assure complete removal of any unreacted starting material.This was followed by three washings with 30 ml portions of diethyl ether. Yield: 0.056 g, 0.043 mmol, 60%. $E_{1/2}$ (V vs. Ag/AgCl): +1.60, -0.10, -0.74, -1.60. λ_{max}^{abs} 630 nm. The MS data for this system, presented in Table 2.2 (full spectrum shown in Appendix E-2), confirms the identity of the product.

$[(phen)_2Ru(dpq)PtCl_2](CF_3SO_3)_2$. $[(phen)_2Ru(dpq)](CF_3SO_3)_2$ (0.10 g, 0.096 mmol) and $Pt(dmso)_2Cl_2$ (0.081 g, 0.19 mmol) were heated at reflux in 40 ml 100% EtOH for 12 h. The solution was then filtered hot, and the resulting dark blue precipitate was washed with six 30 ml portions of hot 100% EtOH. The first washing was a faint red color (denoting possible unreacted starting material), which disappeared by the fourth washing. Two additional washings were accomplished in order to assure complete removal of any unreacted starting material. This was followed by three washings with 30 ml portions of diethyl ether. Yield: 0.067 g, 0.051 mmol, 51%. %. $E_{1/2}$ (V vs. Ag/AgCl): +1.72, -0.20, -0.82, -1.60. λ_{max}^{abs} 584 nm. The MS data for this system, presented in Table 2.3 (full spectrum shown in Appendix E-3), confirms the identity of the product.

Table 2.1 FAB Mass Spectral Data for $[(bpy)_2Ru(dpq)PtCl_2](CF_3SO_3)_2$, *m*-nitrobenzyl alcohol as the matrix. dpq = 2,3-bis(2-pyridyl)quinoxaline, bpy = 2,2′-bipyridine.

m/z	rel. abundance	assignment
1113	60	$[(bpy)_2Ru(dpq)PtCl_2](CF_3SO_3)^+$
964	100	$[(bpy)_2Ru(dpq)PtCl_2]^+$
928	52	$[(bpy)_2Ru(dpq)PtCl\ ]^+$
892	15	$[(bpy)_2Ru(dpq)Pt]^+$

Table 2.2 FAB Mass Spectral Data for $[(bpy)_2Ru(dpb)PtCl_2](CF_3SO_3)_2$, *m*-nitrobenzyl alcohol as the matrix. dpb = 2,3-bis(2-pyridyl)benzoquinoxaline, bpy = 2,2′-bipyridine.

m/z	rel. abundance	assignment
1163	70	$[(bpy)_2Ru(dpb)PtCl_2](CF_3SO_3)^+$
1014	100	$[(bpy)_2Ru(dpb)PtCl_2]^+$
977	67	$[(bpy)_2Ru(dpb)PtCl\ ]^+$
942	21	$[(bpy)_2Ru(dpb)Pt]^+$

Table 2.3 FAB Mass Spectral Data for $[(phen)_2Ru(dpq)PtCl_2](CF_3SO_3)_2$, *m*-nitrobenzyl alcohol as the matrix. dpq = 2,3-bis(2-pyridyl)quinoxaline, phen = 1,10-phenanthroline.

m/z	rel. abundance	assignment
1161	48	$[(phen)_2Ru(dpq)PtCl_2](CF_3SO_3)^+$
1012	100	$[(phen)_2Ru(dpq)PtCl_2]^+$
975	50	$[(phen)_2Ru(dpq)PtCl\ ]^+$
940	25	$[(phen)_2Ru(dpq)Pt]^+$

$[(phen)_2Ru(dpb)PtCl_2](CF_3SO_3)_2$. The synthesis of $[(phen)_2Ru(dpb)PtCl_2](CF_3SO_3)_2$ was a modification of the preparation of $[(phen)_2Ru(dpq)PtCl_2](CF_3SO_3)_2$, in which $[(phen)_2Ru(dpb)](CF_3SO_3)_2$ was substituted for $[(phen)_2Ru(dpq)](CF_3SO_3)_2$. $[(phen)_2Ru(dpb)](CF_3SO_3)_2$ (0.10 g, 0.074 mmol) and $Pt(dmso)_2Cl_2$ (0.046 g, 0.11 mmol) were heated at reflux in 40 ml 100% EtOH for 3 h. The solution was then filtered hot, and the resulting dark green precipitate was washed with six 30 ml portions of hot 100% EtOH. The first washing was a faint red color (denoting possible unreacted starting material), which disappeared by the fourth washing. Two additional washings were accomplished in order to assure complete removal of any unreacted starting material. This was followed by three washings with 30 ml portions of diethyl ether. Yield: 0.076 g, 0.060 mmol, 56%. $E_{1/2}$ (V vs. Ag/AgCl): +1.65, -0.10, -0.77, -1.65. λ_{max}^{abs} 630 nm. The MS data for this system, presented in Table 2.4 (full spectrum shown in Appendix E-4), confirms the identity of the product.

Table 2.4 FAB Mass Spectral Data for $[(phen)_2Ru(dpb)PtCl_2](CF_3SO_3)_2$, *m*-nitrobenzyl alcohol as the matrix. dpb = 2,3-bis(2-pyridyl)benzoquinoxaline, phen = 1,10-phenanthroline.

m/z	rel. abundance	assignment
1211	70	$[(phen)_2Ru(dpb)PtCl_2](CF_3SO_3)^+$
1062	100	$[(phen)_2Ru(dpb)PtCl_2]^+$
1025	70	$[(phen)_2Ru(dpb)PtCl\ ]^+$
989	30	$[(phen)_2Ru(dpb)Pt]^+$

DNA Interaction Studies

Preparation and Purification of Plasmid DNA. The plasmid, pBluescript, was amplified and purified from *E.coli* strain JM109 according to established protocols.[157] Plasmids were isolated using an alkaline lysis procedure, purified in a cesium chloride gradient, and ethidium bromide removed by a 3X extraction with an equivalent volume of ddH_2O-saturated butanol. Following concentration by ethanol precipitation, the DNA was stored in TE at 4 °C. Plasmid DNA was linearized by overnight incubation at 37 °C with *Hin*dIII endonuclease. Typically, 200 μg of plasmid DNA was combined with *Hin*dIII (5 μl) and 40 μl of 10X buffer E in a total volume of 200 μl. Protein was removed by extracting 3X with an equivalent volume of phenol/0.1% hydroxyquinoline (equilibriated with TE pH 8) and 24:1 chloroform/isoamyl alcohol (10μl). Once complete, an additional back-extraction with an equivalent volume of chloroform/isoamyl alcohol was performed. The DNA was then precipitated with 0.2 M NaCl (8 μl of 5M) and 2 volumes of 100% ethanol, resuspended in dionized water, and stored at 4 °C.

Preparation of Molecular Weight Standards. Molecular weight standards for non-denaturing gel electrophoresis were prepared by digesting bacteriophage lambda

DNA with HindIII endonuclease. Lambda DNA (50 μg, 100 μl of stock 500 μg/ml stock solution) was combined with *Hin*dIII (2 μl, 160 U) in 258 μl of ddH_2O containing 10X buffer E (40 μl) and incubated for 12 h at 37 °C. Upon completion, 100 μl of 6X type III dye[123] was added and the solution was stored at 4 °C.

Reaction of Metal Complexes with Plasmid DNA. The preparation of metal-DNA reactions has been described previously.[158] The concentration of the linearized plasmid solution was determined spectrophotometrically.[159] The stock solutions were made by combining solid metal complex with ddH_2O in a 100 ml volumetric flask to give a final concentration of 10^{-5} M. Concentrations of metal solutions were determined using the known extinction coefficients for $[(bpy)_2Ru(dpq)PtCl_2](CF_3SO_3)_2$ ($\varepsilon = 8.0 \times 10^3$ M^{-1} cm^{-1} at 588 nm), $[(bpy)_2Ru(dpb)PtCl_2](CF_3SO_3)_2$ ($\varepsilon = 8.2 \times 10^3$ $M^{-1}cm^{-1}$ at 634 nm), $[(phen)_2Ru(dpq)PtCl_2](CF_3SO_3)_2$ ($\varepsilon = 7.0 \times 10^3$ M^{-1} cm^{-1} at 588 nm), and $[(phen)_2Ru(dpb)PtCl_2](CF_3SO_3)_2$ ($\varepsilon = 7.4 \times 10^3$ M^{-1} cm^{-1} at 634 nm). Metal complex stock solutions were stored at 4 °C in the dark. All reactions contained 1 μg of linearized plasmid DNA and 10 mM sodium phosphate, pH 7 in a total volume of 100 μl. Concentration-dependent studies were performed using DNA base pair (bp) to metal complex (mc) ratios of 5:1 to 300:1. In addition, a sample consisting solely of DNA and ddH_2O (no metal solution added) was included as a control. Reactions were assembled by aliqoting the appropriate amount of metal complex into a suitably marked microcentrifuge tube, followed by addition of cut plasmid DNA and sufficient ddH_2O to bring the final volume to 100 μl. The reactions were then vortexed for 15 s, spun for 2 min (high-speed setting) in a microcentrifuge to bring the solution to the bottom of the tube, and placed in the incubator for 4 h at 37 °C.

Native Gel Electrophoresis. Analysis of metal-DNA interaction reactions has been described previously.[149] Following incubation of the metal-DNA reactions, a 0.8% agarose gel was prepared by combining 0.24 g of low EEO agarose in 30 ml ddH_2O, and heating for 1.5 min. The solution volume was then brought to 24 ml with ddH_2O, and 6 ml of 5X TB buffer (Tris-borate) was added. The resulting agarose melt was then poured

into the electrophoresis apparatus and a 10 well comb was inserted. Solidification typically took 20 minutes, with an additional 40 minutes allotted for complete curing. Electrophoresis buffer (89 mmol Tris, 89 mmol boric acid) was then prepared and poured over the gel and the comb was removed.

Samples were prepared for electrophoresis by the following procedure. Once incubation was complete, the reaction was removed from the incubator, vortexed for 15 s, and spun down in the centrifuge for 2 min (high-speed setting) to bring the solution to the bottom of the tube. For each metal-DNA reaction, 10 μl was mixed with 2 μl of Type III 6X dye. Molecular weight markers were prepared by mixing 5 μl of lambda DNA solution with 2 μl of Type III 6X dye and 5 μl of ddH_2O.

Once sample preparation was complete, the gel was loaded. Electrophoresis was performed at 104 V for 1.5 h, with buffer recirculation initiated after 15 min of initial electrophoresis. Gels were then stained in 0.1 μg/ml ethidium bromide for 1 h, with agitation, and then photographed.

Denaturing Gel Electrophoresis. The DNA-metal reactions were also analyzed by denaturing gel electrophoresis as described previously.[160] A 0.8% agarose gel was prepared by combining 0.24 g of low EEO agarose in 30 ml ddH_2O, and heating for 1.5 min. After heating, the volume of this solution was brought to 29.25 ml using ddH_2O. The solution was then allowed to cool to <60 °C, after which 750 μl of 2 M NaOH was added, to give a final concentration of 50 mM. This was then poured into the electrophoresis apparatus and a 10 well comb was inserted. Solidification typically took 30 minutes, with an additional 2 h allotted for complete curing. Electrophoresis buffer (50 mM NaOH) was then prepared and poured over the gel and the comb was removed.

Samples of metal-DNA reactions for denaturing gel electrophoresis were prepared as previously described.[151] Once incubation was complete, the reaction was removed from the incubator, vortexed for 15 s, and spun down in the centrifuge for 2 min (high-speed setting) to bring the solution to the bottom of the tube. Each sample was prepared by

combining 10 μl of metal-DNA sample with 5 μl of alkaline loading buffer (300mM NaOH, 18% Type 400 Ficoll, 0.15% bromocresol green, 0.25% xylene cyanol FF), and 5 μl of 50 mM NaOH. Standards were prepared by combining 10 μl of lambda DNA solution with 5 μl of alkaline loading buffer and 5 μl of 50 mM NaOH.

Samples were loaded into the gel and electrophoresis was performed at 33 V for 4 h, with buffer recirculation started after 30 min of initial electrophoresis. Once complete, gels were then stained in 0.07 μg/ml ethidium bromide solution for 12 h at 4 °C. The gels were then de-stained in 150 ml ddH_2O for 8 h.

Gel Densitometry. A typical gel densitometry experiment was performed as follows. The Alphaimager 2000™ system was turned on and a gel was placed on the transilluminator, within the light cabinet. The gel was initially illuminated using white light, and the image was optimized in regard to size and clarity. UV exposure time was then set to 6/30 sec, and illumination was then switched to UV. Controls were set to white 0, black 255 and Gamma 1, the image frozen, and the UV illumination turned off. Using the spot densitometry function, the integrated density value of each DNA band was determined. This was accomplished by outlining each DNA band with a box, and fluorescence intensity was then measured by the system. Manual background correction was used. The image was then saved on the system, and all data was printed out.

Gel R_f Values. Upon the completion of a metal-DNA interaction experiment and subsequent analysis by native gel electrophoresis, R_f values were determined by comparing the distance traveled (in mm) by the 2.1 kb band of the lambda DNA standards with the distance traveled by each metal-DNA reaction band (in mm). Measurements were performed manually, measuring from the bottom of the electrophoresis well to the bottom of the DNA band. All measurements were tabulated in Microsoft Excel, and the R_f values calculated according to the following formula:

$$R_f = \frac{D_{mc}}{D_c}$$

where R_f = gel R_f value, D_{mc} is the distance traveled by the metal-reacted DNA band in the gel (mm) , and D_c is the distance traveled by the 2.1 kb band of the lambda DNA standards in the gel (mm).

Metal-DNA Precipitation Experiments. The metal-DNA reaction was monitored by electronic absorbance spectrometry in order to determine if DNA precipitation occurred. Calf thymus DNA was used in the reactions. The metal-DNA interaction experiment was prepared as outlined previously, however only a 5:1 DNA bp: mc ratio was examined. In addition, the amounts of metal, DNA and ddH_2O were increased 10 fold. Total reaction volume was 1.0 ml. Once preparation was complete, an initial UV-vis spectrum was taken. The metal-DNA reaction was then placed in the 37°C incubator. After 4 h, another UV-vis spectrum was obtained.

Ethidium Bromide Emission Quenching. The emission quenching of ethidium bromide by the metal complexes was examined by emission spectrometry. The metal complex solutions used in this study were the same as those used for the metal-DNA interaction studies. A 5 mg/ml solution of ethidium bromide solution was prepared by adding 0.250 g of ethidium bromide to 50 ml ddH_2O, which was then stored at 4 °C in the dark. The experiment was set up as follows. Ten microliters of ethidium bromide was added to the emission cell, with the final volume brought to 3.0 ml with ddH_2O. An excitation scan was performed over the range of 190 to 800 nm. The most intense absorbance was determined to be 347 nm. The emission cell was emptied, and a control experiment, consisting of only ethidium bromide, was performed. 10 μl of ethidium bromide solution was added to the emission cell and the final volume brought to 3.0 ml with ddH_2O. An emission spectrum was then obtained with the excitation wavelength set at 347 nm and the scan range 500 to 700 nm. The emission intensity at 600 nm was noted. Next, the emission cell was again emptied and 10 μl of ethidium bromide solution was added. Sufficient metal complex solution was added, to give a metal complex: ethidium bromide ratio of 100: 1. The final volume was then brought to 3.0 ml with ddH_2O and an

emission spectrum was obtained. This procedure was then repeated for metal complex: ethidium bromide ratios of 20, 10, 5 and 1: 1.

Theoretical Migratory Modeling Studies. The effects of metal binding on DNA migration through agarose electrophoresis gels was examined for the interaction of the Ru-Pt complexes with linearized-plasmid DNA. The effect on molecular weight was examined utilizing the relationship that DNA migration rate is inversely proportional to the log of molecular weight.[24, 26] These experiments were performed as follows. Gel photographs were examined and the distance traveled by the 4.4, 2.3, and 2.0 kb bands of the lambda molecular weight standards were measured (in mm). The molecular weight of each DNA band was determined using the relation that 1 mol of base pairs weighs 660 g/mol.[64] All values were entered into a Microsoft Excel worksheet, and a plot of log molecular weight vs. distance migrated was generated. A least squares regression was then performed and an equation generated. The change in molecular weight for each metal-DNA reaction sample was then computed, assuming 100% binding of the metal complex. This value was then entered into the equation generated by the plot of log molecular weight vs. distance migrated for the lambda molecular weight standards, resulting in a theoretical migration distance.

Chapter 3: Results and Discussion

Synthesis: Ru-Pt complexes containing the bridging bidentate ligands dpq and dpb

The synthesis of these ruthenium-platinum bimetallic systems bridged by the ligands dpq and dpb follows a building block approach, in which the complexes are assembled step by step by alternately adding a ligand followed by a metal center. The utility of this technique is that the nature of each component is known, and sequential reaction of these components imparts the desired molecular architecture on the final complex in high purity. An example of this approach is given in Figure 3.1 for the synthesis of $[(bpy)_2Ru(dpq)PtCl_2](CF_3SO_3)_2$.

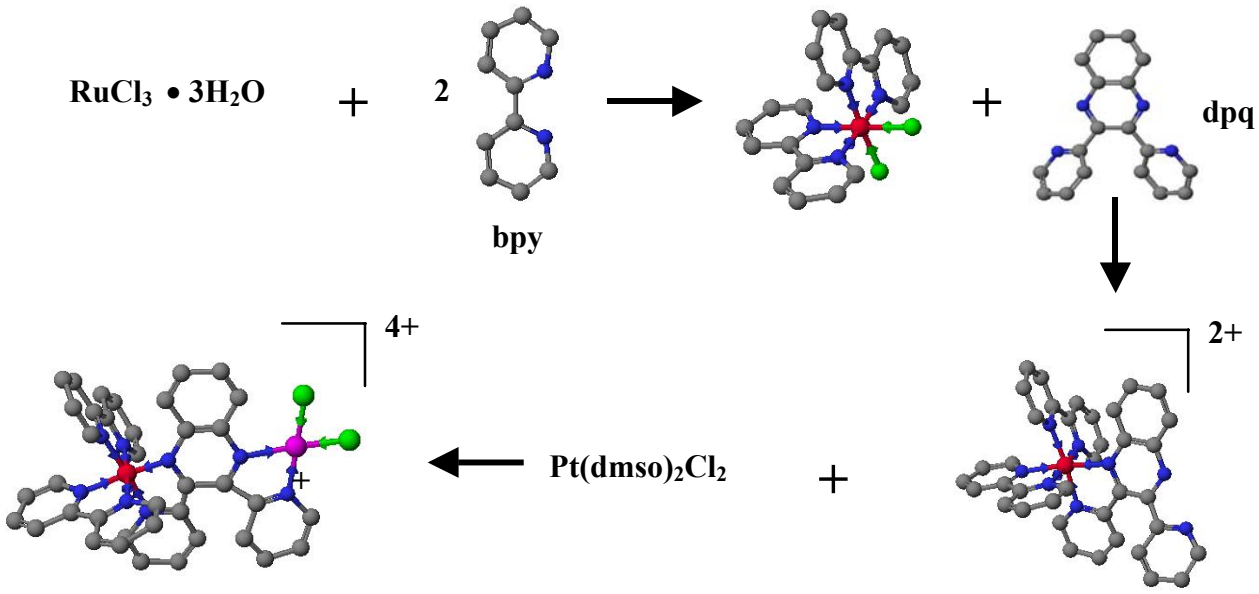

Figure 3.1 Synthetic Scheme for $[(bpy)_2Ru(dpq)PtCl_2](CF_3SO_3)_2$ (where bpy = 2,2′-bipyridine, dpq = 2,3-bis(2-pyridyl)quinoxaline. Red = Ru(II), Green = Cl, Blue = N, Purple = Pt(II). H omitted for clarity.

A desired feature of these ruthenium-platinum complexes is that they provide enhanced water solubility in comparison to the antitumor agent cisplatin. The inclusion of the ruthenium(II) center provides this feature. The selection of a suitable counterion proved to be the critical factor. Early synthetic studies primarily focused on producing the ruthenium-platinum bimetallics as they are a new structural motif. Here the PF_6^- salts were prepared, but these complexes proved to be water-insoluble.

Drawing upon the well-established water-solubility of chloride salts of polyazine Ru complexes, early research focused on the use of Cl^- as counterion. In this area, two approaches were tested, in which the PF_6^- salt was either converted to the chloride salt, or the chloride salt was produced directly from reaction. Conversion to the Cl^- was attempted by metathesis using Bu_4NCl and ion-exchange chromatography.

A review of the literature indicated that trifluoromethanesulfonate (triflate, $CF_3SO_3^-$) could provide water solubility. Initial attempts at producing the triflate salt of the Ru-Pt bimetallics by metathesis of the PF_6^- salts proved unsuccessful. A scheme was devised to produce the triflate salt directly. The chlorides on $[(bpy)_2RuCl_2]$ were removed by reaction with $AgCF_3SO_3$. Next, $[(bpy)_2Ru(CF_3SO_3)_2]$, was reacted with bridging ligand to yield $[(bpy)_2Ru(BL)](CF_3SO_3)_2$. This is reacted with $Pt(dmso)_2Cl_2$ to give the desired bimetallic complex. This product was pure and water-soluble.

Electrochemistry.

The redox properties of these new complexes were studied by cyclic voltammetry. A summary of all electrochemical data for $[(bpy)_2Ru(dpq)PtCl_2](CF_3SO_3)_2$, $[(bpy)_2Ru(dpq)PtCl_2](CF_3SO_3)_2$, $[(phen)_2Ru(dpb)PtCl_2](CF_3SO_3)_2$ and $[(phen)_2Ru(dpq)PtCl_2](CF_3SO_3)_2$ is shown in Table 3.1. Each complex exhibits one reversible oxidation and four reductions within the window +2.0 V to –2.0 V vs Ag/AgCl. Additionally, these systems display an irreversible oxidation that appears as a shoulder, just before the reversible oxidative process.

Table 3.1 Electrochemical data for a series of ruthenium and ruthenium-platinum complexes incorporating the bidentate bridging ligands dpq and dpb. Bpy = 2,2′-bipyridine, phen = 1,10-phenanthroline, dpq = 2,3-bis(2-pyridyl)quinoxaline, dpb = 2,3-bis(2-pyridyl)benzoquinoxaline. Potentials reported in CH_3CN solution with 0.1 M TBAH and reported versus Ag/AgCl (0.29V vs. NHE).

Complex	Oxidations	Reductions	Reference
$[(bpy)_2Ru(dpq)](CF_3SO_3)_2$	+1.50 $Ru^{II/III}$	-0.75 $dpq^{0/-}$	b
		-1.39 $bpy^{0/-}$	
		-1.60 $bpy^{0/-}$	
$[(bpy)_2Ru(dpb)](CF_3SO_3)_2$	+1.49 $Ru^{II/III}$	-0.60 $dpb^{0/-}$	b
		-1.25 $bpy^{0/-}$	
		-1.58 $bpy^{0/-}$	
$[(phen)_2Ru(dpq)](CF_3SO_3)_2$	+1.50 $Ru^{II/III}$	-0.73 $dpq^{0/-}$	c
		-1.39 $phen^{0/-}$	
		-1.59 $phen^{0/-}$	
$[(phen)_2Ru(dpb)](CF_3SO_3)_2$	+1.51 $Ru^{II/III}$	-0.58 $dpb^{0/-}$	d
		-1.25 $phen^{0/-}$	
		-1.57 $phen^{0/-}$	
$[(bpy)_2Ru(dpq)PtCl_2](CF_3SO_3)_2$	+1.67 $Ru^{II/III}$ [a]	-0.20 $dpq^{0/-}$	d
		-0.82 $dpq^{-/2-}$	
$[(bpy)_2Ru(dpb)PtCl_2](CF_3SO_3)_2$	+1.65 $Ru^{II/III}$ [a]	-0.10 $dpb^{0/-}$	e
		-0.74 $dpb^{-/2-}$	
$[(phen)_2Ru(dpq)PtCl_2](CF_3SO_3)_2$	+1.67 $Ru^{II/III}$ [a]	-0.20 $dpq^{0/-}$	d
		-0.95 $dpq^{-/2-}$	
$[(phen)_2Ru(dpb)PtCl_2](CF_3SO_3)_2$	+1.65 $Ru^{II/III}$ [a]	-0.10 $dpb^{0/-}$	d
		-0.77 $dpb^{-/2-}$	

[a] An overlapping, irreversible $Pt^{II/IV}$ is also present just prior to the $Ru^{II/III}$ couple.
[b] The electrochemical properties of this system have been reported in reference 100, but the numbers used here are measured under our conditions.
[c] The electrochemical properties of this system have been reported in reference 181, but the numbers used here are measured under our conditions.
[d] Not previously reported.
[e] Our electrochemical properties of this system were reported in reference 161.

Electrochemical reversibility as used herein represents $i_p^a/i_p^c \cong 1$ (where i_p^a = anodic current and i_p^c = cathodic current).

To serve as a means of comparison, electrochemical data for the ruthenium monometallic synthons, measured under our conditions are also shown in Table 3.1. The electrochemical behavior of complexes of the type $[(bpy)_2Ru(BL)](PF_6)_2$ have been previously studied (where BL= dpq and dpb). [93-101] These systems possess $Ru^{II/III}$ oxidations at 1.47 and 1.48 V vs. Ag/AgCl for BL = dpq and dpb, respectively. They also possess three reductions corresponding to sequential one-electron reductions of the polypyridyl ligands. The first reduction corresponds to the $BL^{0/-}$ couple, with the dpb system undergoing reduction at less negative potentials than the dpq systems ($E_{1/2}^{red}$ = -0.72 (dpq) and –0.62 (dpb) V). The occurrence of the $dpb^{o/-}$ couple at less negative potentials than the $dpq^{0/-1}$ couple is primarily due to the more conjugated π system of the dpb ligand. The bridging ligand reductions are followed by sequential, one-electron reductions of each of the two bpy ligands, with $E_{1/2}^{red}$ = -1.40 and -1.62 for the $[(bpy)_2Ru(dpq)]^{2+}$ system and $E_{1/2}^{red}$ = -1.26 and -1.60 for $[(bpy)_2Ru(dpb)]^{2+}$system. The shift of the bpy-based reductions to less negative potentials for the dpb systems is most likely due to the indirect effect of the increase in positive charge on the metal center, caused by the weaker σ - donor and stronger π-acceptor nature of dpb versus dpq. A short electrochemical mechanism illustrating the redox behavior of these complexes is shown in Figure 3.2.

The triflate salts of these same monometallic synthons, $[(bpy)_2Ru(dpq)](CF_3SO_3)_2$ and $[(bpy)_2Ru(dpb)](CF_3SO_3)_2$ possess nearly identical electrochemical behavior. Metal based oxidations occur at +1.50V and +1.49V for the dpq and dpb systems, with ligand based reductions at -0.75, -1.39, -1.60V (dpq) and -0.60, -1.25, and -1.58 V (dpb). For the complexes containing the terminal bidentate ligand 1,10-phenanthroline, metal based oxidations occur at +1.50V and +1.51V, with ligand based reductions at -0.73, -1.39, -1.59 V(dpq) and -0.58, -1.25, -1.57 V(dpb).

The ruthenium-platinum bimetallics each exhibit two oxidations and four

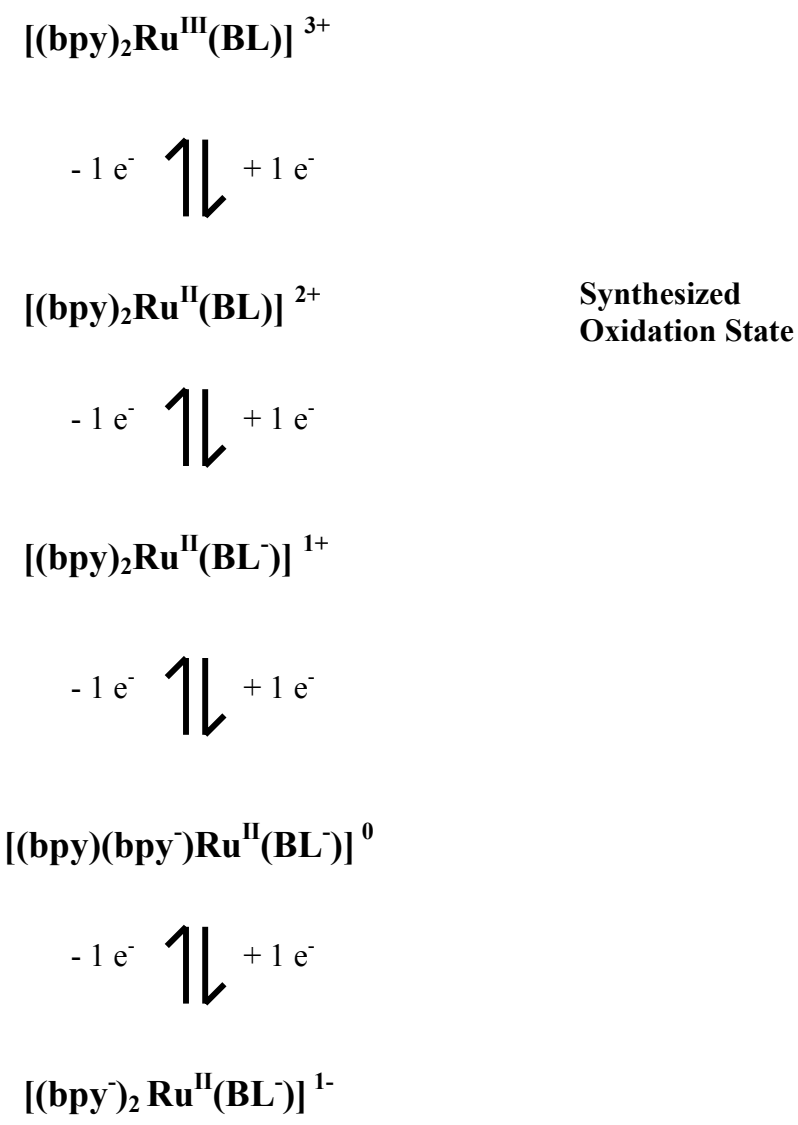

Figure 3.2 Electrochemical mechanism for complexes of the type $[(bpy)_2Ru(BL)]^{2+}$, where bpy = 2,2′-bipyridine, BL = dpq or dpb.

reductions within the solvent window. Cyclic voltammograms for $[(bpy)_2Ru(dpq)PtCl_2](CF_3SO_3)_2$, $[(bpy)_2Ru(dpb)PtCl_2](CF_3SO_3)_2$, $[(phen)_2Ru(dpq)PtCl_2](CF_3SO_3)_2$, and$[(phen)_2Ru(dpb)PtCl_2](CF_3SO_3)_2$ are shown in Figures 3.3 – 3.6. The reversible oxidation is assigned as a metal based $Ru^{II/III}$ couple. In addition to the one reversible oxidation these systems display an irreversible oxidation that appears as a shoulder, immediately prior to the reversible oxidation process. Our data suggests that this process is a platinum-based $Pt^{II/IV}$ couple. Electrochemical studies on $[(bpy)_2Os(dpb)PtCl_2](PF_6)_2$ have also revealed a similar irreversible process, ruling out the possibility of a ruthenium or osmium based process.[161] Substitution of the bpy ligand with phen or BL variation also does not impact this process. This clearly establishes this couple as Pt based. In a recent study, Yam and co-workers reported the electrochemical properties of $[(bpy)_2Ru(dpp)PtCl_2]^{2+}$.[162] In acetonitrile, they observed a $Ru^{II/III}$ couple at 1.56 V, and a dpp/dpp^- couple at –0.54 V vs SCE. They also reported an irreversible oxidation at 1.47 vs. SCE but presented no assignment for this process. The data presented here indicates that this irreversible wave in their system also represents a platinum-based process as well.

The Ru-Pt bimetallics exhibit a $BL^{0/-}$ reduction at substantially less negative potentials than their monometallic precursors, $[(bpy)_2Ru(BL)]^{2+}$ and $[(phen)_2Ru(BL)]^{2+}$. An electrochemical mechanism illustrating the redox behavior of these complexes is shown in Figure 3.7. In addition, these systems possess a second reversible reduction at relatively positive potential, assigned as the $BL^{-/2-}$ couple. The presence of two one-electron reductions at low potentials is indicative of bimetallic complex formation when the dpq or dpb ligand is bridging.[112, 114-124, 133, 134, 163-167] Following these two one-electron reductions, two more reductions occur but are not well behaved. This is most likely due to the formation of a neutral complex by the two previous BL-based one-electron reductions, $[(bpy)_2Ru(BL^{2-})PtCl_2]$, which can adsorb onto the electrode surface. Absorption and desorption spikes often are seen in CVs recorded past the second reduction. These two additional reductions represent sequential reduction of the terminal bidentate ligands (2,2′-bipyridine or 1,10-phenanthroline), but resolution of these waves is very difficult.

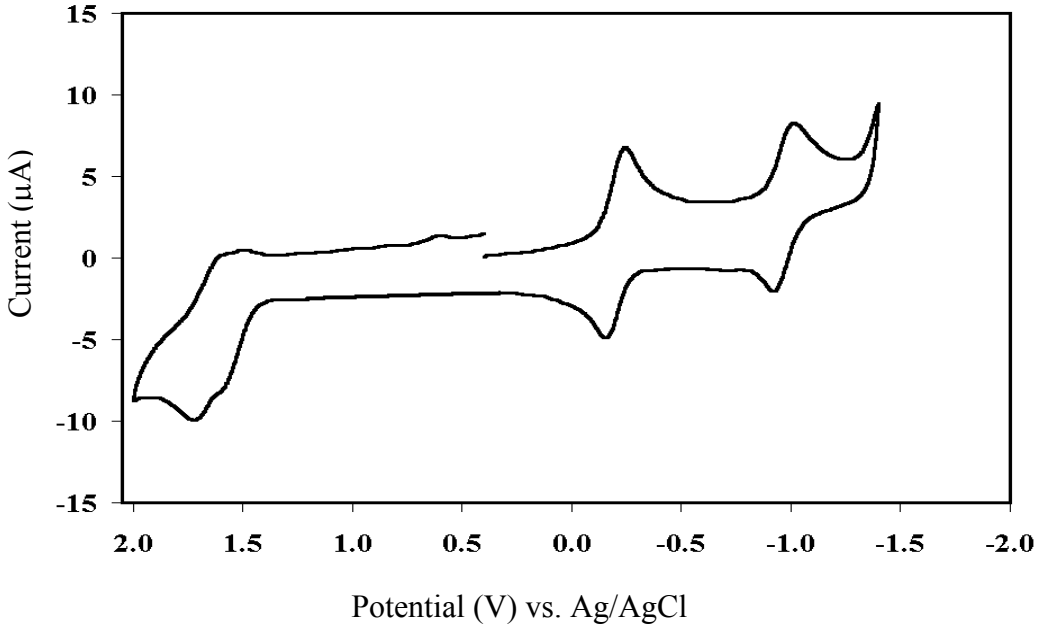

Figure 3.3 Cyclic Voltammogram of $[(bpy)_2Ru(dpq)PtCl_2](CF_3SO_3)_2$ (where bpy = 2,2′-bipyridine, dpq = 2,3-bis(2-pyridyl)quinoxaline) in CH_3CN, 0.1 M TBAH supporting electrolyte.

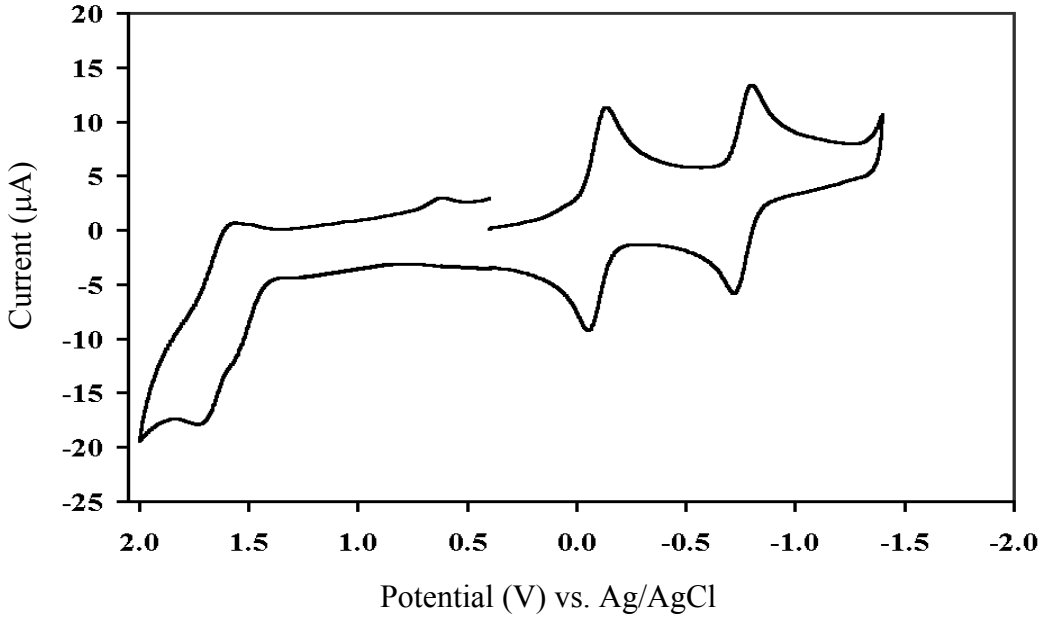

Figure 3.4 Cyclic Voltammogram of $[(bpy)_2Ru(dpb)PtCl_2](CF_3SO_3)_2$ (where bpy = 2,2′-bipyridine, dpb = 2,3-bis(2-pyridyl)benzoquinoxaline) in CH_3CN, 0.1 M TBAH supporting electrolyte.

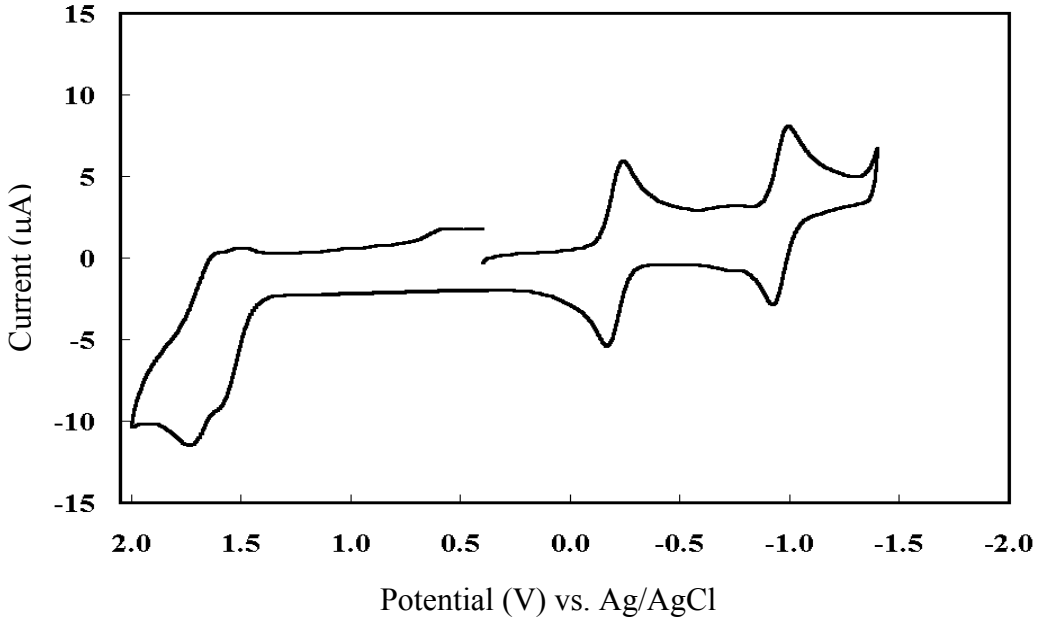

Figure 3.5 Cyclic Voltammogram of $[(phen)_2Ru(dpq)PtCl_2](CF_3SO_3)_2$ (where phen = 1,10-phenanthroline, dpq = 2,3-bis(2-pyridyl)quinoxaline) in CH_3CN, 0.1 M TBAH supporting electrolyte.

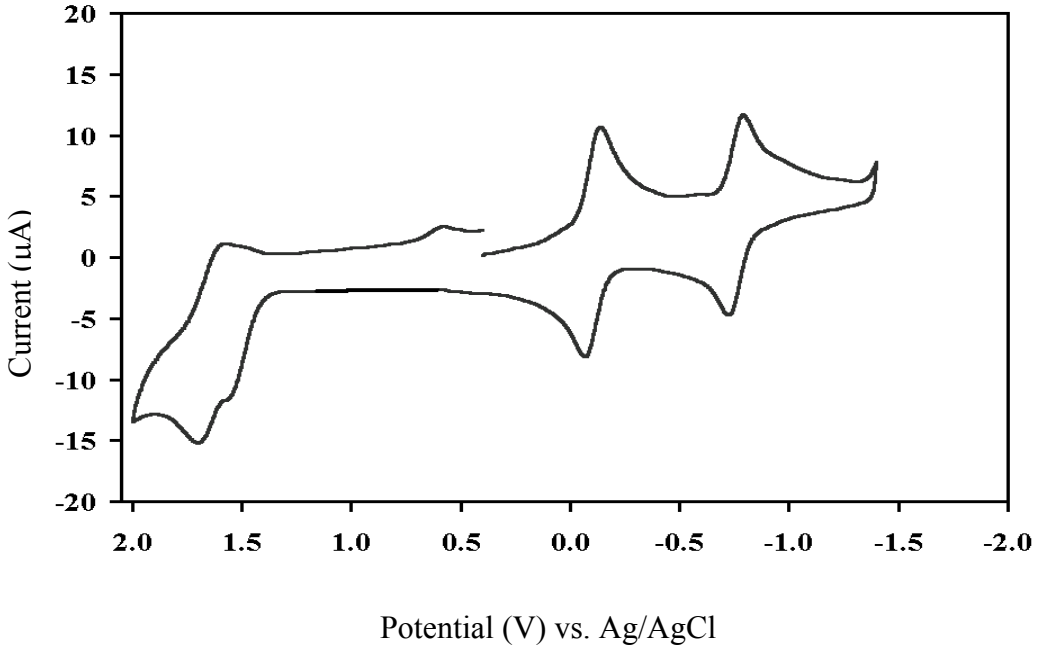

Figure 3.6 Cyclic Voltammogram of $[(phen)_2Ru(dpb)PtCl_2](CF_3SO_3)_2$ (where phen = 1,10-phenanthroline, dpb = 2,3-bis(2-pyridyl)benzoquinoxaline) in CH_3CN, 0.1 M TBAH supporting electrolyte.

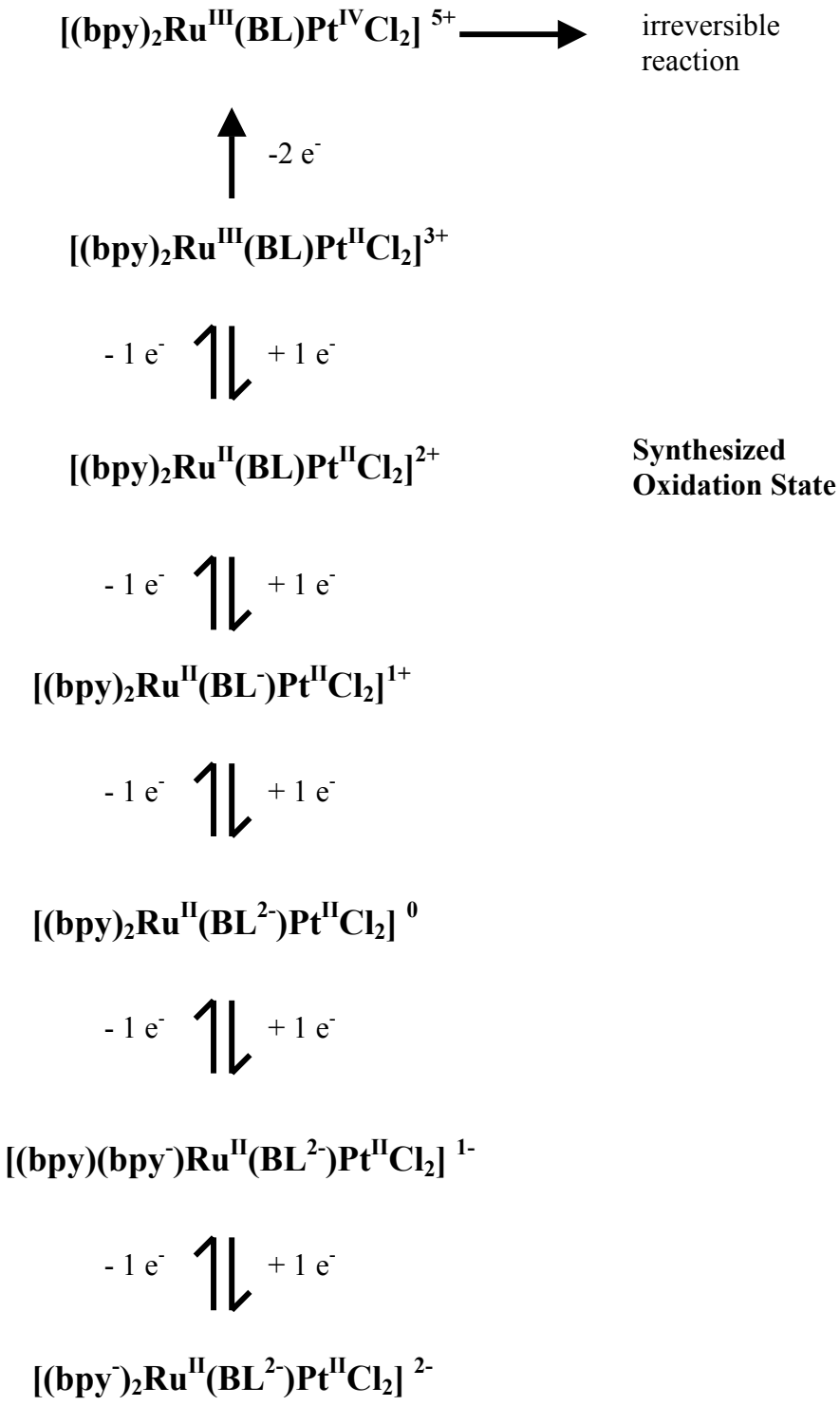

Figure 3.7 Electrochemical mechanism for complexes of the type $[(bpy)_2Ru(BL)PtCl_2](CF_3SO_3)_2$, where bpy = 2,2′-bipyridine, BL = dpq, dpb (where dpq = 2,3-bis(2-pyridyl)quinoxaline and dpb = 2,3-bis(2-pyridyl)benzoquinoxaline).

A representative cyclic voltammogram illustrating these remaining, sequential reductions of the terminal bridging ligands is shown in Appendix A-1.

Electronic Absorption Spectroscopy.

Electronic absorption spectroscopy was used to characterize the light absorbing properties of the four ruthenium-platinum bimetallic complexes. The electronic absorption spectra for the monometallic complexes $[(bpy)_2Ru(BL)](CF_3SO_3)_2$ are shown in Figure 3.8, and for the phen-derivatives $[(phen)_2Ru(BL)](CF_3SO_3)_2$ in Figure 3.9 (BL = dpq and dpb). The spectra for the $[(bpy)_2Ru(BL)PtCl_2](CF_3SO_3)_2$ bimetallic complexes are shown in Figure 3.10, and for $[(phen)_2Ru(BL)PtCl_2](CF_3SO_3)_2$ in Figure 3.11 (BL = dpq and dpb). Spectra of the bpy-based bimetallics overlaid with the phen-based bimetallics are included in Appendix A-2 and A-3.

The electronic absorption spectra of $[(bpy)_2Ru(BL)]^{2+}$ complexes have been extensively studied.[91-100] These complexes exhibit intense bands in the UV attributed to bpy- and BL based $\pi \rightarrow \pi^*$ and $n \rightarrow \pi^*$ transitions. In the visible region, MLCT transitions to each ligand are present, with Ru$\rightarrow$ bpy CT transitions occurring at 434 and 414 nm for the dpq and dpb systems, respectively. Also, Ru $\rightarrow$ BL-based MLCT transitions occur at 517 and 550 nm for dpq and dpb, respectively.[93, 94, 100] For the $[(phen)_2Ru(BL)]^{2+}$ complexes, intense bands in the UV attributed to phen-and BL-based $\pi \rightarrow \pi^*$ and $n \rightarrow \pi^*$ transitions. In addition, the $[(phen)_2Ru(BL)]^{2+}$ complexes also display MLCT transitions in the visible region, with the Ru$\rightarrow$ phen-based transitions occurring at 425 and 406 nm for dpq and dpb, respectively. Ru$\rightarrow$ BL MLCT transitions occur at 530 nm for the dpq system, and at 552 nm for the dpb system. The shift of M $\rightarrow$ dpb CT to lower energy compared to the analogous M $\rightarrow$ dpq CT within each series results from the lower energy π^*-acceptor orbitals on dpb relative to dpq.[161]

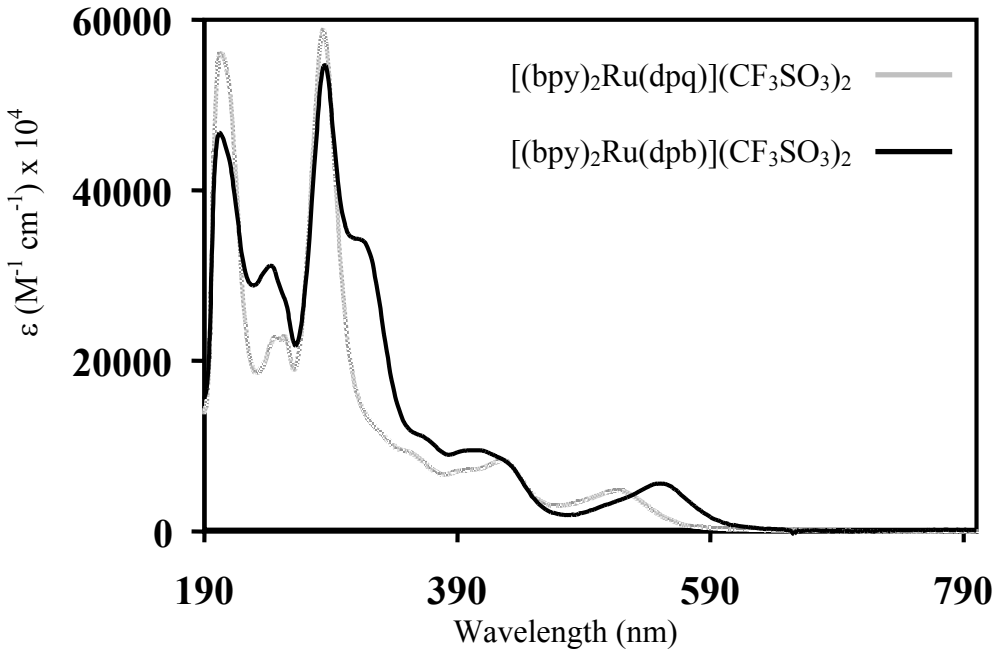

Figure 3.8 Electronic absorption spectrum for $[(bpy)_2Ru(dpq)](CF_3SO_3)_2$ and $[(bpy)_2Ru(dpb)](CF_3SO_3)_2$ (where bpy = 2,2′-bipyridine, dpq = 2,3-bis(2-pyridyl)quinoxaline, dpb = 2,3-bis(2-pyridyl)benzoquinoxaline) in ddH_2O.

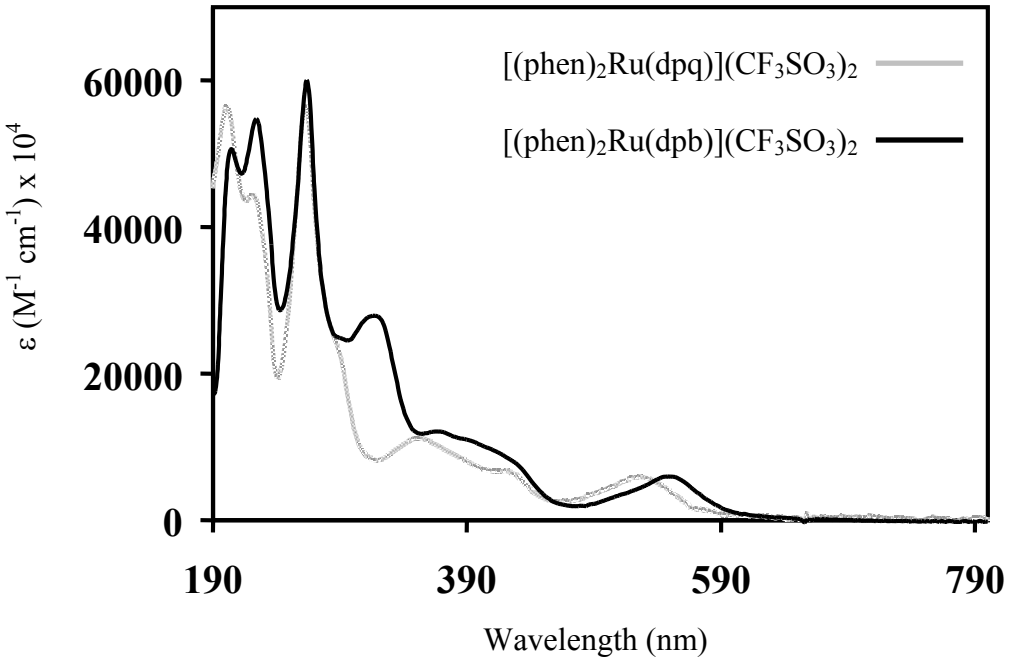

Figure 3.9 Electronic absorption spectrum of $[(phen)_2Ru(dpq)](CF_3SO_3)_2$ and $[(phen)_2Ru(dpb)](CF_3SO_3)_2$ (where phen = 1,10-phenanthroline, dpq = 2,3-bis(2-pyridyl)quinoxaline, dpb = 2,3-bis(2-pyridyl)benzoquinoxaline) in ddH_2O.

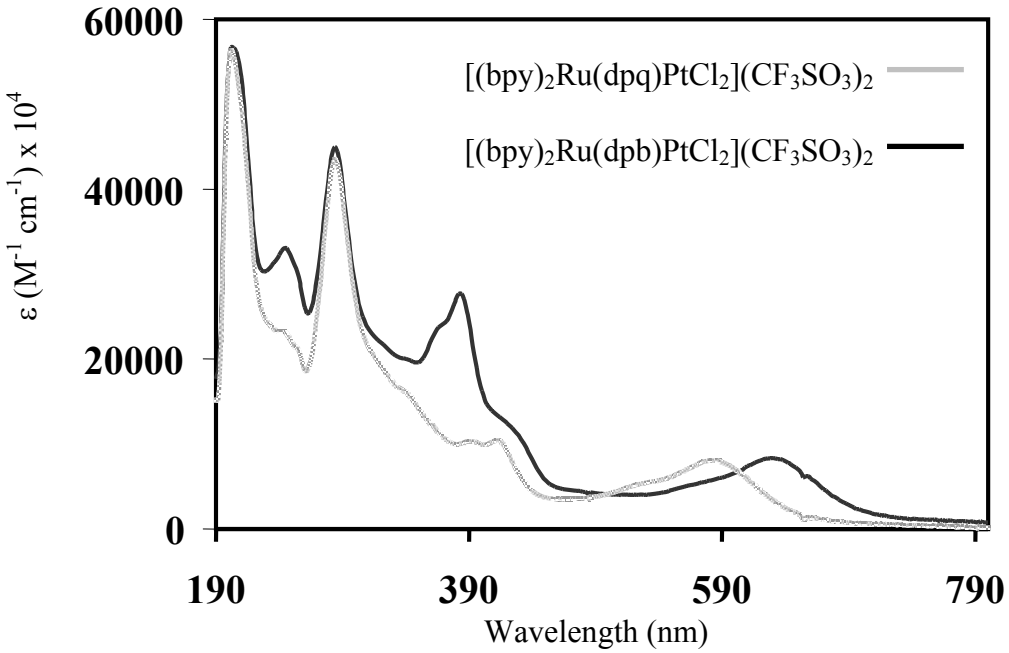

Figure 3.10 Electronic absorption spectrum of $[(bpy)_2Ru(dpq)PtCl_2](CF_3SO_3)_2$ and $[(bpy)_2Ru(dpb)PtCl_2](CF_3SO_3)_2$ (where bpy = 2,2′-bipyridine, dpq = 2,3-bis(2-pyridyl)quinoxaline, dpb = 2,3-bis(2-pyridyl)benzoquinoxaline in ddH_2O.

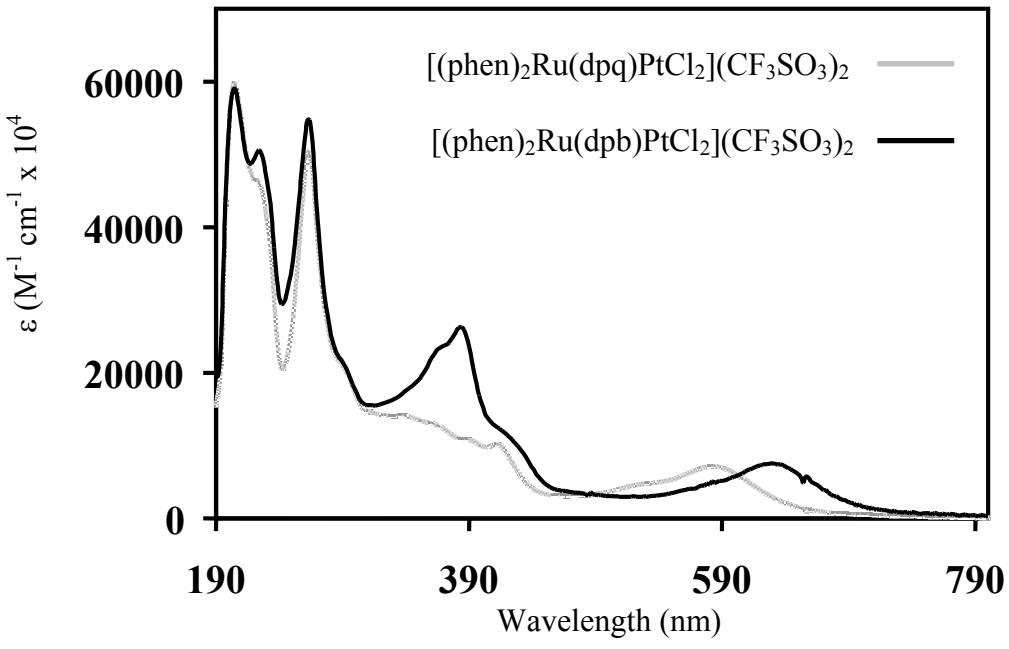

Figure 3.11 Electronic absorption spectrum of $[(phen)_2Ru(dpq)PtCl_2](CF_3SO_3)_2$ and $[(phen)_2Ru(dpb)PtCl_2](CF_3SO_3)_2$ (where phen = 1,10-phenanthroline, dpq = 2,3-bis(2-pyridyl)quinoxaline, dpb = 2,3-bis(2-pyridyl)benzoquinoxaline) in ddH_2O.

For the $[(bpy)_2Ru(BL)PtCl_2]^{2+}$ systems, Ru → BL CT bands occur at 588 nm (dpq) and 638 nm (dpb). This represents a 71 nm (dpq system) and 88 nm (dpb system) shift versus the respective $[(bpy)_2Ru(BL)]^{2+}$ monometallics. For the $[(phen)_2Ru(BL)PtCl_2]^{2+}$ systems, Ru → BL CT bands occur at 588 nm (dpq) and 638 nm (dpb). This represents a 58 (dpq system) and 86 (dpb system) nm shift versus the respective $[(phen)_2Ru(BL)]^{2+}$ monometallics. For the $[(bpy)_2Ru(BL)]^{2+}$and $[(phen)_2Ru(BL)]^{2+}$ systems, bimetallic formation results in the lowering in energy of the M → BL CT band. [91-101, 131-135, 163-166] Yam and co-workers have reported that $[(bpy)_2Ru(dpp)PtCl_2]^{2+}$ possesses a Ru → dpp CT band at 509 nm. This Ru → dpp CT is red-shifted relative to that of $[(bpy)_2Ru(dpp)]^{2+}$, which is at 468 nm.[91, 92, 162] In the homobimetallic system $[(bpy)_2Ru(dpp)Ru(bpy)_2]^{4+}$, the Ru → dpp CT occurs at 526 nm.[91, 92] This suggests that the $Pt^{II}Cl_2$ coordination to the remote nitrogens on the dpp ligand is less stabilizing than the coordination of another $Ru^{II}(bpy)_2$ moiety. This is also true for dpq and dpb as the homobimetallic systems $[(bpy)_2Ru]_2(dpq)]^{4+}$ and $[(bpy)_2Ru]_2(dpb)]^{4+}$ have Ru → BL CT bands at 603 and 644 nm, respectively.[100]

These systems also exhibit transitions in the 410-420 nm region, assigned as M → bpy CT transitions.[91-101] The transitions in the UV are typical of $\pi \rightarrow \pi^*$ and $n \rightarrow \pi^*$ transitions in mixed-ligand polyazine systems, with some differences due to the identity of the terminal ligand. For the bpy-based systems, bands at ca. 290 nm are attributed to bpy, with BL-based transitions at 340-350 nm for the dpq systems and at 380-390 for the dpb systems. For the phen-based systems, similar transitions in the UV are observed, but with the phen-based transition at ca. 264 nm. The phen complexes display transitions at 340-350 nm and 380-390 nm for the dpq and dpb systems, which are very nearly equivalent to the bpy-based systems indicating they are likely BL $\pi \rightarrow \pi^*$ in nature. A summary of electronic absorption spectroscopy data for all four Ru-Pt bimetallics is shown in Table 3.2.

It has been previously shown that a correlation can be drawn between the electrochemical energy gap and the spectroscopic energy gap within a series of related

Table 3.2 Electronic absorption spectroscopy for a series of Ru^{II}, Pt^{II} complexes measured in CH_3CN at RT. bpy = 2,2′-bipyridine, phen = 1,10-phenanthroline, dpq = 2,3-bis(2-pyridyl)quinoxaline, dpb = 2,3-bis(2-pyridyl)benzoquinoxaline.

Complex	λ_{max}^{abs} (nm)	Assignment
$[(bpy)_2Ru(dpq)PtCl_2](CF_3SO_3)_2$	204	bpy n$\rightarrow \pi^*$, $\pi \rightarrow \pi^*$
	254	
	286	bpy $\pi \rightarrow \pi^*$
	352	dpq $\pi \rightarrow \pi^*$
	422	Ru $\rightarrow$ bpy CT
	590	Ru $\rightarrow$ dpq CT
$[(bpy)_2Ru(dpb)PtCl_2](CF_3SO_3)_2$	206	bpy n$\rightarrow \pi^*$, $\pi \rightarrow \pi^*$
	250	
	286	bpy $\pi \rightarrow \pi^*$
	386	dpb $\pi \rightarrow \pi^*$
	432	Ru $\rightarrow$ bpy CT
	638	Ru $\rightarrow$ dpb CT
$[(phen)_2Ru(dpq)PtCl_2](CF_3SO_3)_2$	206	phen n$\rightarrow \pi^*$, $\pi \rightarrow \pi^*$
	226	
	264	phen $\pi \rightarrow \pi^*$
	348	dpq $\pi \rightarrow \pi^*$
	422	Ru $\rightarrow$ phen CT
	590	Ru $\rightarrow$ dpq CT
$[(phen)_2Ru(dpb)PtCl_2](CF_3SO_3)_2$	206	phen n$\rightarrow \pi^*$, $\pi \rightarrow \pi^*$
	228	
	264	phen $\pi \rightarrow \pi^*$
	386	dpb $\pi \rightarrow \pi^*$
	432	Ru $\rightarrow$ phen CT
	638	Ru $\rightarrow$ dpb CT

metal complexes.[91, 134, 167-174] If the electrochemical processes (metal-based oxidation and bridging ligand based reduction) involve the same orbitals as the spectroscopic transition (Ru $\rightarrow$ BL MLCT), the plot of these two measures of the energy difference should show a correlation. A plot of ΔE ½ versus E_{abs} (MLCT) for the $[(bpy)_2Ru(BL)]^{2+}$, $[(phen)_2Ru(BL)]^{2+}$, $[(bpy)_2Ru(BL)PtCl_2]^{2+}$ and $[(phen)_2Ru(BL)PtCl_2]^{2+}$systems is shown in Figure 3.12. The data used to construct this correlation is shown in Appendix A-4. As shown in this figure, the data gives good correlation (correlation coefficient of 0.97). This

is further evidence of the equivalence of the orbitals involved with the redox processes and the Ru → BL MLCT transition.

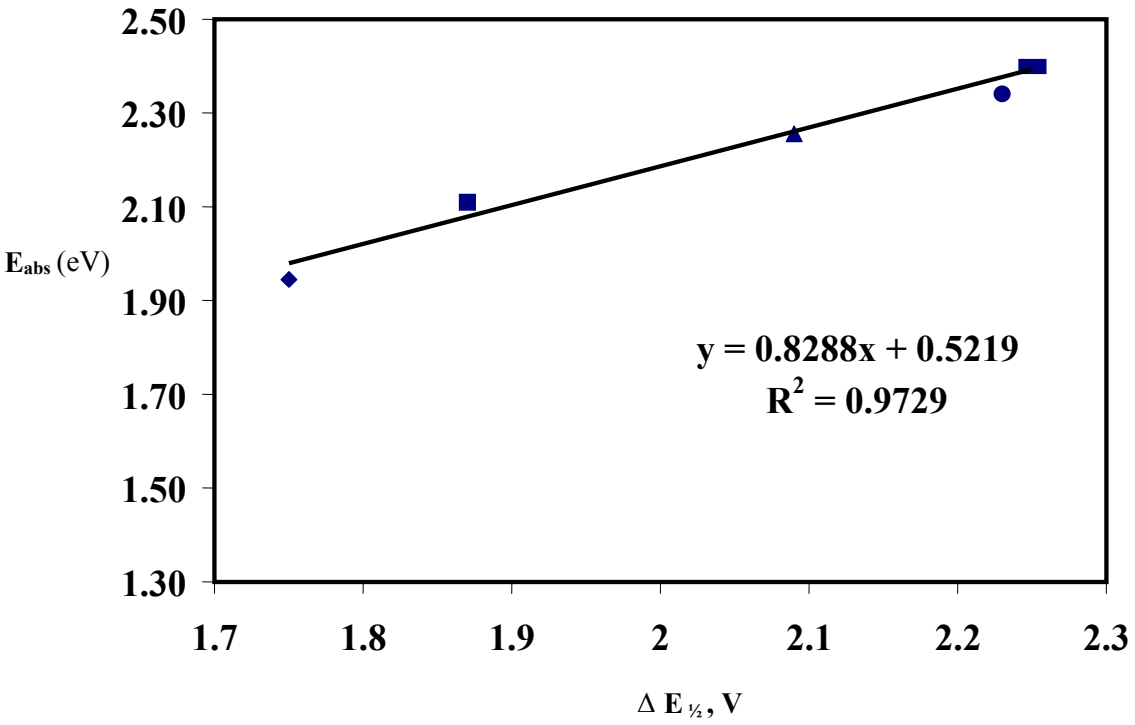

Figure 3.12 Plot of energies of the lowest energy absorption band (eV) vs. $E_{1/2}$ (V) of $[(bpy)_2Ru(dpq)]^{2+}$(■), $[(bpy)_2Ru(dpb)]^{2+}$ (▲) , $[(phen)_2Ru(dpq)]^{2+}$ (●), $[(phen)_2Ru(dpb)]^{2+}$ (▲), $[(bpy)_2Ru(dpq)PtCl_2]^{2+}$ (■), $[(bpy)_2Ru(dpb)PtCl_2]^{2+}$ (◆), $[(phen)_2Ru(dpq)PtCl_2]^{2+}$ (■), $[(phen)_2Ru(dpb)PtCl_2]^{2+}$ (◆), where bpy = 2,2′-bipyridine, phen = 1,10-phenanthroline, dpq = 2,3-bis(2-pyridyl)quinoxaline, dpb = 2,3-bis(2-pyridyl)benzoquinoxaline. In general, between the bpy- and phen- series, points overlap due to the lowest energy absorbance being Ru → BL CT in nature.

The Interaction of Ru-Pt Bimetallic Complexes with DNA

Native Gel Studies: Concentration-Dependent Interaction with DNA

In order to determine whether the Ru-Pt bimetallic complexes $[(bpy)_2Ru(dpq)PtCl_2](CF_3SO_3)_2$, $[(bpy)_2Ru(dpb)PtCl_2](CF_3SO_3)_2$, $[(phen)_2Ru(dpq)PtCl_2](CF_3SO_3)_2$, and $[(phen)_2Ru(dpb)PtCl_2](CF_3SO_3)_2$ exhibit DNA binding activity, reactions were performed with linearized plasmid DNA over a range of DNA base pair (bp) to metal complex (mc) ratios. To provide a basis for comparison, two positive controls were included with these studies, the known DNA binders *cis*-$[Pt(NH_3)_2Cl_2]$ (cisplatin) and *trans*-$\{[PtCl(NH_3)_2]_2(\mu\text{-}H_2N(CH_2)_6NH_2)\}^{2+}$(1,1/t,t). Cisplatin is known to form primarily intrastrand DNA cross-links, and (1,1/t,t) is known to form primarily inter-strand crosslinks. Both complexes, however, form covalent bonds to DNA via the Pt center.

The concentration-dependent DNA binding studies for the positive controls and Ru-Pt bimetallic complexes were analyzed by native gel electrophoresis. The reasons for using this technique were threefold. First, native gel electrophoresis may provide a means to detect interactions of these complexes with DNA. As stated previously, these Ru-Pt bimetallic complexes are designed to be DNA binding agents. Binding to the DNA helix may alter the migration of the DNA through the gel. Secondly, this method may provide insight into the mode of binding of these complexes. Since these complexes have many possible forms of DNA binding, native gel electrophoresis may provide some insight into whether the DNA interaction is primarily covalent. Thirdly, this method may serve to probe the individual binding properties and differences of the Ru-Pt complexes. Differential binding of a complex may lead to different DNA migration characteristics.

The results of the concentration-dependent DNA binding study for cisplatin and 1,1/t,t are shown in Figure 3.13. Linearized plasmid DNA was incubated with the Ru-Pt at ratios ranging from 5:1 to 300: 1 for 4 h at 37°C. Although cisplatin forms

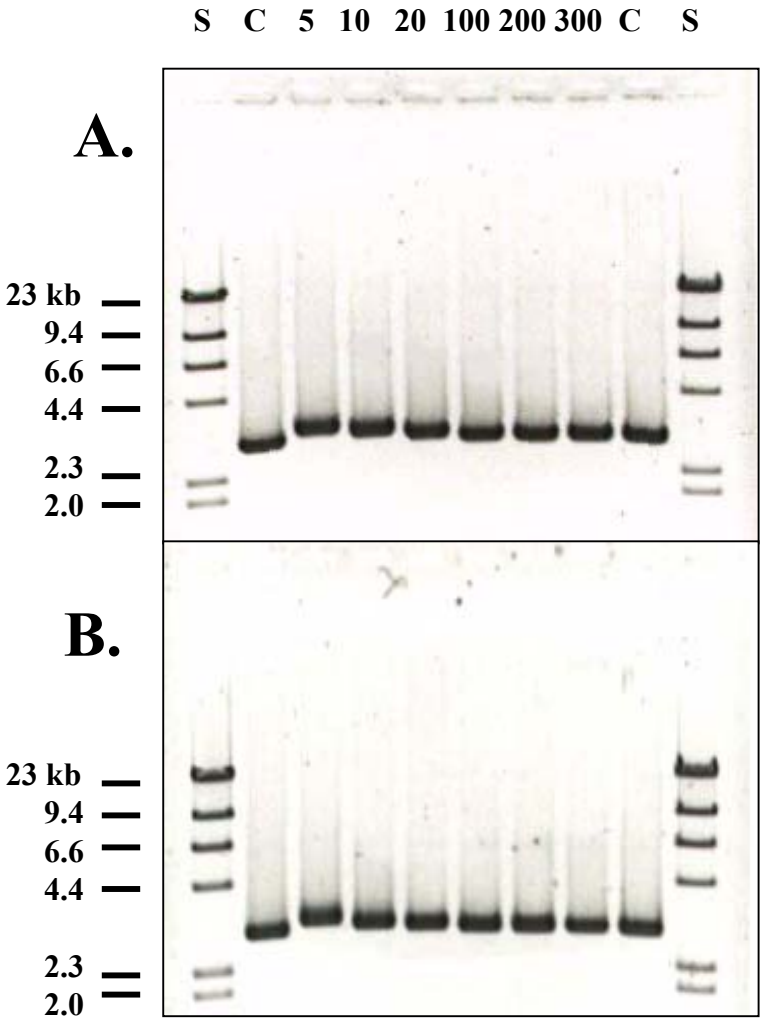

Figure 3.13 Native agarose gel electrophoresis of interaction of *cis*-$[Pt(NH_3)_2Cl_2]$ (cisplatin) **(A)** and *trans*-$\{[PtCl(NH_3)_2]_2(\mu\text{-}H_2N(CH_2)_6NH_2)\}(NO_3)_2$ (1,1/t,t) **(B)** with linearized plasmid DNA. One μg of linearized plasmid DNA was incubated with metal complex at a ratio of 5, 10, 20, 100, 200 or 300 base pairs to 1 metal complex at 37 °C for 4 h . A control sample (C) containing only plasmid DNA was incubated under identical conditions. Samples containing 100 ng of DNA were analyzed on a 0.8% native agarose gels, which were then stained with 0.5 mg/ml ethidium bromide for 1 h and photographed under UV illumination. A molecular weight standard (S) was included for reference.

predominantly intrastrand crosslinks and 1,1/t,t forms predominantly interstrand crosslinks,[18, 19, 23, 29,.30] both complexes affected the migration of linearized plasmid DNA in the gel in a similar fashion. In the absence of metal complex, the plasmid control (C) migrated at a rate inversely proportional to the logarithm of its molecular weight, 3.0 kb, relative to the size standard (S). After incubation with cisplatin or 1,1/t,t, DNA migration was reduced relative to the control. This effect was most pronounced for the lowest ratio of DNA bp: mc, 5: 1, which is the highest relative concentration of metal complex. As the DNA bp: mc ratio is increased to 10:1 and higher, reflecting a decrease in metal complex, this effect decreased to the point that at 100: 1 bp: mc the DNA migrated at the same rate as the untreated control (C).

An equivalent study for the Ru-Pt bimetallic complexes $[(bpy)_2Ru(dpq)PtCl_2](CF_3SO_3)_2$ and $[(bpy)_2Ru(dpb)PtCl_2](CF_3SO_3)_2$ is shown in Figure 3.14. The Ru-Pt complexes had a significant effect on the migration of linearized plasmid DNA through the gel, producing a reduction in migration as with cisplatin and 1,1/t,t that was much more pronounced for all DNA bp: mc ratios examined. The most dramatic effect occurred at the lowest DNA bp: mc ratio, 5: 1, which again reflects the highest metal concentration added. As the DNA bp: mc ratio was increased from 10: 1 onward, this effect diminished but the rate of DNA migration does not approach the untreated control (C) at 100: 1 DNA bp: mc. Instead, a small effect continues to be observed for the remaining two samples, 200 and 300: 1.

For both metal complexes at DNA bp: mc ratios of 20, 10 and 5: 1, the fluorescence intensity of the DNA band was significantly reduced relative to the untreated plasmid control. As with the effects on migration, this apparent reduction in ethidium bromide fluorescence intensity appears to be concentration dependent, with more pronounced effects observed with decreasing ratios of bp to mc (corresponding to a higher concentration of metal added).

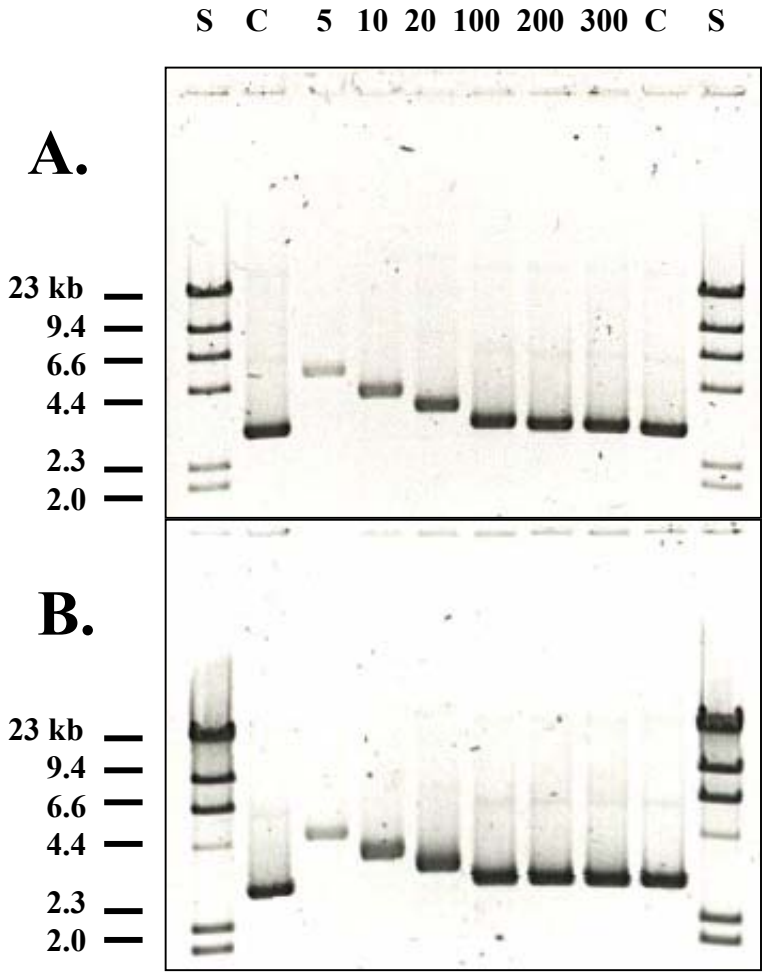

Figure 3.14 Native agarose gel electrophoresis of interaction of $[(bpy)_2Ru(dpq)PtCl_2](CF_3SO_3)_2$ **(A)** and $[(bpy)_2Ru(dpb)PtCl_2](CF_3SO_3)_2$ **(B)** (where bpy = 2,2′-bipyridine, dpq = 2,3-bis(2-pyridyl)quinoxaline, dpb = 2,3-bis(2-pyridyl)benzoquinoxaline) with linearized plasmid DNA. One μg of linearized plasmid DNA was incubated with metal complex at a ratio of 5, 10, 20, 100, 200 or 300 base pairs to 1 metal complex at 37 °C for 4 h. A control sample (C) containing only plasmid DNA was incubated under identical conditions. Samples containing 100 ng of DNA were analyzed on a 0.8% native agarose gels, which were then stained with 0.5 mg/ml ethidium bromide for 1 h and photographed under UV illumination. A molecular weight standard (S) was included for reference.

A similar study for the complexes $[(phen)_2Ru(dpq)PtCl_2](CF_3SO_3)_2$ and $[(phen)_2Ru(dpb)PtCl_2](CF_3SO_3)_2$ is shown in Figure 3.15. Incubation with these complexes produced a strikingly similar reduction in DNA migration as observed for the bpy-analogs. The trend and magnitude of inhibition also appeared to be equivalent. In addition, ethidium bromide staining was also affected, with increasing effects observed with decreasing ratios of bp to mc.

An equivalent study for the ruthenium monometallic synthons was conducted to establish the role of the Pt^{II} center. Gels for $[(bpy)_2Ru(dpq)](CF_3SO_3)_2$ and $[(bpy)_2Ru(dpb)](CF_3SO_3)_2$ are presented in Figure 3.16, and results for $[(phen)_2Ru(dpq)](CF_3SO_3)_2$ and $[(phen)_2Ru(dpb)](CF_3SO_3)_2$ are shown in Figure 3.17. Incubation with these complexes produced no observable effect on the migration of the plasmid DNA through the gel. All DNA bands, regardless of the concentration of the metal complex added, migrated at approximately the same rate as the untreated control. In addition, ethidium bromide staining did not appear to be affected at any DNA bp: mc ratio.

The native gel electrophoresis studies clearly showed that the four Ru-Pt complexes bind to linearized plasmid DNA. All four complexes exhibited a significant effect on the migration of linearized plasmid DNA in these experiments. The staining of the fluorescing, intercalating dye ethidium bromide was also affected. Both effects are proportional to the amount of metal complex present. This provides strong evidence that these complexes bind directly to double-stranded DNA. The absence of this effect in the Ru monometallic studies clearly establishes the role of the Pt^{II} site on this binding. A comparison with the results for our Ru-Pt systems to the known DNA-crosslinkers cisplatin and 1,1/t,t provides additional evidence for this binding. The Ru-Pt complexes exhibit a similar, yet more pronounced retardation of DNA migration than these known DNA-crosslinkers. The effect on ethidium bromide fluorescence was not observed for cisplatin or 1,1/t,t.

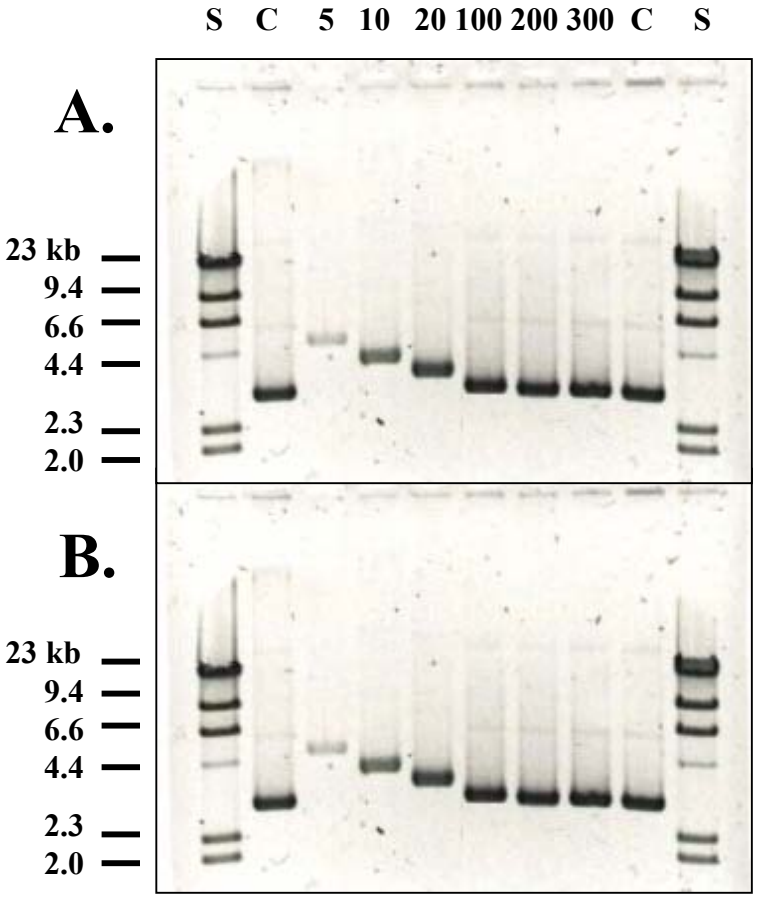

Figure 3.15 Native agarose gel electrophoresis of interaction of $[(phen)_2Ru(dpq)PtCl_2](CF_3SO_3)_2$ **(A)** and $[(phen)_2Ru(dpb)PtCl_2](CF_3SO_3)_2$ **(B)** (where phen = 1,10-phenanthroline, dpq = 2,3-bis(2-pyridyl)quinoxaline, dpb = 2,3-bis(2-pyridyl)benzoquinoxaline) with linearized plasmid DNA. One μg of linearized plasmid DNA was incubated with metal complex at a ratio of 5, 10, 20, 100, 200 or 300 base pairs to 1 metal complex at 37 °C for 4 h. A control sample (C) containing only plasmid DNA was incubated under identical conditions. Samples containing 100 ng of DNA were analyzed on a 0.8% native agarose gels, which were then stained with 0.5 mg/ml ethidium bromide for 1 h and photographed under UV illumination. A molecular weight standard (S) was included for reference.

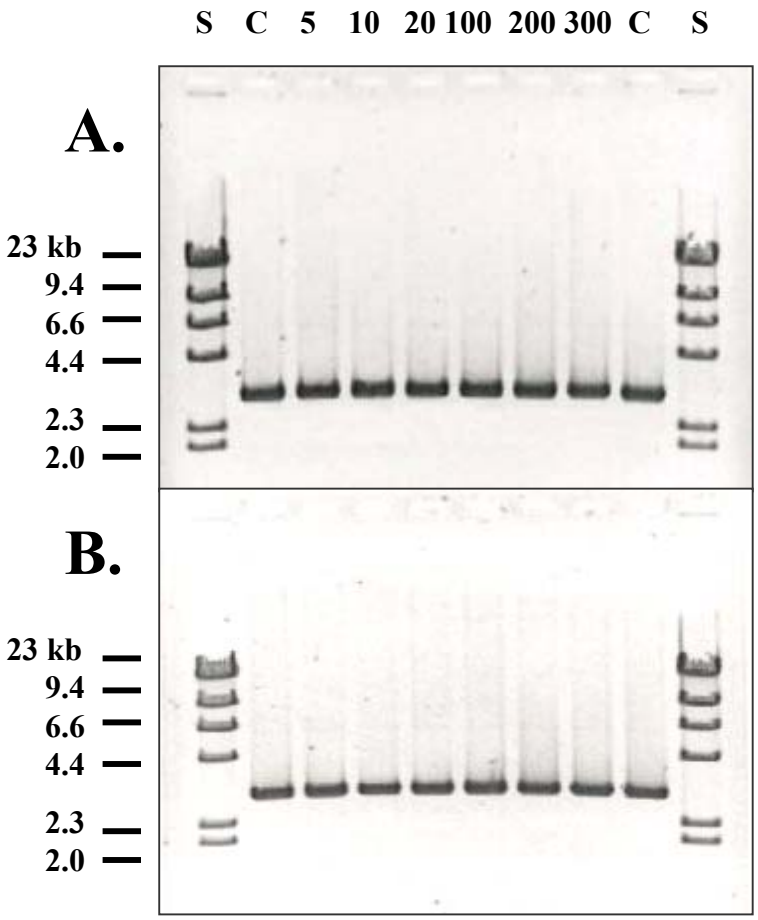

Figure 3.16 Native agarose gel electrophoresis of interaction of $[(bpy)_2Ru(dpq)](CF_3SO_3)_2$ **(A)** and $[(bpy)_2Ru(dpb)](CF_3SO_3)_2$ **(B)**, (where bpy = 2,2′ -bipyridine, dpq = 2,3-bis(2-pyridyl)quinoxaline, dpb = 2,3-bis(2-pyridyl)benzoquinoxaline) with linearized plasmid DNA. One μg of linearized plasmid DNA was incubated with metal complex at a ratio of 5, 10, 20, 100, 200 or 300 base pairs to 1 metal complex at 37 °C for 4 h. A control sample (C) containing only plasmid DNA was incubated under identical conditions. Samples containing 100 ng of DNA were analyzed on a 0.8% native agarose gels, which were then stained with 0.5 mg/ml ethidium bromide for 1 h and photographed under UV illumination. A molecular weight standard (S) was included for reference.

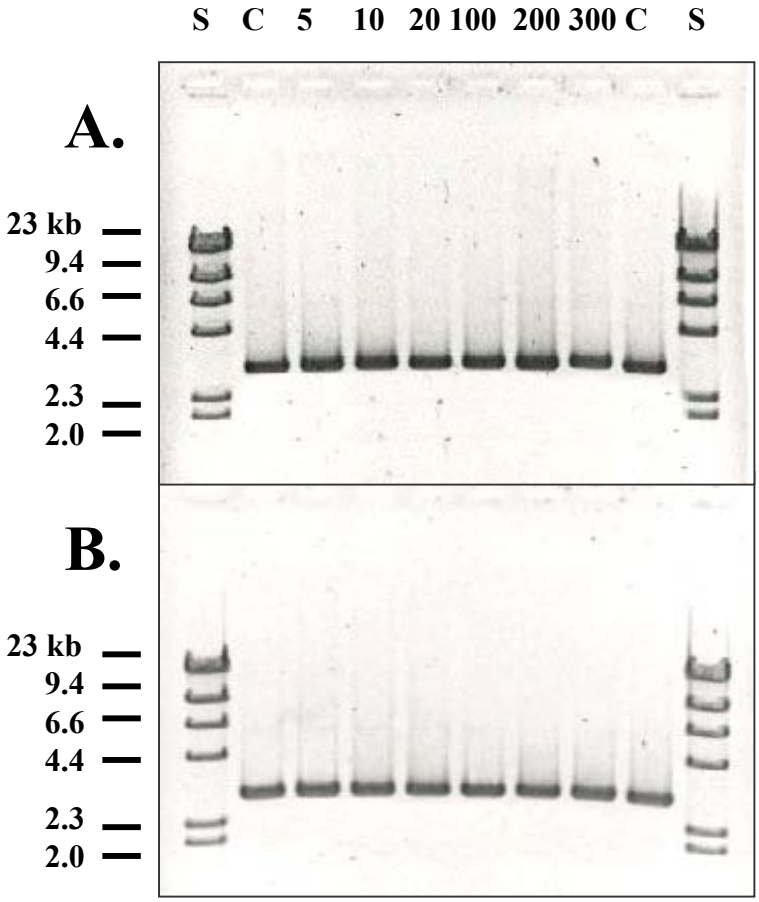

Figure 3.17 Native agarose gel electrophoresis of interaction of $[(phen)_2Ru(dpq)](CF_3SO_3)_2$ **(A)** and $[(phen)_2Ru(dpb)](CF_3SO_3)_2$ **(B)** (where phen = 1,10-phenanthroline, dpq = 2,3-bis(2-pyridyl)quinoxaline, dpb = 2,3-bis(2-pyridyl)benzoquinoxaline) with linearized plasmid DNA. One μg of linearized plasmid DNA was incubated with metal complex at a ratio of 5, 10, 20, 100, 200 or 300 base pairs to 1 metal complex at 37 °C for 4 h. A control sample (C) containing only plasmid DNA was incubated under identical conditions. Samples containing 100 ng of DNA were analyzed on a 0.8% native agarose gels, which were then stained with 0.5 mg/ml ethidium bromide for 1 h and photographed under UV illumination. A molecular weight standard (S) was included for reference.

The electrophoretic mobility of DNA is determined by many factors, including molecular weight, molecular shape, charge, and gel voltage. Alteration of any of these factors may affect the migration of DNA through the gel; i.e., a shorter DNA molecule will move farther and faster than a larger one, as will a more compact or more negatively charged DNA molecule.[21, 24, 26] The effect on DNA migration observed in these gels is due to the binding of the metal complexes to the DNA. Such binding will alter the molecular weight of the DNA. Since the Ru-Pt complexes have considerably higher molecular weights than cisplatin or 1,1/t,t, one would expect a more dramatic sized based effect on the retardation of the DNA through the gel. At this point, however, the efficiency of metal-DNA binding is not known. A comparison of the molecular weights of cisplatin, 1,1/t,t and the four Ru-Pt complexes is shown in Table 3.3. Also, the molecular weight of the linearized plasmid DNA, assuming 100% metal binding, is shown. This data suggests why the Ru-Pt systems have a more dramatic effect than cisplatin or 1,1/t,t on DNA migration.

Binding of the metal complexes to DNA will not only affect molecular mass, but also the overall charge of the DNA molecule. The Ru-Pt complexes, as well as 1,1/t,t and cisplatin, contain labile chloride ligands that can be substituted with a neutral water ligand. This labilization and substitution would lead to a 4+ cationic complex for the ruthenium-platinum bimetallics and 1,1/t,t and a 2+ cationic complex for cisplatin. Subsequent binding of these 4+ cationic complexes would significantly reduce the overall negative charge of the DNA, which could further reduce the rate of migration of the DNA in an electrophoresis gel. Since the charge is the same for the Ru-Pt systems and 1,1/t,t, any impact on charge on DNA migration would only be observed if a higher percentage of the Ru-Pt complexes bind DNA since 1,1/t,t treated DNA exhibits a more rapid migration.

Another important issue to consider is that the binding of these ruthenium-platinum bimetallic complexes to DNA may induce local or global changes in DNA conformation. It has been well established that the binding of cisplatin to DNA unwinds,

Table 3.3 Change in molecular weight of DNA upon binding of *cis*-$[Pt(NH_3)_2Cl_2]$ (cisplatin), *trans*-$\{[PtCl(NH_3)_2]_2(\mu\text{-}H_2N(CH_2)_6NH_2)\}(NO_3)_2$ (1,1/t,t), $[(bpy)_2Ru(dpq)PtCl_2](CF_3SO_3)_2$, $[(bpy)_2Ru(dpb)PtCl_2](CF_3SO_3)_2$, $[(phen)_2Ru(dpq)PtCl_2](CF_3SO_3)_2$, $[(phen)_2Ru(dpb)PtCl_2](CF_3SO_3)_2$ (where bpy = 2,2′-bipyridine, phen = 1,10-phenanthroline, dpq = 2,3-bis(2-pyridyl)quinoxaline, dpb = 2,3-bis(2-pyridyl)benzoquinoxaline), given in atomic mass units (amu). Molecular weight of DNA with 100% metal binding was calculated assuming a 5: 1 bp: mc ratio. Molecular weight of plasmid DNA used in these experiments was calculated based on 1 mol base pairs = 660 g/mol. Linearized plasmid DNA is 2961 bp in length. The actual location of the 5: 1 band on the gel is given for reference. The location of this band was determined by comparison with the DNA molecular weight standards.

Complex	MW, Metal Complex (amu)	MW, DNA (amu)	MW, DNA 100% metal bound	Location of 5:1 band on gel (MW, amu)
cis-$[Pt(NH_3)_2Cl_2]$ (cisplatin)	300	2.0×10^6	2.2×10^6	2.3×10^6
trans-$\{[PtCl(NH_3)_2]_2(\mu\text{-}H_2N(CH_2)_6NH_2)\}(NO_3)_2$ (1,1/t,t)	646	2.0×10^6	2.4×10^6	2.3×10^6
$[(bpy)_2Ru(dpq)PtCl_2](CF_3SO_3)_2$	1263	2.0×10^6	2.8×10^6	3.3×10^6
$[(bpy)_2Ru(dpb)PtCl_2](CF_3SO_3)_2$	1313	2.0×10^6	2.8×10^6	3.3×10^6
$[(phen)_2Ru(dpq)PtCl_2](CF_3SO_3)_2$	1360	2.0×10^6	2.8×10^6	3.3×10^6
$[(phen)_2Ru(dpb)PtCl_2](CF_3SO_3)_2$	1310	2.0×10^6	2.8×10^6	3.3×10^6

and bends the helix to a degree dictated by the type of adduct formed.[30-32] Since the Ru-Pt complexes contain the same *cis*-$PtCl_2$ active site as cisplatin, it is reasonable to assume that the binding of complexes will alter the three dimensional shape of the DNA helix. To what extent the overall shape of the DNA is changed cannot be determined from these native gel analyses.

Our bimetallic complexes were designed to be capable of binding DNA through an intercalation of the bridging ligand into the DNA helix and/or through covalent binding via the platinum metal site. Analysis of the interaction of the monometallic ruthenium synthons, $[(bpy)_2Ru(dpq)](CF_3SO_3)_2$, $[(bpy)_2Ru(dpb)](CF_3SO_3)_2$, $[(phen)_2Ru(dpq)](CF_3SO_3)_2$, and $[(phen)_2Ru(dpb)](CF_3SO_3)_2$, with DNA suggest that intercalation of the bridging ligand is not responsible for the observed change in migration of DNA exposed to the Ru-Pt bimetallic complexes. This indicates that the platinum site is needed for the observed trends and that these complexes exhibit covalent binding to DNA. The presence of a rapid intercalation interaction prior to covalent binding is possible and may influence the site of covalent binding of our complexes.

Determination of R_f Values

As observed in the native gel electrophoresis studies, the DNA binding of all four Ru-Pt compounds and the standards, cisplatin and 1,1/t,t, decreased the electrophoretic mobility of DNA in agarose gels. In comparison with the untreated control, a significantly greater effect was observed for the Ru-Pt complexes than for cisplatin and 1,1/t,t. These observations, however, were made in a purely qualitative fashion. It was therefore desirable to quantitate the migration of the metal-reacted DNA, through the determination of a R_f value. Equivalent determinations were also performed for the untreated control and the cisplatin and 1,1/t,t standards.

The results of the R_f determinations are shown in Table 3.4, with full data for the R_f determinations included in Appendices B-1 through B-12. Graphs comparing R_f values for the untreated controls are shown in Figure 3.18. Graphs comparing R_f values for all

Table 3.4. R_f values for *cis*-$[Pt(NH_3)_2Cl_2]$ (cisplatin), *trans*-$\{[PtCl(NH_3)_2]_2(\mu\text{-}H_2N(CH_2)_6NH_2)\}(NO_3)_2$ (1,1/t,t), $[(bpy)_2Ru(dpq)PtCl_2](CF_3SO_3)_2$, $[(bpy)_2Ru(dpb)PtCl_2](CF_3SO_3)_2$, $[(phen)_2Ru(dpq)PtCl_2](CF_3SO_3)_2$, and $[(phen)_2Ru(dpb)PtCl_2](CF_3SO_3)_2$ (where bpy = 2,2′-bipyridine, phen = 1,10-phenanthroline, dpq = 2,3-bis(2-pyridyl)quinoxaline, dpb = 2,3-bis(2-pyridyl)benzoquinoxaline). Values represent the distance traveled by the metal-reacted DNA band (in mm) divided by the distance traveled by the 2.1 kb band of the molecular weight standards (in mm), averaged over three equivalent metal-DNA interaction experiments for each respective metal complex. **Bold face** values represent %**RSD** over the three equivalent metal-DNA interaction experiments.

Complex	Ratio, bp: mc						
	Control	5:1	10:1	20:1	100:1	200:1	300:1
cis-$[Pt(NH_3)_2Cl_2]$	0.875 **(0.365)**	0.823 **(1.73)**	0.838 **(1.65)**	0.838 **(1.65)**	0.854 **(1.56)**	0.854 **(1.56)**	0.854 **(1.56)**
trans-$\{[PtCl(NH_3)_2]_2(\mu\text{-}H_2N(CH_2)_6NH_2)\}^{2+}$	0.844 **(0.579)**	0.812 **(0.722)**	0.828 **(0.649)**	0.828 **(0.649)**	0.844 **(0.579)**	0.844 **(0.579)**	0.844 **(0.579)**
$[(bpy)_2Ru(dpq)PtCl_2](CF_3SO_3)_2$	0.866 **(0.68)**	0.715 **(2.81)**	0.769 **(1.53)**	0.806 **(0.775)**	0.844 **(1.27)**	0.849 **(2.29)**	0.866 **(0.677)**
$[(bpy)_2Ru(dpb)PtCl_2](CF_3SO_3)_2$	0.855 **(1.19)**	0.724 **(2.76)**	0.775 **(2.75)**	0.805 **(2.52)**	0.839 **(2.82)**	0.845 **(1.76)**	0.850 **(0.799)**
$[(phen)_2Ru(dpq)PtCl_2](CF_3SO_3)_2$	0.861 **(1.17)**	0.712 **(1.73)**	0.764 **(0.748)**	0.805 **(0.747)**	0.841 **(0.901)**	0.851 **(0.405)**	0.861 **(1.17)**
$[(phen)_2Ru(dpb)PtCl_2](CF_3SO_3)_2$	0.852 **(1.22)**	0.689 **(1.11)**	0.735 **(1.03)**	0.775 **(1.47)**	0.826 **(2.34)**	0.826 **(2.34)**	0.826 **(2.34)**

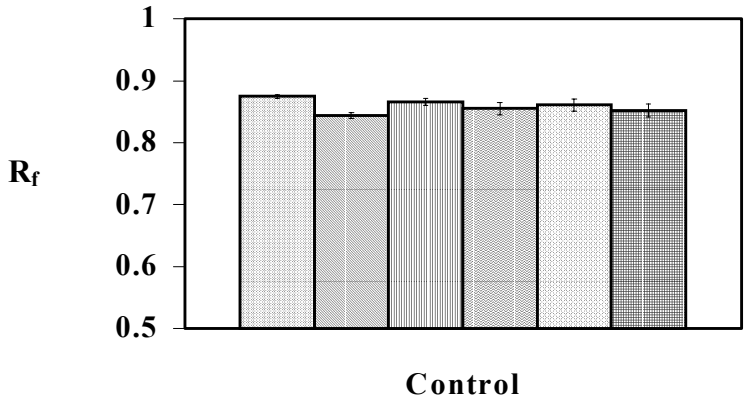

Legend:

- **untreated control from *cis*-[$(Pt(NH_3)_2PtCl_2]$ (cisplatin) study**
- **untreated control from *trans*-{$[PtCl(NH_3)_2]_2(\mu\text{-}H_2N(CH_2)_6NH_2)\}^{2+}$ (1,1/t,t) study**
- **untreated control from $[(bpy)_2Ru(dpb)PtCl_2](CF_3SO_3)_2$ study**
- **untreated control from $[(bpy)_2Ru(dpq)PtCl_2](CF_3SO_3)_2$ study**
- **untreated control from $[(phen)_2Ru(dpq)PtCl_2](CF_3SO_3)_2$ study**
- **untreated control from $[(phen)_2Ru(dpb)PtCl_2](CF_3SO_3)_2$ study**

Figure 3.18 Comparison of R_f values for the untreated control. Each histogram represents the R_f value of the untreated control obtained from each respective metal-DNA interaction study listed above. R_f is defined as the migration distance of the metal reacted DNA divided by the migration distance of the 2.1 kb band of the molecular weight standards. n = 3 for each control.

four Ru-Pt complexes at various DNA bp: mc ratios are shown in Figure 3.19. Along the y-axis of each graph the average R_f is indicated. This value represents the distance traveled (in mm) by the metal-reacted DNA, divided by the distance traveled (in mm) of the 2.1 kb band in the molecular weight standards, averaged over three equivalent metal-DNA interaction experiments (3 separate electrophoretic gels) for each respective metal complex. On the x-axis, individual histograms corresponding to each metal complex are represented, along with one representing an average R_f value for the untreated control.

The results for the R_f value determinations for the untreated controls are presented in Figure 3.18. An untreated control from each respective metal-DNA study is represented. These are presented together to assess the reproducibility of the R_f value determination. The R_f values for the untreated controls are approximately equal for all the Ru-Pt, cisplatin and 1,1/t,t metal-DNA interaction studies. This result clearly shows the reproducibility of the R_f values derived from independent electrophoresis experiments.

A comparison of the R_f values at the 5, 10, 20, 100, 200 and 300 DNA bp: mc ratio for all four Ru-Pt complexes and the cisplatin and 1,1/t,t standards is shown in Figure 3.19. A value is also included for the untreated DNA control, which is the average of all R_f values observed for the untreated control in each of the metal-DNA interaction experiments. At the 5:1 ratio (high amounts of metal added) the R_f values determined for the four Ru-Pt complexes are considerably less than those determined for cisplatin, 1,1/t,t, and the untreated control. In addition, the R_f values for the four Ru-Pt complexes are approximately equivalent. This trend continues for the 10 and 20: 1 DNA bp: mc ratios (representing progressively lower amounts of metal added), with the R_f values increasing in magnitude. At the 100, 200 and 300: 1 DNA bp: mc ratios (again, representing progressively lower amounts of metal added) this trend disappears, with the R_f values for the Ru-Pt complexes, cisplatin, 1,1/t,t and the untreated control becoming essentially identical.

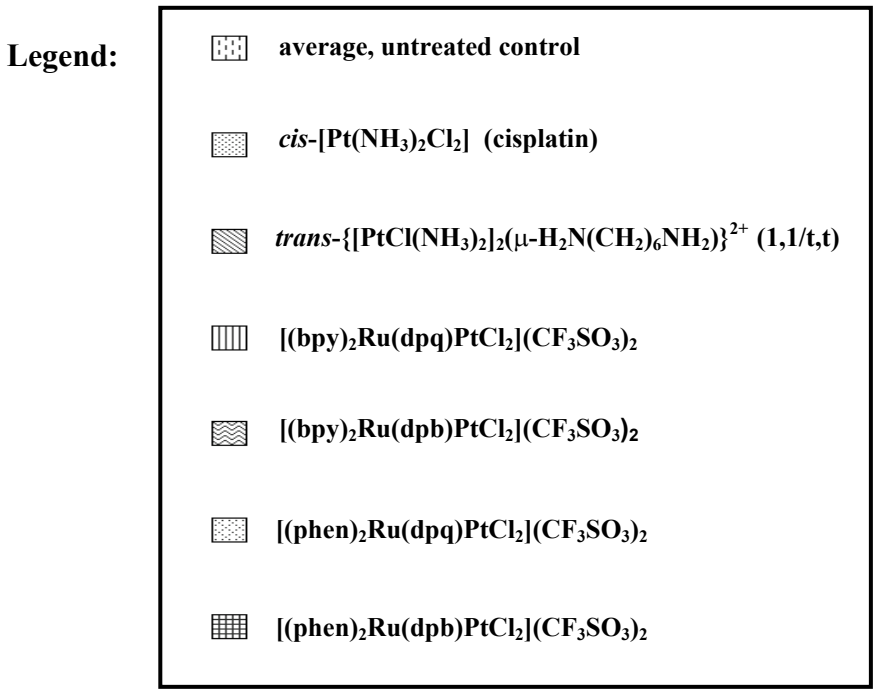

Figure 3.19 **(following page)**. Comparison of R_f values for *cis*-$[Pt(NH_3)_2Cl_2]$ (cisplatin), *trans*-$\{[PtCl(NH_3)_2]_2(\mu\text{-}H_2N(CH_2)_6NH_2)\}(NO_3)_2$ (1,1/t,t), $[(bpy)_2Ru(dpq)PtCl_2](CF_3SO_3)_2$, $[(bpy)_2Ru(dpb)PtCl_2](CF_3SO_3)_2$, $[(phen)_2Ru(dpq)PtCl_2](CF_3SO_3)_2$, and $[(phen)_2Ru(dpb)PtCl_2](CF_3SO_3)_2$, (where bpy = 2,2′-bipyridine, phen = 1,10-phenanthroline, dpq = 2,3-bis(2-pyridyl)quinoxaline, dpb = 2,3-bis(2-pyridyl)benzoquinoxaline) 5:1 ratio. R_f is defined as the migration distance of the metal reacted DNA divided by the migration distance of the 2.1 kb band of the molecular weight standards. n = 3 for each metal complex.

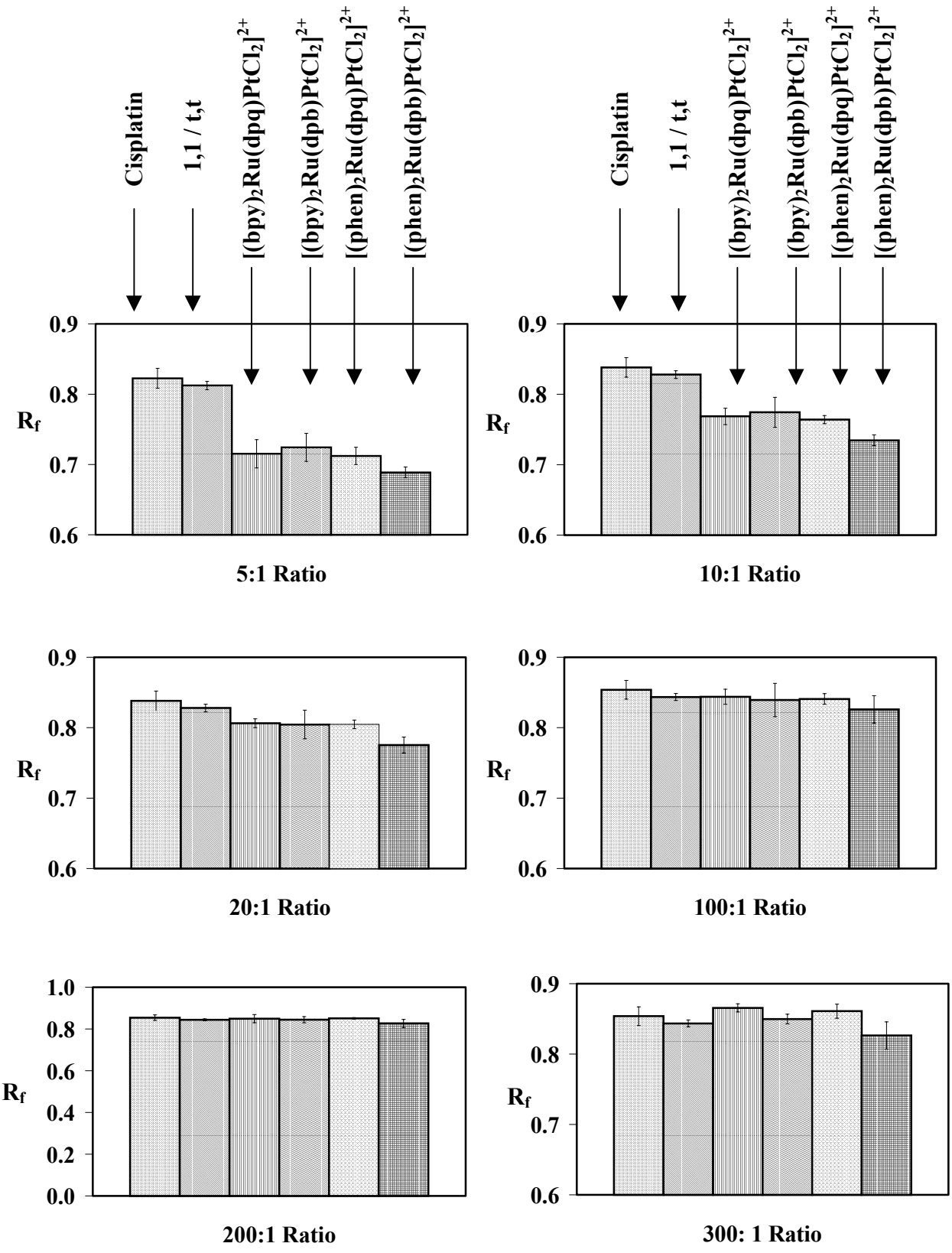
Cisplatin
1,1 / t,t
[(bpy)2Ru(dpq)PtCl2]2+
[(bpy)2Ru(dpb)PtCl2]2+
[(phen)2Ru(dpq)PtCl2]2+
[(phen)2Ru(dpb)PtCl2]2+
Rf
0.9
0.8
0.7
0.6
5:1 Ratio
10:1 Ratio
20:1 Ratio
100:1 Ratio
1.0
0.4
0.2
0.0
200:1 Ratio
300: 1 Ratio

The results in Figures 3.18-3.19 clearly show the utility of this technique for quantitating the migration of metal-reacted DNA. As stated previously, the retardation effects observed in the native gels were purely qualitative. By calculating a R_f value, numbers may be compared. It is easy to see that the Ru-Pt compounds more profoundly effect the migration of linearized plasmid DNA than cisplatin or 1,1/t,t. Examination of the data in Table 3.2 shows that %RSDs for all measurements are quite low. This indicates that the technique of native gel electrophoresis is highly reproducible.

Theoretical Modeling of DNA Migration, Molecular Weight Effect

The migration of DNA through an electrophoresis gel is inversely proportional to the logarithm of its molecular weight, a relationship that is well established in the literature and is used routinely to determine the size of DNA fragments.[24–26] Since the binding of metal-complexes to DNA constitutes an increase in molecular weight of the DNA, a theoretical migration distance for metal-reacted DNA can be determined by utilizing a standard curve. In these studies, a standard curve was constructed using molecular weight and migration distance data for the 4.4, 2.3 and 2.0 kb bands of the lambda DNA standards. These DNA bands were selected because they migrate in approximately the same region as the metal-reacted DNA. In order to investigate the most dramatic effects due to molecular weight, 100% metal binding was assumed for all theoretical calculations.

For comparison purposes, an equivalent study for the cisplatin and 1,1/t,t standards was conducted. Migration distance and molecular weight data for the lambda molecular weight standards, used to construct the molecular weight vs. migration distance standard curve, are shown in Table 3.5– 3.6. The molecular weight vs. migration distance standard curve is shown in Figure 3.20.

Table 3.5 Migration distance data for the 4361, 2322 and 2027 bp bands of the lambda DNA molecular weight standards. DNA band migration distance is measured from the bottom of the electrophoresis gel well to the bottom of the respective DNA band. Data taken from six native gel analyses.

DNA Band (kb)	DNA Band Migration Distance (mm)						Average Distance Migrated (mm)	Std. Deviation
	I	II	III	IV	V	VI		
4361	26.0	23.5	24.5	26.0	25.0	23.5	24.8	1.13
2322	33.0	30.0	31.0	32.5	31.5	29.0	31.2	1.50
2027	35.0	31.5	32.5	34.0	33.5	31.5	33.0	1.41

Table 3.6 Molecular weight and average migration distance data for 4361, 2322, 2027 bp fragments of lambda molecular weight standards. Molecular weight of DNA is calculated using the relation that 1 mol base pairs = 660 g/mol. Average migration distance data reproduced from table 3.4. Data used to construct log MW vs. migration distance standard curve shown in Figure 3.23.

DNA Band (kb)	MW of DNA Band (amu)	Log MW	Average Distance Migrated (mm)
4361	2.9×10^6	6.46	24.8
2322	1.5×10^6	6.19	31.2
2027	1.3×10^6	6.13	33.0

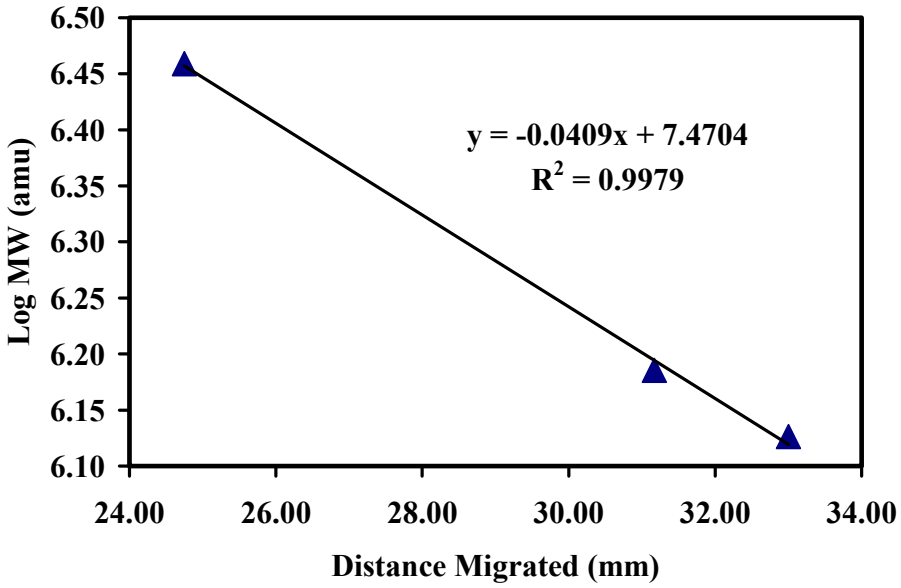

Figure 3.20 Standard curve relating the relationship between the molecular weight of DNA and distance traveled through a native gel. Plot of log MW of 4361, 2322, 2027 bp fragments of lambda MW standards vs. distance migrated. Equation of line determined by least-squares method. Data used to construct this graph shown in Tables 3.4 – 3.5.

Theoretical migration calculations (assuming 100% metal binding) and experimental DNA migration distances for all metal complexes are shown in Tables 3.7 – 3.12. The calculated DNA migration distances follow an obvious trend. At low-DNA bp: mc ratios (high amounts of metal present) the DNA migrates less distance than at high-DNA bp: mc ratios (low amounts of metal present). Calculated migration distances follow a similar trend. The calculated and observed migration distances differ for the Ru-Pt complexes, cisplatin, and 1,1/t,t, due to differences in the molecular weights of these compounds.

Significant variance, however, exists between theoretical and experimental migration distances. This occurs for all metal complexes examined, and appears to be greatest at low DNA bp: mc ratios (high amounts of metal added). The experimental migrations are lower than the theoretical numbers assuming 100% binding. The differences appear to be slightly higher in magnitude for the Ru-Pt complexes than for cisplatin and 1,1/t,t. These variances point to other factors than molecular weight impacting the R_f value. This treatment did not address the effect on DNA migration by other factors. Changes in three-dimensional structure of DNA are expected after binding of these metal complexes. Also, the bound Ru-Pt complexes will carry a 4+ charge, thereby diminishing the overall charge of the DNA molecule and reducing migration distance. The degree to which each of the above described factors is occurring cannot be easily determined. This study does clearly show that molecular weight change alone does not account for the degree of observed perturbations of DNA migration and highlights the type of migration expected due to MW increases alone.

Gel Densitometry Studies: Concentration Dependent Interaction with DNA

Gel desitometry is a technique commonly used in molecular biology to quantitate DNA.[175-177] It involves the use of the fluorescent, intercalating dye ethidium bromide. Intercalation of this dye into the DNA helix greatly enhances its quantum yield for emission, which is linear throughout a wide range. Therefore, the measurement of fluorescence intensity of ethidium bromide reacted DNA can be used to measure DNA concentration in comparison to a control with known molecular weight. Various factors

Table 3.7 Experimental and theoretical DNA migration distances for the interaction of *cis*-[$Pt(NH_3)_2Cl_2$] (cisplatin) with linearized plasmid DNA. Migration distances represent the distance traveled by the DNA band, measured from the bottom of the electrophoresis gel loading well to the bottom of the DNA band. Molecular weight of DNA is calculated using the relation that 1 mol DNA base pairs = 660 g/mol. Total molecular weight is the sum of the molecular weight of the DNA and the bound metal complex, assuming 100% metal binding. This value was then used in conjunction with the log MW vs. migration distance standard curve for the lambda molecular weight standards to determine a theoretical migration distance. Experimental migration distances are provided for comparison purposes and are derived from the native gel analysis of an actual metal-DNA interaction study. The difference between theoretical and experimental migration distances was calculated by simple subtraction and is included to facilitate comparison between these two classifications of data.

DNA Band	MW Added Through Metal Binding (amu)	MW of DNA (amu)	Total MW (amu)	Theoretical Migration Distance (mm)	Experimental Migration Distance (mm)	Difference, (Theoretical – Experimental) (mm)
Control	0	2.0×10^6	2.0×10^6	28.8	28.0	0.8
5:1 Ratio	2.0×10^5	2.0×10^6	2.1×10^6	27.9	26.5	1.4
10: 1 Ratio	9.0×10^4	2.0×10^6	2.0×10^6	28.4	27.0	1.4
20: 1 Ratio	4.0×10^4	2.0×10^6	2.0×10^6	28.6	27.0	1.6
100: 1 Ratio	9.0×10^3	2.0×10^6	2.0×10^6	28.8	27.5	1.3
200: 1 Ratio	4.0×10^3	2.0×10^6	2.0×10^6	28.8	27.5	1.3
300: 1 Ratio	3.0×10^3	2.0×10^6	2.0×10^6	28.8	27.5	1.3

Table 3.8 Experimental and theoretical DNA migration distances for the interaction of *trans*-$\{[PtCl(NH_3)_2]_2(\mu\text{-}H_2N(CH_2)_6NH_2)\}^{2+}$ (1,1/t,t) with linearized plasmid DNA Migration distances represent the distance traveled by the DNA band, measured from the bottom of the electrophoresis gel loading well to the bottom of the DNA band. Molecular weight of DNA is calculated using the relation that 1 mol DNA base pairs = 660 g/mol. Total molecular weight is the sum of the molecular weight of the DNA and the bound metal complex, assuming 100% metal binding. This value was then used in conjunction with the log MW vs. migration distance standard curve for the lambda molecular weight standards to determine a theoretical migration distance. Experimental migration distances are provided for comparison purposes and are derived from the native gel analysis of an actual metal-DNA interaction study. The difference between theoretical and experimental migration distances was calculated by simple subtraction and is included to facilitate comparison between these two classifications of data.

DNA Band	MW Added Through Metal Binding (amu)	MW of DNA (amu)	Total MW (amu)	Theoretical Migration Distance (mm)	Experimental Migration Distance (mm)	Difference, (Theoretical – Experimental) (mm)
Control	0	2.0×10^6	2.0×10^6	28.8	28.0	0.8
5 : 1 Ratio	4.6×10^5	2.0×10^6	2.4×10^6	26.6	27.0	1.4
10: 1 Ratio	2.3×10^5	2.0×10^6	2.2×10^6	27.7	27.5	0.2
20: 1 Ratio	1.1×10^5	2.0×10^6	2.1×10^6	28.2	27.5	0.7
100: 1 Ratio	2.3×10^4	2.0×10^6	2.0×10^6	28.7	28.0	0.7
200: 1 Ratio	1.1×10^4	2.0×10^6	2.0×10^6	28.8	28.0	0.8
300: 1 Ratio	7.6×10^3	2.0×10^6	2.0×10^6	28.8	28.0	0.8

Table 3.9 Experimental and theoretical DNA migration distances for the interaction of $[(bpy)_2Ru(dpq)PtCl_2](CF_3SO_3)_2$ (where bpy = 2,2′-bipyridine, dpq = 2,3-bis(2-pyridyl)quinoxaline) with linearized plasmid DNA. Migration distances represent the distance traveled by the DNA band, measured from the bottom of the electrophoresis gel loading well to the bottom of the DNA band. Molecular weight of DNA is calculated using the relation that 1 mol DNA base pairs = 660 g/mol. Total molecular weight is the sum of the molecular weight of the DNA and the bound metal complex, assuming 100% metal binding. This value was then used in conjunction with the log MW vs. migration distance standard curve for the lambda molecular weight standards to determine a theoretical migration distance. Experimental migration distances are provided for comparison purposes and are derived from the native gel analysis of an actual metal-DNA interaction study. The difference between theoretical and experimental migration distances was calculated by simple subtraction and is included to facilitate comparison between these two classifications of data.

DNA Band	MW Added Through Metal Binding (amu)	MW of DNA (amu)	Total MW (amu)	Theoretical Migration Distance (mm)	Experimental Migration Distance (mm)	Difference (Theoretical – Experimental) (mm)
Control	0	2.0×10^6	2.0×10^6	28.8	27.5	1.3
5 : 1 Ratio	7.5×10^5	2.0×10^6	2.7×10^6	25.4	23.0	2.4
10: 1 Ratio	3.7×10^5	2.0×10^6	2.3×10^6	27.0	25.0	2.0
20: 1 Ratio	1.9×10^5	2.0×10^6	2.1×10^6	27.9	26.0	1.9
100: 1 Ratio	3.7×10^4	2.0×10^6	2.0×10^6	28.6	27.0	1.6
200: 1 Ratio	1.9×10^4	2.0×10^6	2.0×10^6	28.7	27.0	1.7
300: 1 Ratio	1.2×10^4	2.0×10^6	2.0×10^6	28.8	27.5	1.3

Table 3.10 Experimental and theoretical DNA migration distance calculations for the interaction of $[(bpy)_2Ru(dpb)PtCl_2](CF_3SO_3)_2$ (where bpy = 2,2′-bipyridine, dpb = 2,3-bis(2-pyridyl)benzoquinoxaline)with cut plasmid DNA. Migration distances represent the distance traveled by the DNA band, measured from the bottom of the electrophoresis gel loading well to the bottom of the DNA band. Molecular weight of DNA is calculated using the relation that 1 mol DNA base pairs = 660 g/mol. Total molecular weight is the sum of the molecular weight of the DNA and the bound metal complex, assuming 100% metal binding. This value was then used in conjunction with the log MW vs. migration distance standard curve for the lambda molecular weight standards to determine a theoretical migration distance. Experimental migration distances are provided for comparison purposes and are derived from the native gel analysis of an actual metal-DNA interaction study. The difference between theoretical and experimental migration distances was calculated by simple subtraction and is included to facilitate comparison between these two classifications of data.

DNA Band	MW Added Through Metal Binding (amu)	MW of DNA (amu)	Total MW (amu)	Theoretical Migration Distance (mm)	Experimental Migration Distance (mm)	Difference (Theoretical – Experimental) (mm)
Control	0	2.0×10^6	2.0×10^6	28.8	28.5	0.3
5 : 1 Ratio	7.8×10^5	2.0×10^6	2.7×10^6	25.3	24.0	1.3
10: 1 Ratio	3.9×10^5	2.0×10^6	2.3×10^6	26.9	26.0	0.9
20: 1 Ratio	1.9×10^5	2.0×10^6	2.2×10^6	27.8	27.0	0.8
100: 1 Ratio	3.9×10^4	2.0×10^6	2.0×10^6	28.6	28.0	0.6
200: 1 Ratio	1.9×10^4	2.0×10^6	2.0×10^6	28.7	28.0	0.7
300: 1 Ratio	1.9×10^4	2.0×10^6	2.0×10^6	28.8	28.0	0.8

Table 3.11 Experimental and theoretical DNA migration distances for the interaction of $[(phen)_2Ru(dpq)PtCl_2](CF_3SO_3)_2$ (where phen = 1,10-phenanthroline, dpq = 2,3-bis(2-pyridyl)quinoxaline) with linearized plasmid DNA. Migration distances represent the distance traveled by the DNA band, measured from the bottom of the electrophoresis gel loading well to the bottom of the DNA band. Molecular weight of DNA is calculated using the relation that 1 mol DNA base pairs = 660 g/mol. Total molecular weight is the sum of the molecular weight of the DNA and the bound metal complex, assuming 100% metal binding. This value was then used in conjunction with the log MW vs. migration distance standard curve for the lambda molecular weight standards to determine a theoretical migration distance. Experimental migration distances are provided for comparison purposes and are derived from the native gel analysis of an actual metal-DNA interaction study. The difference between theoretical and experimental migration distances was calculated by simple subtraction and is included to facilitate comparison between these two classifications of data.

DNA Band	MW Added Through Metal Binding (amu)	MW of DNA (amu)	Total MW (amu)	Theoretical Migration Distance (mm)	Experimental Migration Distance (mm)	Difference (Theoretical – Experimental) (mm)
Control	0	2.0×10^6	2.0×10^6	28.8	28.5	0.3
5 : 1 Ratio	7.8×10^5	2.0×10^6	2.7×10^6	25.3	23.5	1.8
10: 1 Ratio	3.9×10^5	2.0×10^6	2.3×10^6	26.9	25.0	1.9
20: 1 Ratio	1.9×10^5	2.0×10^6	2.2×10^6	27.8	26.5	1.3
100: 1 Ratio	3.9×10^4	2.0×10^6	2.0×10^6	28.6	28.0	0.6
200: 1 Ratio	1.9×10^4	2.0×10^6	2.0×10^6	28.7	28.0	0.7
300: 1 Ratio	1.3×10^4	2.0×10^6	2.0×10^6	28.8	28.5	0.3

Table 3.12 Experimental and theoretical DNA migration distances for the interaction of $[(phen)_2Ru(dpb)PtCl_2](CF_3SO_3)_2$ (where phen = 1,10-phenanthroline, dpb = 2,3-bis(2-pyridyl)benzoquinoxaline) with cut plasmid DNA. Migration distances represent the distance traveled by the DNA band, measured from the bottom of the electrophoresis gel loading well to the bottom of the DNA band. Molecular weight of DNA is calculated using the relation that 1 mol DNA base pairs = 660 g/mol. Total molecular weight is the sum of the molecular weight of the DNA and the bound metal complex, assuming 100% metal binding. This value was then used in conjunction with the log MW vs. migration distance standard curve for the lambda molecular weight standards to determine a theoretical migration distance. Experimental migration distances are provided for comparison purposes and are derived from the native gel analysis of an actual metal-DNA interaction study. The difference between theoretical and experimental migration distances was calculated by simple subtraction and is included to facilitate comparison between these two classifications of data.

DNA Band	MW Added Through Metal Binding (amu)	MW of DNA (amu)	Total MW (amu)	Theoretical Migration Distance (mm)	Experimental Migration Distance (mm)	Difference (Theoretical – Experimental) (mm)
Control	0	2.0×10^6	2.0×10^6	28.8	28.0	0.8
5 : 1 Ratio	8.1×10^5	2.0×10^6	2.8×10^6	25.2	22.5	2.7
10: 1 Ratio	4.0×10^5	2.0×10^6	2.4×10^6	26.9	24.0	1.9
20: 1 Ratio	2.0×10^5	2.0×10^6	2.2×10^6	27.8	25.5	2.3
100: 1 Ratio	4.0×10^4	2.0×10^6	2.0×10^6	28.6	27.0	1.6
200: 1 Ratio	2.0×10^4	2.0×10^6	2.0×10^6	28.7	27.0	1.7
300: 1 Ratio	1.3×10^4	2.0×10^6	2.0×10^6	28.8	27.0	0.8

can affect the fluorescence intensity of ethidium bromide-reacted DNA. In these experiments, the DNA concentration was held constant and changes in ethidium bromide fluorescence intensity provides a means of detecting the binding of the Ru-Pt complexes to DNA.

The binding of all four Ru-Pt complexes significantly affected the ethidium bromide fluorescence after staining of metal-treated DNA. In comparison to the untreated control, the fluorescence intensity of the ethidium bromide-stained DNA was diminished at low DNA bp: mc ratios (high concentrations of metal). Gel densitometry experiments were conducted in order to quantify this reduced fluorescence intensity. These experiments were performed immediately following the ethidium bromide-staining step of the previously described native gel electrophoresis studies. Equivalent experiments for the standards cisplatin and 1,1/t,t were also conducted.

A comparison of the densitometry results for the untreated controls included in each metal-DNA interaction study are shown in Figure 3.21. The purpose of this comparison was to determine the reproducibility of this technique. The untreated control consists of a metal-DNA reaction sample in which no metal is added. Numerical data used to construct this figure and all remaining figures in this section is included in Appendices C-1 through C-13. As shown in Figure 3.21, the IDV (integrated density value) values for the untreated control do vary from one gel to the next, but all are within experimental error.

Figure 3.22 shows the densitometry results for the interaction of cisplatin, 1,1/t,t, and the Ru-Pt complexes with linearized plasmid DNA at 5, 10, 20, 100, 200 and 300 DNA bp: mc ratios. These results are expressed as a % IDV of the untreated control, averaged over three experiments. For cisplatin and 1,1 /t,t, the ethidium bromide fluorescence intensity is not appreciably affected at any DNA bp: mc ratio.

The Ru-Pt complexes significantly affected the ethidium bromide fluorescence intensity. At the 5, 10, and 20: 1 DNA bp: mc ratios, the ethidium bromide fluorescence

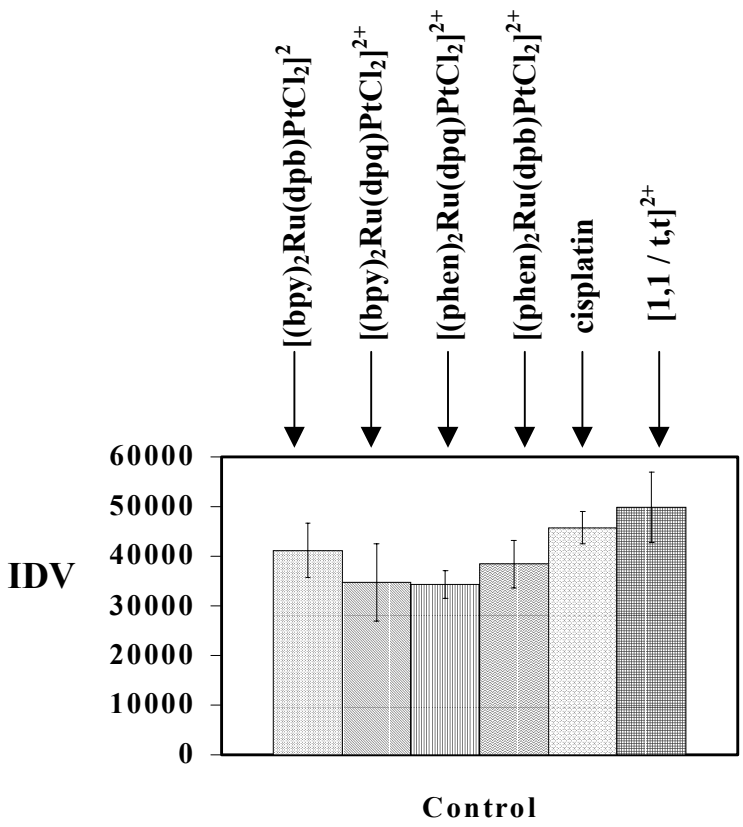

Legend:

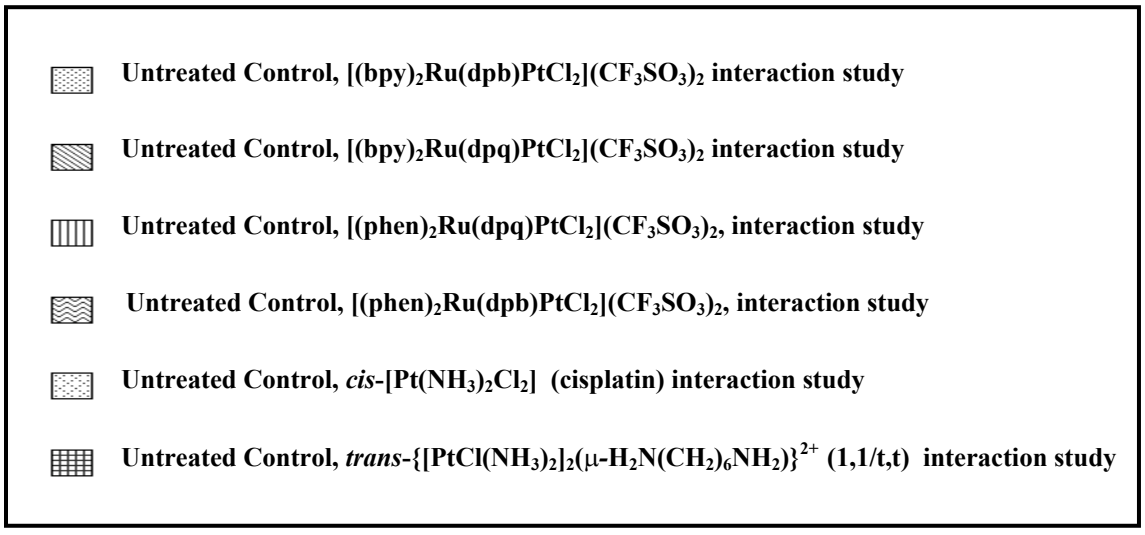

Figure 3.21 Comparison of gel densitometry results for the untreated control (no metal added), included with each respective metal-DNA interaction study. Along the y-axis, the designation "**IDV**" indicates the integrated density value, averaged over three experiments for each respective metal-DNA interaction study. Along the x-axis, the histograms represent the untreated control taken from each respective metal-DNA interaction study.

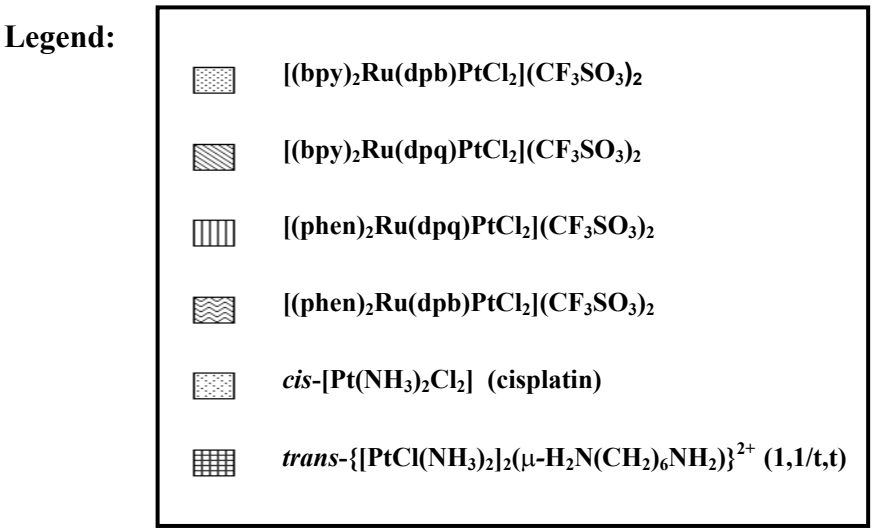

Figure 3.22 **(following page)** Comparison of gel densitometry results for the interaction of $[(bpy)_2Ru(dpq)PtCl_2](CF_3SO_3)_2$, $[(bpy)_2Ru(dpb)PtCl_2](CF_3SO_3)_2$, $[(phen)_2Ru(dpq)PtCl_2](CF_3SO_3)_2$, $[(phen)_2Ru(dpb)PtCl_2](CF_3SO_3)_2$, *cis*-$[Pt(NH_3)_2Cl_2]$ (cisplatin), and *trans*-$\{[PtCl(NH_3)_2]_2(\mu\text{-}H_2N(CH_2)_6NH_2)\}(NO_3)_2$ (1,1/t,t) (where bpy = 2,2′-bipyridine, phen = 1,10-phenanthroline, dpq = 2,3-bis(2-pyridyl)quinoxaline, dpb = 2,3-bis(2-pyridyl)benzoquinoxaline) with linearized plasmid DNA at 5, 10, 20, 100, 200, 300 DNA bp: mc ratios. All results represented as a percent of the untreated control. Along the y-axis, the designation "IDV" represents the integrated density value of the ethidium bromide fluorescence averaged over three equivalent metal-DNA experiments for each respective metal complex. Along the x-axis, individual histograms corresponding to each metal complex are shown.

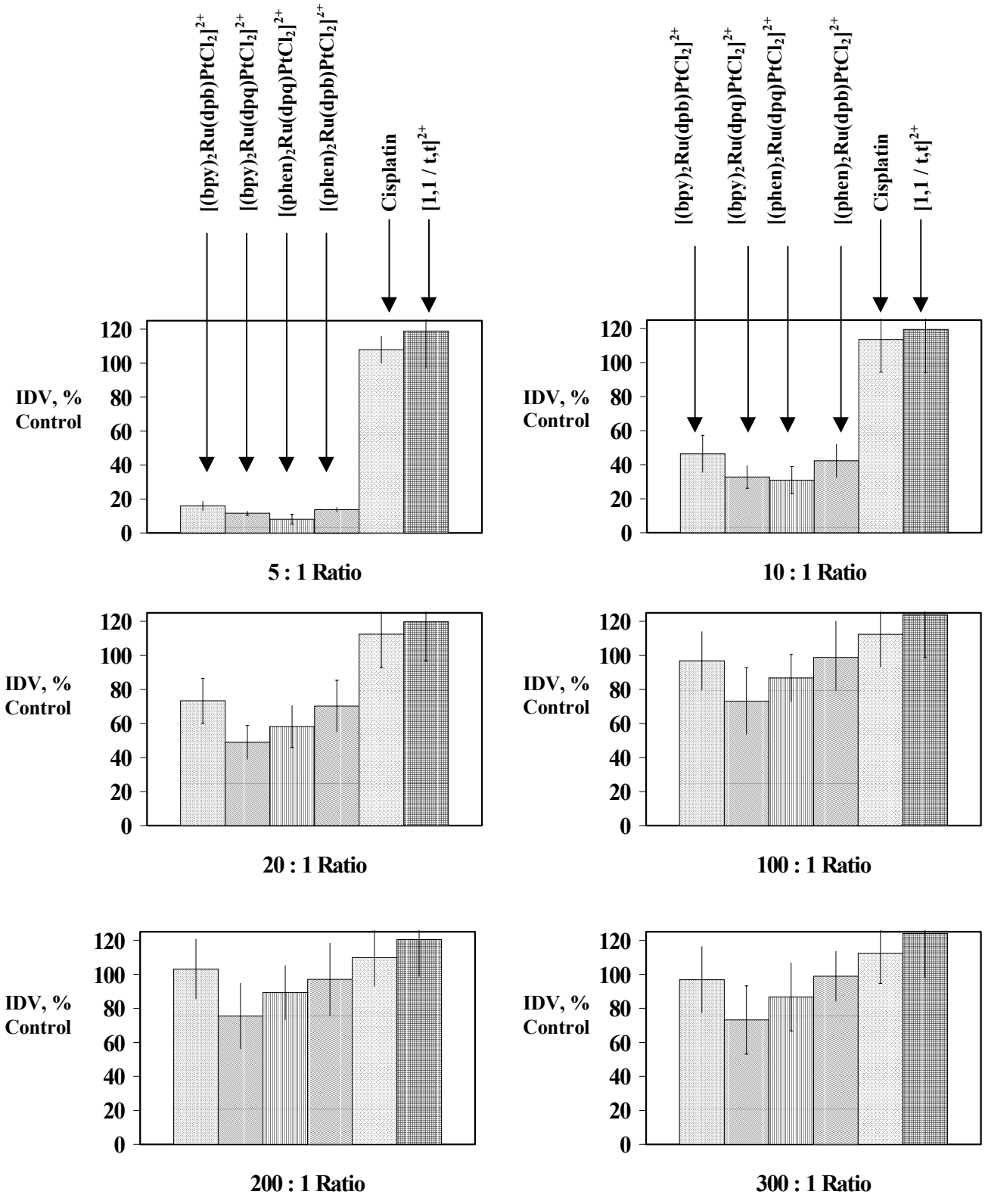
[(bpy)2Ru(dpb)PtCl2]2+
[(bpy)2Ru(dpq)PtCl2]2+
[(phen)2Ru(dpq)PtCl2]2+
[(phen)2Ru(dpb)PtCl2]2+
Cisplatin
[1,1 / t,t]2+
IDV, % Control
0
20
40
60
80
100
120
5 : 1 Ratio
10 : 1 Ratio
20 : 1 Ratio
100 : 1 Ratio
200 : 1 Ratio
300 : 1 Ratio

intensity is significantly reduced relative to the untreated control. This effect is most pronounced for the 5:1 ratio, in which the average IDV values are in the range of 0-20% of the untreated control. As the DNA bp: mc ratio was increased (corresponding to a decrease in metal concentration), there is less of an effect on ethidium bromide fluorescence intensity. This corresponds to a range of 25-50% for the 10: 1 DNA bp: mc ratio and 50-80% for the 20: 1 ratio. At the 100:1 DNA bp: mc ratio the average IDV values begin to closely resemble that observed for the untreated control, a trend which continues through the 300: 1 DNA bp: mc ratio. For these ratios, the average IDV values all fall within 75-100% of the untreated control.

Appendices C-1 to C-13 show the numerical data used to construct Figures 3.21 and 3.22, and included is the %RSD information for each metal complex at the DNA bp: mc ratios examined. This data shows that the binding of the four Ru-Pt complexes to DNA reduces the fluorescence intensity of intercalated ethidium bromide. The %RSD data indicates that the comparison of relative fluorescence intensity within a gel quantitates the reduction of emission as our Ru-Pt complexes are added. The direct reproducibility of these gel densitometry results are not high while relative reproducibility is quite reasonable. This data shows a remarkable difference between the Ru-Pt complexes and the cisplatin and 1,1/t,t standards.

The binding of cisplatin and 1,1/t,t to DNA does not cause a measurable decrease in ethidium bromide fluorescence intensity in comparison to the untreated control. As stated previously, the binding of cisplatin distorts the structure of the DNA double helix, unwinding and bending it to a magnitude dictated by the type of adduct formed.[27-29] These results suggest that the structural distortions caused by cisplatin-DNA binding do not affect the intercalation of ethidium bromide. In addition, these complexes do not quench the fluorescence of ethidium bromide.

The observed concentration-dependent decrease in ethidium bromide fluorescence intensity (decreased average IDV) for the binding of the Ru-Pt complexes to DNA may be due to several factors. First, the binding of the Ru-Pt complexes to the DNA may distort

DNA structure, inhibiting the intercalation of ethidium bromide. Second, the Ru-Pt complexes may intercalate into DNA, interfering with ethidium bromide intercalation. Third, the Ru-Pt complexes may quench the fluorescence of ethidium bromide. Fourth, the DNA may be precipitating from the metal-DNA reaction.

The first possible factor suggests binding of the Ru-Pt complexes may distort DNA structure and therefore inhibit intercalation of ethidium bromide. Since the Ru-Pt complexes share the *cis*- $PtCl_2$ active site of cisplatin, it is reasonable to suggest that the binding of the Ru-Pt complexes to DNA may induce similar structural distortions as cisplatin upon binding to DNA. These structural distortions may inhibit the intercalation of ethidium bromide, thereby causing a reduction in fluorescence intensity. The results obtained for cisplatin, however, cast doubt on this possibility. However, it is possible that the Ru- Pt complexes, due to their different structure and/or DNA binding mode, may induce more dramatic DNA distortions and therefore inhibit ethidium bromide intercalation to a higher degree than cisplatin. The validity of this idea cannot be confirmed at this time and is the subject for future investigations.

The second possible factor suggests intercalation of the Ru-Pt complex into the DNA helix could lead to decreased ethidium bromide fluorescence. Lippard and co-workers have shown that a series of monometallic platinum and palladium complexes having planar aromatic ligands terpy, phen and bpy (terpy = 2, 2′, 2′′-terpyridine, phen = 1,10-phenanthroline, bpy = 2,2′ -bipyridine) interfered with the fluorescence enhancement of ethidium bromide by competing for intercalation sites on calf-thymus DNA.[73] These complexes also unwind plasmid DNA as analyzed by gel electrophoresis. These two observations strongly suggest intercalation.[68] Since the Ru-Pt complexes contain similar, planar aromatic ligands and also interfere with the fluorescence enhancement of ethidium bromide, intercalation of these complexes into the DNA helix may be occurring.

The native gel analysis for the interaction of the monometallic synthons $[(bpy)_2Ru(BL)](CF_3SO_3)_2$ and $[(phen)_2Ru(BL)](CF_3SO_3)_2$ (where BL = dpq and dpb) shows no effect on fluorescence of ethidium bromide. This data suggests that intercalation

into DNA is not responsible for the fluorescence quenching by the Ru-Pt complexes. These complexes may exhibit a weaker intercalative interaction than the Pt-polypyridyl compounds examined by Lippard and co-workers.[68, 73] Under electrophoresis conditions, these cationic complexes might be "pulled" out of the DNA helix. The DNA would then migrate towards the negative electrode at an otherwise "normal" rate. This would then lead to no reduction in ethidium bromide fluorescence and no effect on DNA migration. At this time, this idea has not been explored and is the subject of further investigations.

The third possible factor suggests fluorescence quenching by the Ru-Pt complexes could also be a cause of this effect. Numerous molecules have been shown to quench the fluorescence of intercalated ethidium bromide.[178- 180] Examples include the porphryin cations, *meso*-tetrakis-(4-*N*-trimethylaminobenzyl)porphin (TTP), *meso*-tetrakis-(4-*N*-dimethylaminobenzyl)porphin (TDP), the pyridyl cationic surfactant hexadecylpyridium bromide (HPB), the antitumor agent amsacrine, and the terbium cation. The quenching mechanism of the porphyrins, the surfactant and the terbium cation are presently unknown, while an electron transfer mechanism has been implicated for amsacrine. At present, the mechanism by which the Ru-Pt complexes could quench the ethidium bromide fluorescence is undetermined. Due to the spectral overlap between the absorption spectra of the Ru-Pt complexes (dpq complexes, MLCT at 588 nm, dpb complexes MLCT at 634 nm) and the emission spectrum of ethidium (λ_{max} emission = 600 nm) an energy transfer mechanism is possible. Studies exploring this possibility have been conducted and the results are shown in a later section of this manuscript.

The fourth possible factor suggests DNA precipitation by the positively charged Ru-Pt complexes could also account of the decrease of ethidium bromide fluorescence intensity. If precipitation occurred during the metal-DNA reactions prior to gel electrophoresis, then less DNA would be loaded on the gel. Once the DNA ran through the gel less DNA would be available for ethidium bromide staining and hence result in a decrease in ethidium bromide fluorescence intensity. DNA precipitation and emission quenching studies have been performed to probe further the cause of this reduction in fluorescence of ethidium bromide.

DNA Precipitation Studies

It has previously been shown that a concentration-dependent loss of ethidium fluorescence intensity is observed upon the binding of all four Ru-Pt complexes to DNA. A possible explanation for this occurrence is precipitation of the DNA from the metal-DNA reaction solution owing to the cationic nature of our metal complexes and the known "salting out" ability of DNA. This would result in less DNA in solution and thus less DNA being loaded onto the electrophoresis gel. This would then bind less ethidium bromide, and hence exhibit less fluorescence. In order to determine if the DNA is precipitating during the metal-DNA binding reactions, reactions were monitored by electronic absorption spectroscopy. Examining an initial and final UV-vis spectrum of the metal-DNA reaction solution should provide some insight into this possibility. All four Ru-Pt complexes as well as the cisplatin and 1,1/t,t standards were examined in this study.

The rationale behind this experimental technique is Beer's Law. Beer's Law is defined as:

$$\mathbf{A = \varepsilon cL}$$

Where A = absorbance of the solution, ε = extinction coefficient in $M\text{-}cm^{-1}$, c = concentration in mol/l, L = path length of spectrophotometric cell in cm.
Since absorbance is directly related to concentration, any loss of absorbance of the metal-DNA solution may be indicative of DNA/ metal complex precipitation. These experiments were conducted independently of the other metal-DNA interaction experiments, due to the different amounts of metal and DNA used and a reaction volume of 1.0 ml (please refer to the experimental chapter for additional details). The 5: 1 DNA bp: mc ratio was examined since this ratio should produce the most metal-DNA binding and hence the greatest possibility for precipitation. An additional centrifugation step was included after incubation was complete in order to separate any possible precipitate. All experiments were performed in triplicate to assure reproducibility.

Figures 3.23 through 3.28 show the results of the DNA precipitation study for cisplatin, 1,1/t,t, and the four Ru-Pt complexes. Two electronic absorption spectra are represented in each figure. The spectrum labeled "initial" represents the metal-DNA reaction solution immediately after the mixing of the DNA and metal components. The spectrum labeled "final" represents the metal-DNA reaction solution after 4 h incubation (at 37°C) and centrifugation. For each metal complex, both the "initial" spectrum and the "final" spectrum almost completely overlap. This indicates that very little change in absorbance of the metal-DNA reaction solution is occurred over the incubation time period. The percent differences between initial and final absorbance recorded at 260 nm for each metal-DNA precipitation study are shown in Table 3.13.

The results show that DNA/ metal complex was not precipitating from the reaction solution. Evidence for this was the near absence of any loss of absorbance observed after the 4 h incubation and subsequent centrifugation (varying between 0-8.4% difference). This result was observed for all the Ru-Pt complexes as well as the cisplatin and 1,1/t,t standards. If DNA/metal complex precipitation was indeed occurring, the concentration of the DNA should decrease, resulting in a loss of absorbance in accordance with Beer's Law. In addition, differences this small cannot be significant. Even at the highest percent difference (8.4%) observed for $[(bpy)_2Ru(dpb)PtCl_2]^{2+}$, these results cannot account for the dramatic loss in ethidium bromide fluorescence intensity shown in the densitometry studies. In those studies, at 5: 1 bp: mc ratio, the ethidium bromide fluorescence for $[(bpy)_2Ru(dpb)PtCl_2]^{2+}$-bound DNA was approximately 18% of that observed for the untreated control. A 8.4% loss in DNA cannot account of 82% loss in ethidium bromide fluorescence (relative to the untreated control). These results therefore clearly show the loss of fluorescence intensity discussed previously in the native gel studies was not caused by precipitation of the DNA.

Ethidium Bromide Fluorescence Quenching by Ru-Pt Complexes

The native gel electrophoresis studies have shown that the binding of all four Ru-Pt complexes significantly affects the ethidium bromide emission. In order to determine if

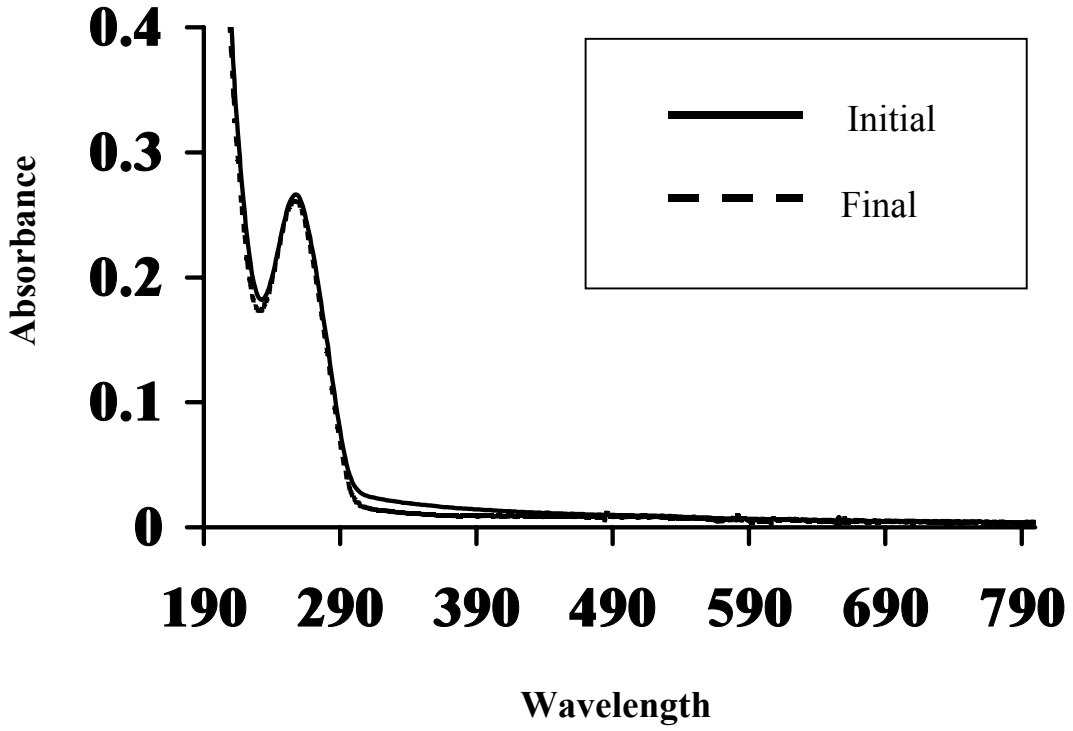

Figure 3.23 DNA precipitation study for *cis*-$[Pt(NH_3)_2Cl_2]$ (cisplatin). Graph of absorbance vs. wavelength for metal-DNA reaction (5:1 DNA bp: mc ratio) immediately following preparation (initial) and after 4 h incubation (37°C) and centrifugation (final). Three trials were accomplished to assure reproducibility.

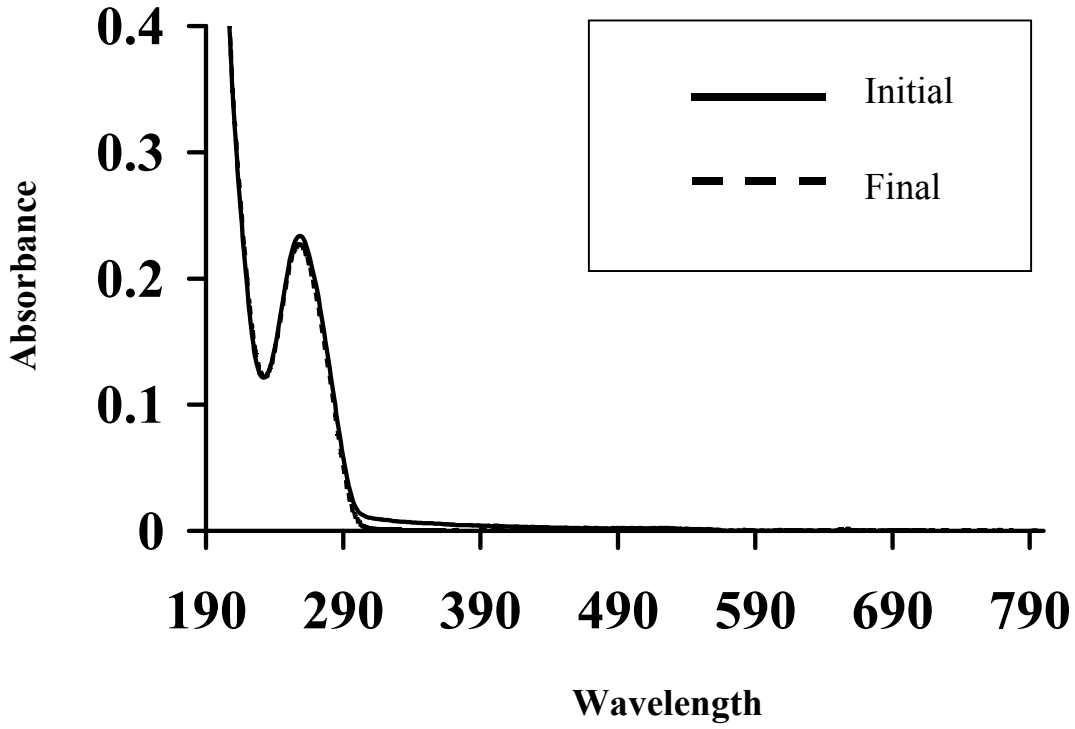

Figure 3.24 DNA precipitation study for *trans*-{[$PtCl(NH_3)_2]_2(\mu$-$H_2N(CH_2)_6NH_2)\}(NO_3)_2$ (1,1/t,t). Graph of absorbance vs. wavelength for metal-DNA reaction (5:1 DNA bp: mc ratio) immediately following preparation (initial) and after 4 h incubation (37°C) and centrifugation (final). Three trials were accomplished to assure reproducibility.

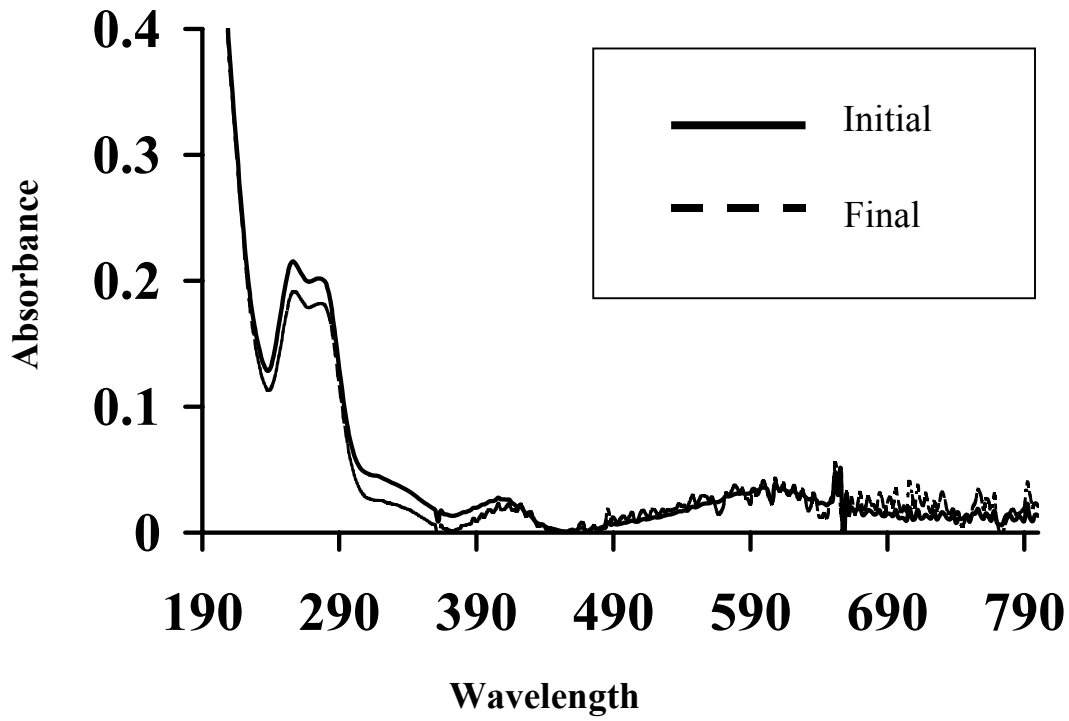

Figure 3.25 DNA precipitation study for $[(bpy)_2Ru(dpq)PtCl_2](CF_3SO_3)_2$ (where bpy = 2,2′-bipyridine and dpq = 2,3-bis(2-pyridyl)quinoxaline). Graph of absorbance vs. wavelength for metal-DNA reaction (5:1 DNA bp: mc ratio) immediately following preparation (initial) and after 4 h incubation (37°C) and centrifugation (final). Three trials were accomplished to assure reproducibility.

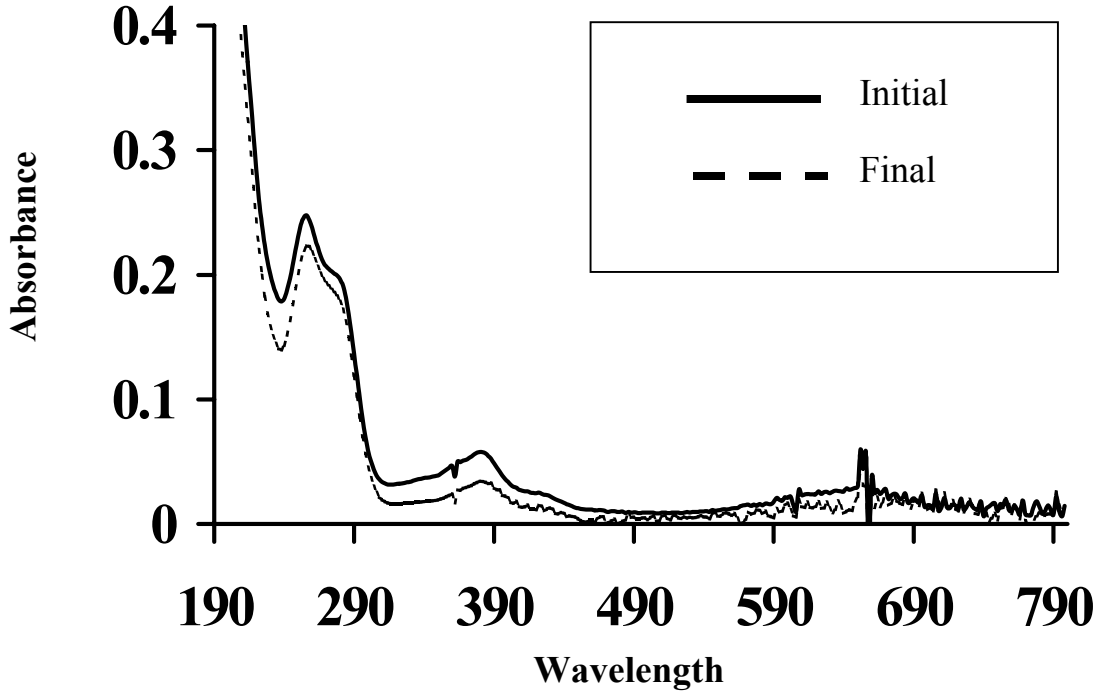

Figure 3.26 DNA precipitation study for $[(bpy)_2Ru(dpb)PtCl_2](CF_3SO_3)_2$ (where bpy = 2,2′-bipyridine, dpb = 2,3-bis(2-pyridyl)benzoquinoxaline). Graph of absorbance vs. wavelength for metal-DNA reaction (DNA Bp: mc ratio) immediately following preparation (initial) and after 4 h incubation (37°C) and centrifugation (final). Three trials were accomplished to assure reproducibility.

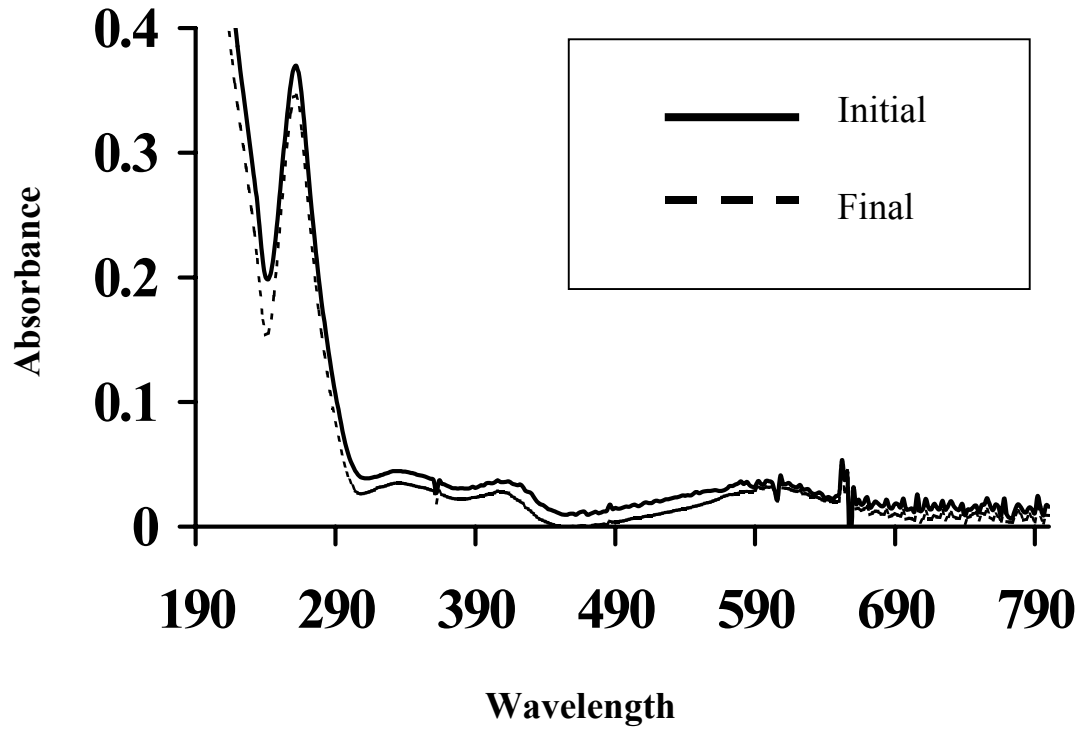

Figure 3.27 DNA precipitation study for $[(phen)_2Ru(dpq)PtCl_2](CF_3SO_3)_2$ (where phen = 1,10-phenanthroline, dpq = 2,3-bis(2-pyridyl)quinoxaline). Graph of absorbance vs. wavelength for metal-DNA reaction (5:1 DNA bp: mc ratio) immediately following preparation (initial) and after 4 h incubation (37°C) and centrifugation (final). Three trials were accomplished to assure reproducibility.

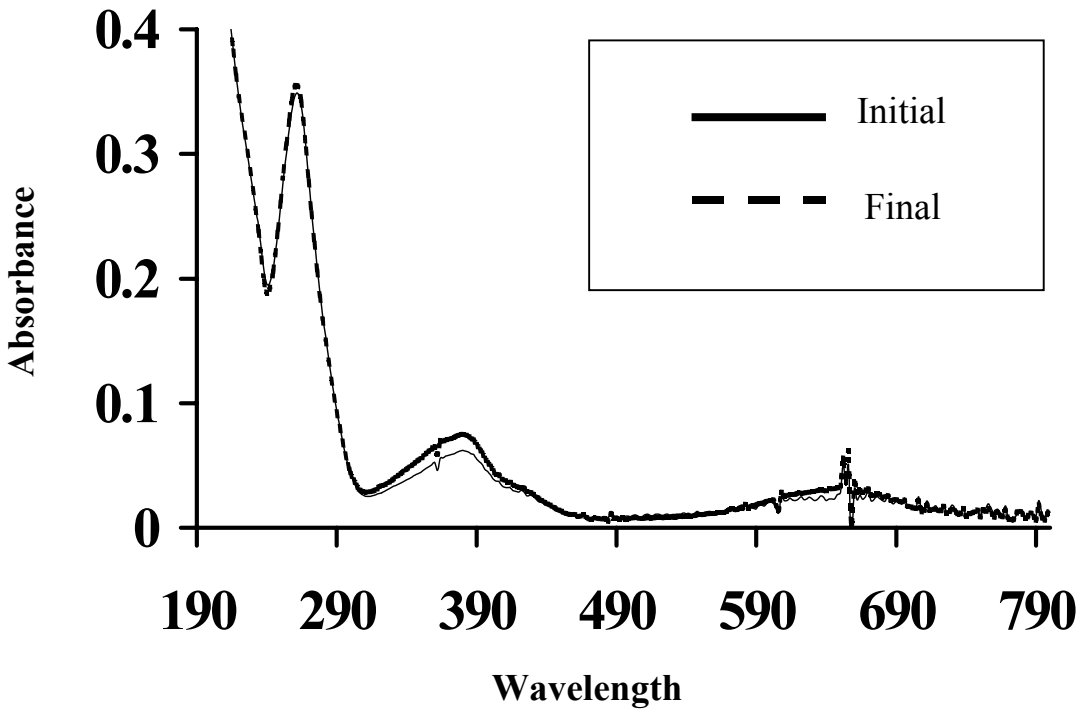

Figure 3.28 DNA precipitation study for $[(phen)_2Ru(dpb)PtCl_2](CF_3SO_3)_2$ (where phen = 1,10-phenanthroline dpb = 2,3-bis(2-pyridyl)benzoquinoxaline). Graph of absorbance vs. wavelength for metal-DNA reaction (5:1 DNA bp: mc ratio) immediately following preparation (initial) and after 4 h incubation (37°C) and centrifugation (final). Three trials were accomplished to assure reproducibility.

Table 3.13 Percent differences between initial and final absorbance recorded at 260 nm, for each metal-DNA precipitation study. Percent differences were calculated by $(A_{Initial} - A_{Final})/ A_{initial} \times 100$. bpy = 2,2′-bipyridine, phen = 1,10-phenanthroline, dpq = 2,3-bis(2-pyridyl)quinoxaline, dpb = 2,3-bis(2-pyridyl)benzoquinoxaline.

Complex	% difference, abs @ 260 nm
cisplatin	2.3 %
1,1/t,t	0 %
$[(bpy)_2Ru(dpq)PtCl_2](CF_3SO_3)_2$	5.2 %
$[(bpy)_2Ru(dpb)PtCl_2](CF_3SO_3)_2$	8.4 %
$[(phen)_2Ru(dpq)PtCl_2](CF_3SO_3)_2$	6.0 %
$[(phen)_2Ru(dpb)PtCl_2](CF_3SO_3)_2$	2.3 %

the Ru-Pt complexes quench the fluorescence of ethidium bromide, the emission of ethidium bromide in fluid solution was examined holding the concentration of ethidium bromide constant while varying the concentration of metal complex. To provide a basis for comparison, similar experiments were conducted for cisplatin and 1,1/t,t. One trial was accomplished for each respective metal complex.

The results for the emission quenching study for cisplatin and 1,1/t,t are shown in Figure 3.29. Emission spectra and intensity data used to construct this figure and all remaining figures for this section are shown in Appendices D-1 to D-6. All experiments were conducted at room temperature in ddH_2O, with a 3.0 ml final volume. An excitation spectrum of ethidium bromide was first obtained, and as a result the excitation wavelength was set at 347 nm and the 500 – 700 nm range scanned for emission. A control experiment using only ethidium bromide (no metal added) was examined first. The emission intensity of the ethidium bromide was then measured in the presence of increasing amounts of metal complex. The results are reported as a percentage of the emission intensity observed in the control experiment (100% ethidium bromide, no metal added). As shown in Figure 3.29, the emission intensity of ethidium bromide in the presence of cisplatin or 1,1/t,t was constant.

The results of an equivalent study for $[(bpy)_2Ru(dpq)PtCl_2](CF_3SO_3)_2$ and $[(bpy)_2Ru(dpb)PtCl_2](CF_3SO_3)_2$ are shown in Figure 3.30. The results here contrast markedly with that obtained for cisplatin and 1,1/t,t. In this case, the emission intensity of ethidium bromide was strongly affected, decreasing in intensity with increasing amounts of metal complex. At the 100:1 ethidium bromide: Ru-Pt complex ratio, the emission was slightly less than the ethidium bromide control containing no metal complex. At the 20 and 10: 1 ratio, the emission decreased, falling within 80 – 100% of the ethidium bromide control. At the 5: 1 ratio, the emission was further reduced, falling within 60- 80% of the ethidium bromide control. However at the final ratio examined, 1:1 ethidium bromide: metal complex, the emission was 20 – 40% of the ethidium bromide control.

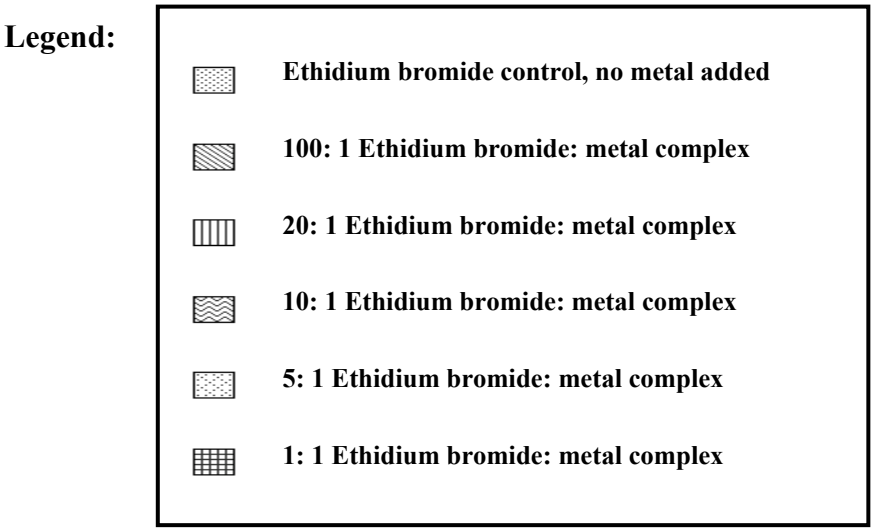

Figure 3.29 **(following page)** Ethidium bromide quenching study for *cis*-$[Pt(NH_3)_2Cl_2]$ (cisplatin) and *trans*-$\{[PtCl(NH_3)_2]_2(\mu\text{-}H_2N(CH_2)_6NH_2)\}(NO_3)_2$ (1,1/t,t). Emission intensity was monitored keeping the concentration of ethidium bromide constant while varying the concentration of metal complex at 100, 20, 10, 5, and 1 ethidium bromide: metal complex ratios. For comparison purposes, a solution containing 100% ethidium bromide (no metal added) was also examined under the same conditions. Emission intensity reported as a percentage of the emission intensity for 100% ethidium bromide (no metal added) experiment.

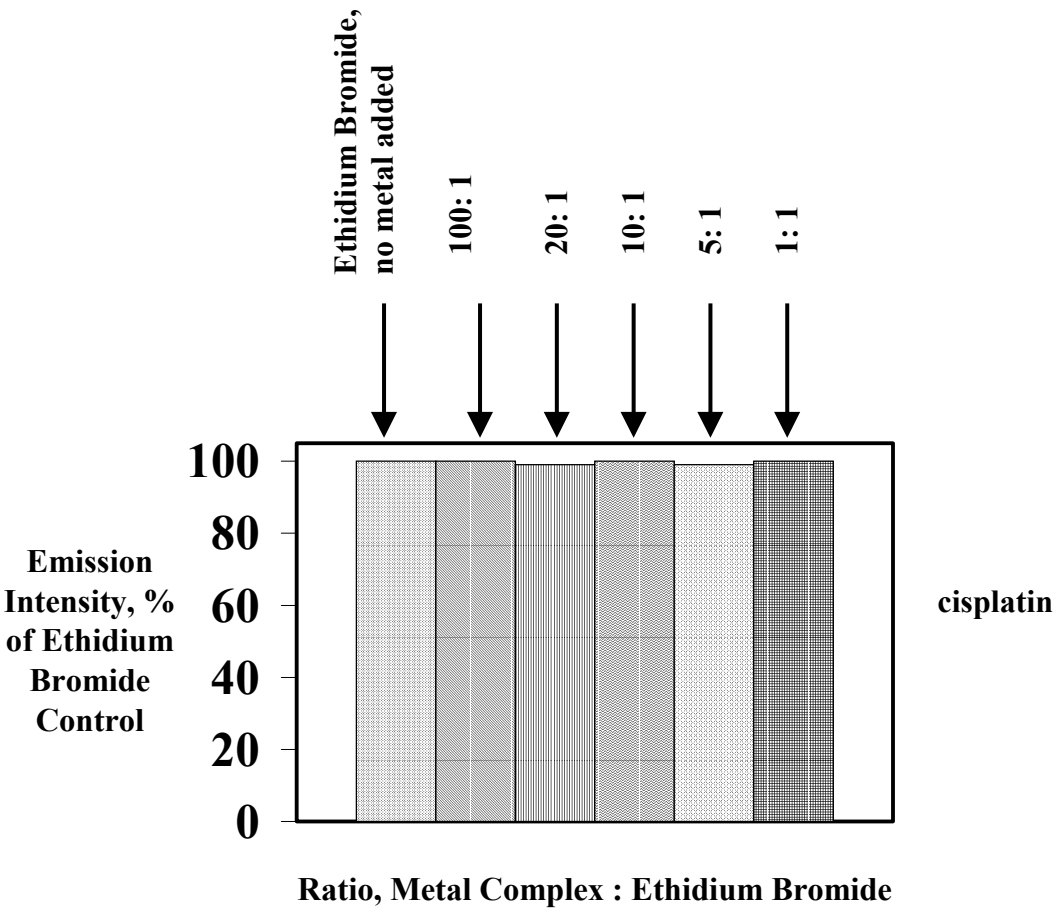
Ethidium Bromide, no metal added
100: 1
20: 1
10: 1
5: 1
1: 1
100
80
60
40
20
0
Emission Intensity, % of Ethidium Bromide Control
cisplatin
Ratio, Metal Complex : Ethidium Bromide

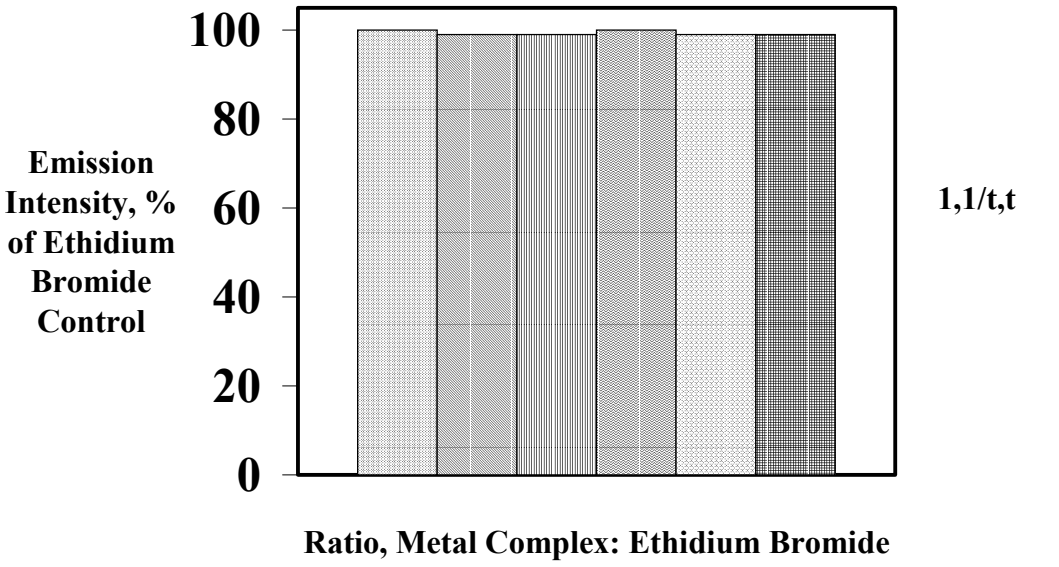
100
80
60
40
20
0
Emission Intensity, % of Ethidium Bromide Control
1,1/t,t
Ratio, Metal Complex: Ethidium Bromide

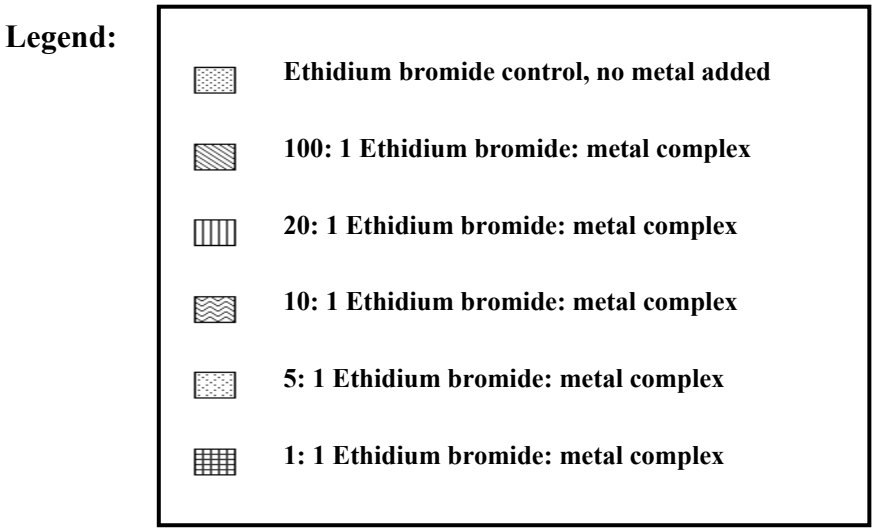

Figure 3.30 **(following page)**. Ethidium bromide quenching study for $[(bpy)_2Ru(dpq)PtCl_2](CF_3SO_3)_2$ and $[(bpy)_2Ru(dpb)PtCl_2](CF_3SO_3)_2$ (where bpy = 2,2′-bipyridine, dpq = 2,3-bis(2-pyridyl)quinoxaline, 2,3-bis(2-pyridyl)benzoquinoxaline). Emission intensity was monitored keeping the concentration of ethidium bromide constant while varying the concentration of metal complex at 100, 20, 10, 5, and 1 ethidium bromide: metal complex ratios. For comparison purposes, a solution containing 100% ethidium bromide (no metal added) was also examined under the same conditions. Emission intensity reported as a percentage of the emission intensity for the 100% ethidium bromide (no metal added) experiment.

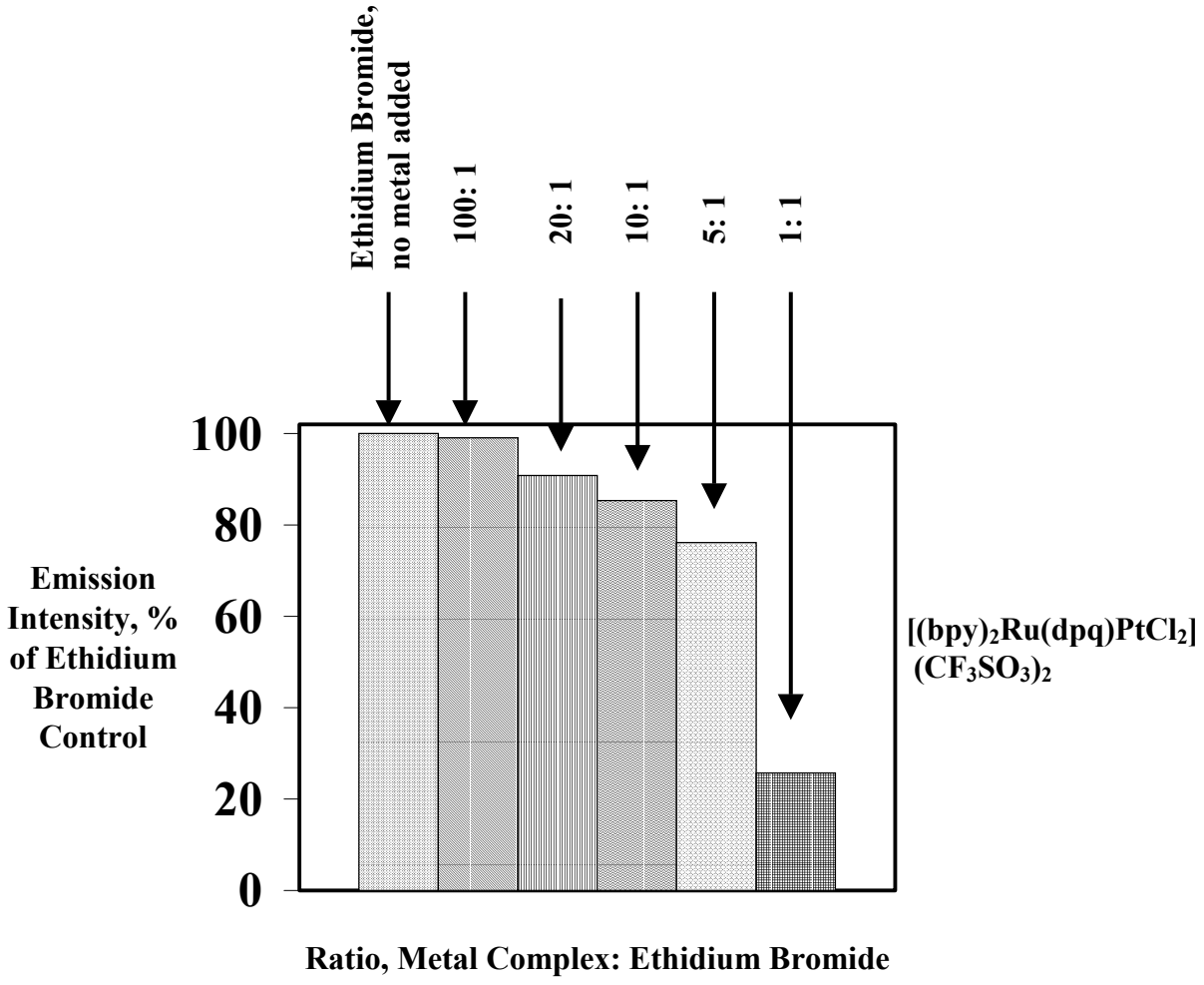
Ethidium Bromide, no metal added
100: 1
20: 1
10: 1
5: 1
1: 1
100
80
60
40
20
0
Emission Intensity, % of Ethidium Bromide Control
[(bpy)2Ru(dpq)PtCl2] (CF3SO3)2
Ratio, Metal Complex: Ethidium Bromide

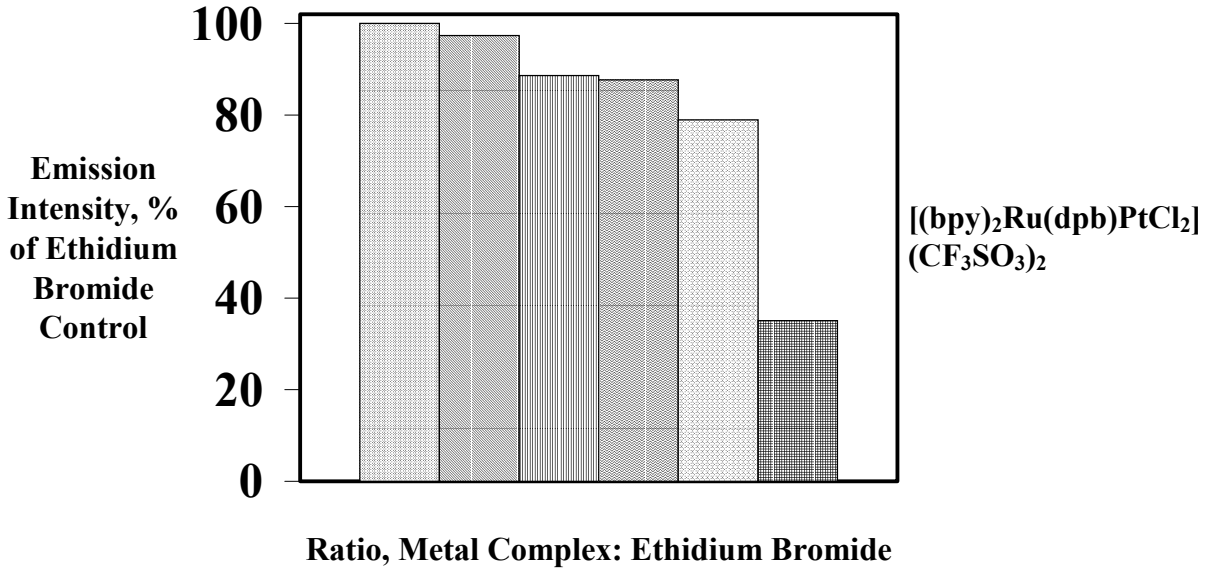
100
80
60
40
20
0
Emission Intensity, % of Ethidium Bromide Control
[(bpy)2Ru(dpb)PtCl2] (CF3SO3)2
Ratio, Metal Complex: Ethidium Bromide

The results of an equivalent study for $[(phen)_2Ru(dpq)PtCl_2](CF_3SO_3)_2$ and $[(phen)_2Ru(dpb)PtCl_2](CF_3SO_3)_2$ are shown in Figure 3.31. The results for these complexes are quite similar to the bpy-analogs. At the 100:1 ethidium bromide: Ru-Pt complex ratio, the ethidium bromide emission was barely affected (approx. 100% of the ethidium bromide control). At the 20 and 10: 1 ratio, the ethidium bromide emission decreased, falling within 80 – 100% of the ethidium bromide control. At the 5: 1 ratio, the ethidium bromide emission was further reduced, falling within 60- 80% of the ethidium bromide control. At the final ratio examined, 1:1 ethidium bromide: metal complex, the ethidium bromide emission was 20 – 40% of the ethidium bromide control.

The results presented here demonstrate that all four Ru-Pt complexes quench the ethidium bromide emission. Complexes of this type are known energy transfer quenchers of many chromophores. This suggests that the reduced ethidium bromide fluorescence observed in the native gels could be due to fluorescence quenching of intercalated ethidium bromide by the Ru-Pt complexes. Within these gel experiments, the DNA could be considered as a type of "support," bringing the emitter (ethidium bromide) and potential quencher (Ru-Pt complex) very close together. This should therefore enhance the efficiency for energy transfer quenching. This effect has been the subject of many studies as local concentration is enhanced. It should be noted however, that these experiments were not repeated and that additional work should be accomplished to further demonstrate reproducibility.

Denaturing Gel Studies: Concentration-Dependent Interaction with DNA

In a previous section, native gel electrophoresis was used to analyze the reaction of our Ru-Pt complexes with DNA. It was determined that the complexes retarded the migration of DNA through the gel in a concentration-dependent fashion. Similar, but less dramatic results were obtained for cisplatin and 1,1/t,t. This shows the Ru-Pt complexes undergo a strong covalent reaction that significantly alters the size, shape and/ or charge of the DNA molecules. However, the similarity of the results for cisplatin and 1,1/t,t indicated that these experiments did not differentiate between complexes that form

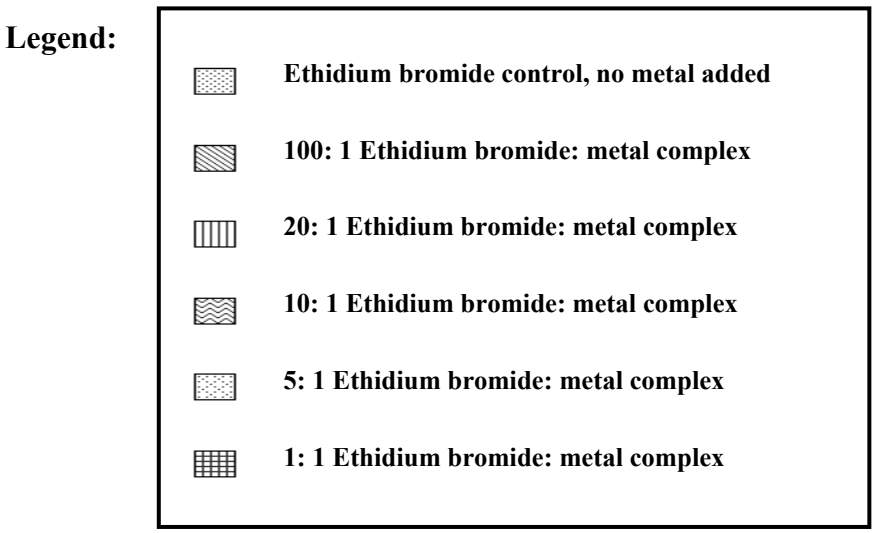

Figure 3.31 **(following page).** Ethidium bromide quenching study for $[(phen)_2Ru(dpq)PtCl_2](CF_3SO_3)_2$ and $[(phen)_2Ru(dpb)PtCl_2](CF_3SO_3)_2$ (where phen= 1,10-phenanthroline, dpq = 2,3-bis(2-pyridyl)quinoxaline, 2,3-bis(2-pyridyl)benzoquinoxaline).. Fluorescence intensity was monitored keeping the concentration of ethidium bromide constant while varying the concentration of metal complex at 100, 20, 10, 5, and 1 ethidium bromide: metal complex ratios. For comparison purposes, a solution containing 100% ethidium bromide (no metal added) was also examined under the same conditions. Fluorescence intensity reported as a percentage of emission intensity for the 100% ethidium bromide (no metal added) experiment.

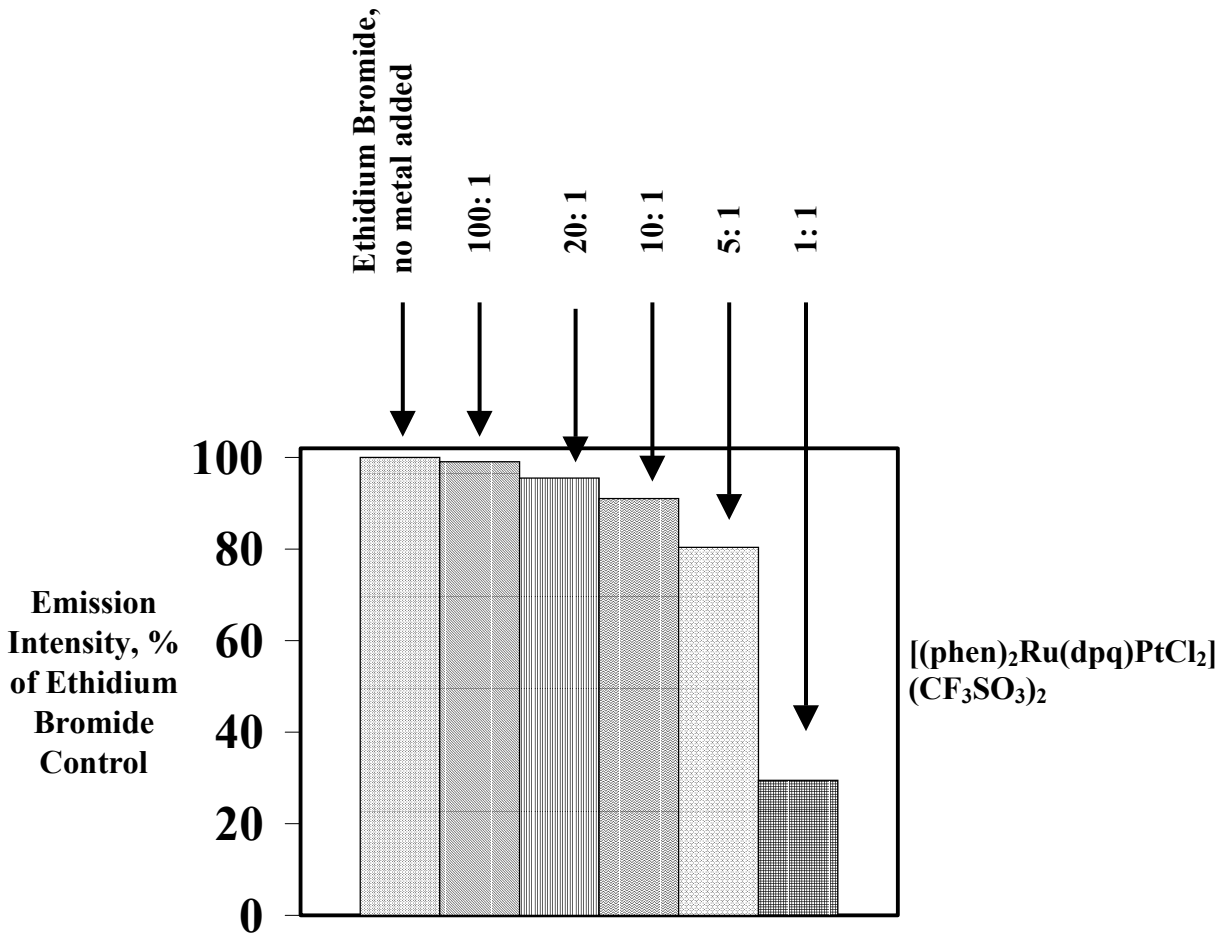
Ethidium Bromide, no metal added
100: 1
20: 1
10: 1
5: 1
1: 1
100
80
60
40
20
0
Emission Intensity, % of Ethidium Bromide Control
[(phen)2Ru(dpq)PtCl2] (CF3SO3)2
Ratio, Metal Complex: Ethidium Control

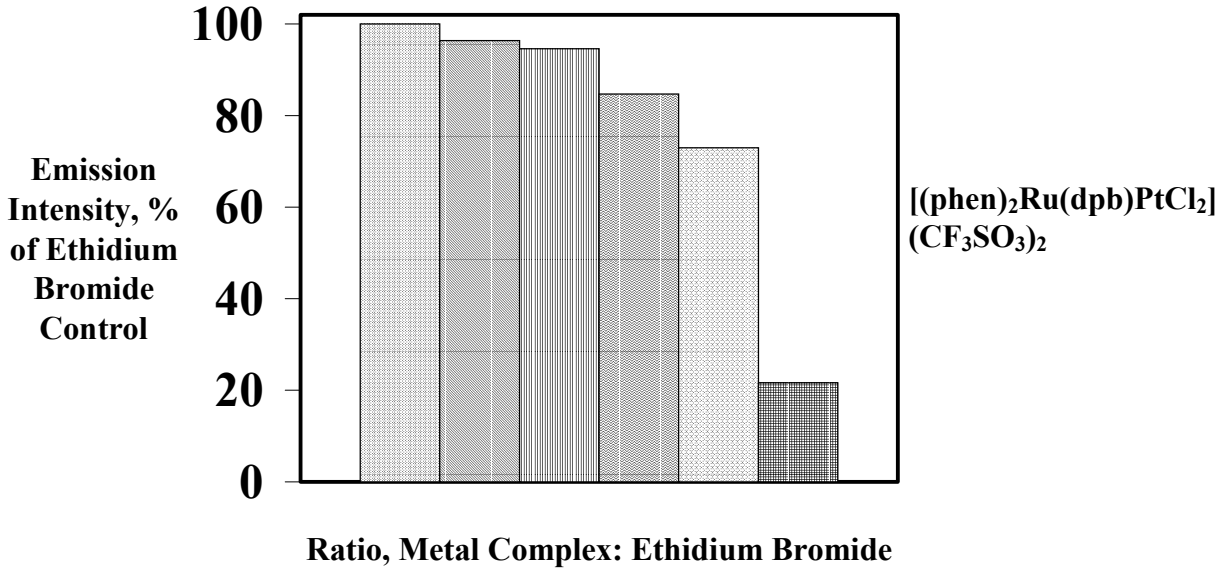
100
80
60
40
20
0
Emission Intensity, % of Ethidium Bromide Control
[(phen)2Ru(dpb)PtCl2] (CF3SO3)2
Ratio, Metal Complex: Ethidium Bromide

primarily intrastrand crosslinks (cisplatin) and those that form primarily interstrand crosslinks (1,1/t,t). The difference between intrastrand and interstrand crosslinks is illustrated in Figure 3.32.

As with the native gel studies, metal-DNA reactions were performed with linearized plasmid DNA in a range of DNA base pair (bp) to metal complex (mc) ratios. During the incubation, the DNA was double stranded. The DNA was then denatured in the gel loading solution, which is 50 mM in NaOH. Following this, the DNA is loaded on the gel, which is also 50 mM in NaOH. Next, the DNA on the gel is renatured and stained with ethidium bromide for detection of the DNA bands. To provide a basis of comparison, equivalent experiments were conducted with the known DNA binders cisplatin and 1,1/t,t. These two complexes served to show the behavior of intrastrand and interstrand crosslinked DNA under the conditions of these experiments, as cisplatin

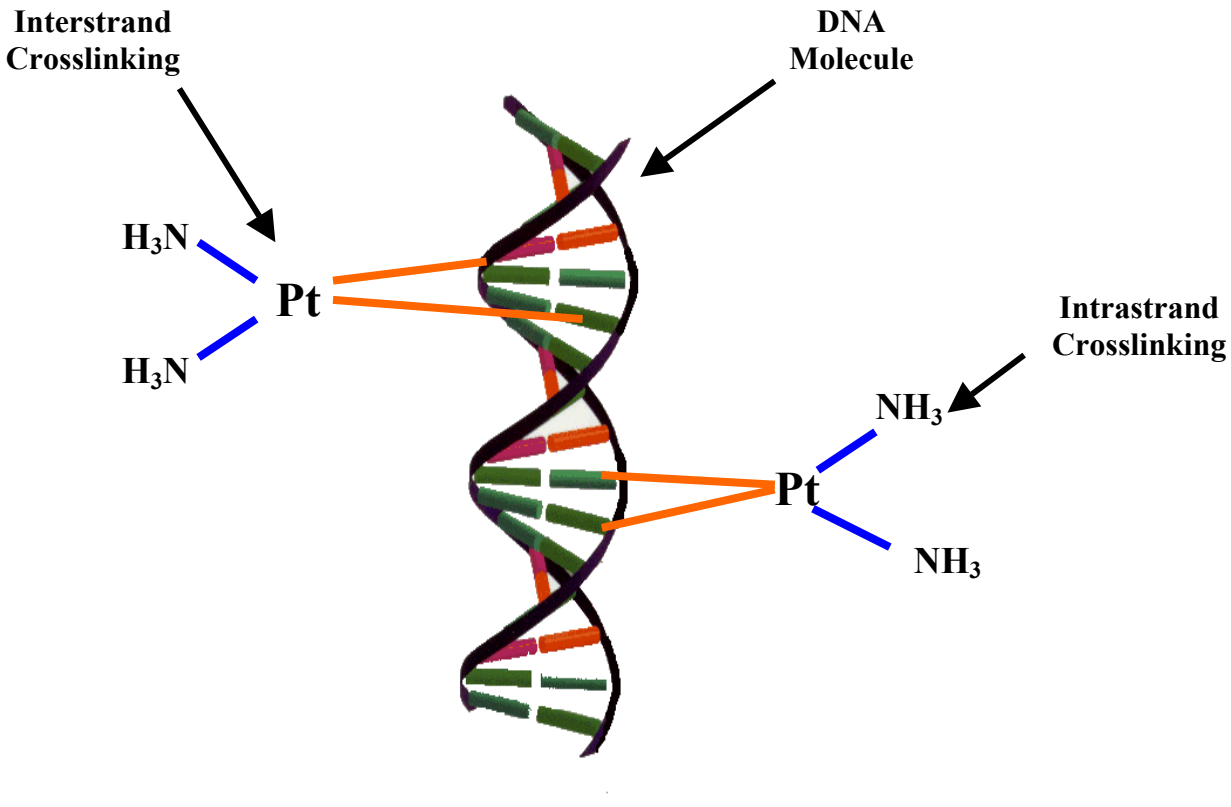

Figure 3.32 Schematic representation of intrastrand and interstrand crosslinking.

undergoes ≈ 3% interstrand crosslinking and 1,1/t,t ≈ 100% interstrand crosslinking.[160]

The results of denaturing gel analysis of the DNA binding of cisplatin are shown in Figure 3.33. At the 300: 1 bp: mc ratio, which represents the lowest amount of metal complex, the DNA migrates through the gel at approximately the same rate as the control that was not treated with metal complex (C). As the amount of metal complex was increased and the DNA bp: mc ratio decreased, two forms of DNA begin to appear in the gel (illustrated in Figure 3.33 as Form I & II). The second form (Form II) appeared at bp: mc ratios of ≤ 20. Under conditions at which the two forms were present, one form migrated at a rate similar to the untreated control (2958 nucleotides (nt)) and the other migrated much more slowly through the gel, just ahead of the 6557 nt DNA fragment in the standard (Form II). For cisplatin, the predominant form of DNA observed at all bp: mc ratios except the lowest used, 5:1, is the form that migrated at a rate similar to the untreated control (Form I).

The results of the denaturing gel analysis of the binding of 1,1/t,t to linearized plasmid DNA are shown in Figure 3.34. The results observed for 1,1/t,t were remarkably different than those for cisplatin. At the highest bp: mc ratios, representing the lowest amount of metal complex, the majority of the DNA was in a form that migrated much more slowly through the gel (Form II) than the untreated control, slightly ahead of the 6557 nt standard. Only a very small fraction of the DNA migrated through the gel at a rate similar to that of the untreated control (Form I) and only at bp: mc ratios in excess of 200: 1. In addition, the migration of the major from of DNA observed in this study changed as the bp: mc ratio was reduced from 200: 1 to 20: 1. The migration of DNA through the gel increased as the bp: mc ratio was decreased and then leveled off at a position near that of the 4361 nt standard. At the bp: mc ratio where the migration of this form of the DNA was changing, the band was also more diffuse.

Examination of the results for cisplatin and 1,1/t,t has revealed the usefulness of denaturing agarose gel electrophoresis for differentiating between complexes that form

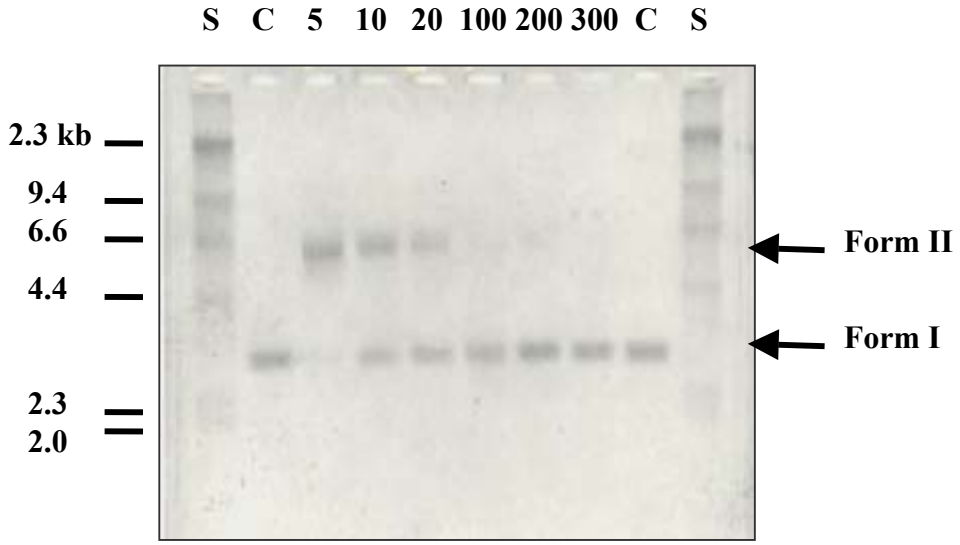

Figure 3.33 Denaturing agarose gel electrophoresis of the interaction of *cis*-$[Pt(NH_3)_2Cl_2]$ (cisplatin) with linearized plasmid DNA. One μg of linearized plasmid DNA was incubated with metal complexes at a ratio of 5, 10, 20, 100, 200, or 300 base pairs to 1 metal complex at 37 °C for 4 h. A control sample (C) containing only linearized plasmid DNA (no metal added) was incubated under identical conditions. Samples containing 100 ng of DNA were analyzed on denaturing agarose gels, which were then stained with 0.5 mg/ml ethidium bromide and photographed under UV illumination. A molecular weight standard (S) was included for reference.

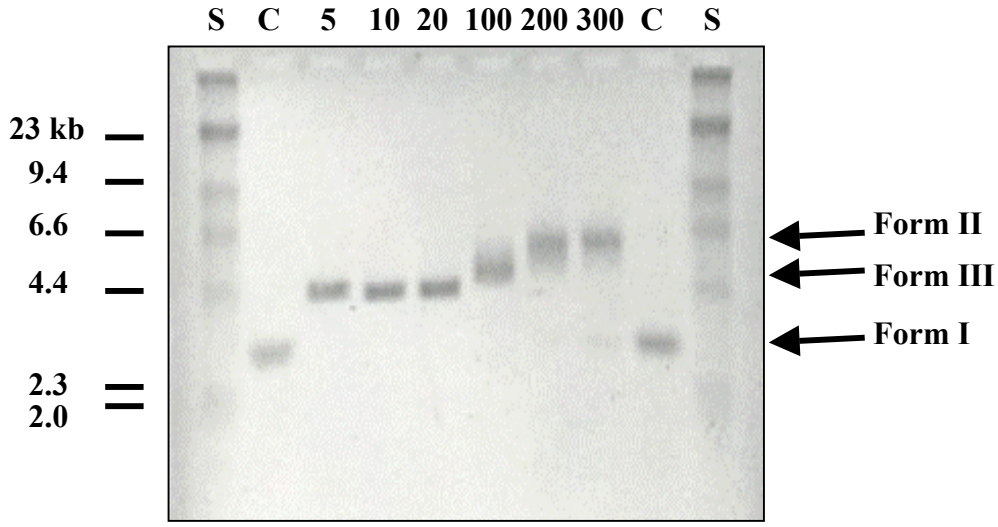

Figure 3.34 Denaturing agarose gel electrophoresis of the interaction of [{ *trans*-$PtCl(NH_3)_2\}_2(\mu\text{-}H_2N(CH_2)_4NH_2)](NO_3)_2$ (1,1/t,t) with linearized plasmid DNA. One μg of linearized plasmid DNA was incubated with metal complexes at a ratio of 5, 10, 20, 100, 200, or 300 base pairs to 1 metal complex at 37 °C for 4 h. A control sample (C) containing only linearized plasmid DNA(no metal added) was incubated under identical conditions. Samples containing 100 ng of DNA were analyzed on denaturing agarose gels which were then stained with 0.5 mg/ml ethidium bromide and photographed under UV illumination. A molecular weight standard (S) was included for reference.

primarily intrastrand crosslinks, such as cisplatin, and those that form interstrand crosslinks, such as 1,1/t,t. Under the denaturing conditions of this study, DNA that has only intrastrand crosslinks was able to separate into single-stranded DNA and migrated at a rate similar to the control DNA that was not treated with any metal complex (Form I). This was evident for cisplatin at high DNA bp: mc ratios. As the DNA bp: mc ratio was decreased, a detectable amount of interstrand crosslinking occurs at ratios ≤ 20: 1, due to a higher relative concentration of metal complex. As an interstrand crosslink occurred, the DNA was no longer able to separate into single-stranded DNA under these conditions since the two strands were held together by cisplatin. The result would be a DNA molecule that would migrate much more slowly through the gel than the control (Form II). This would explain the second form of DNA (Form II) observed in the gel, at DNA bp: mc ratios ≤ 20: 1, which migrated at a rate consistent with the two strands bound together, 5916 nt.

The behavior of the 1,1/t,t standard under these denaturing conditions was quite different from cisplatin. In studies by Farrell and co-workers, which used a 65 bp fragmentand denaturing polyacrylamide gel electrophoresis, crosslinking was observed at concentrations as low as 0.5 μM (bp: mc ratio of 12.7: 1) and approximately half of the DNA shifted to a much slower-migrating form at 10 μM 1,1/t,t (bp: mc ratio of 0.63: 1).[44, 45]

Under the conditions of the present study, the results of denaturing gel analysis of 1,1/t,t were quite different than those obtained by Farrell and co-workers. The primary form of DNA migrating through the gel was the interstrand crosslinked form, which was observed at all DNA bp: mc ratios (Form II). Unlike cisplatin and the earlier 1,1/t,t studies, interstrand crosslinks in our method for studying 1,1/t,t appeared at much lower metal concentrations (higher DNA bp: mc ratios), and the DNA bp: mc ratio must be increased to ≥ 300: 1 to detect any of the other form of DNA (Form I). These observations are entirely consistent with the ability of 1,1/t,t to form primarily interstrand crosslinks. In addition, the rate of DNA migration for the 1,1/t,t-reacted DNA varied as the DNA bp: mc ratio changes from 300 to 20: 1. At DNA bp: mc ratios of 200-300: 1,

the interstrand crosslinked DNA migrated at a rate that was consistent with a molecular weight twice that of the single stranded control, i.e. 5916 nt. This result was consistent with the DNA having a few interstrand crosslinks and behaving to a large degree like a DNA strand twice the length of the fragment used. As the bp: mc ratio was decreased, the band became quite diffuse and then sharpened and migrated more rapidly, finally leveling off at a rate consistent with a size of ~ 4.4 kb (Form III). This plateau at a region of smaller molecular weight than the two single strands which are bound together may be indicative of the extensive interstrand crosslinking giving rise to a more compact shape of this 5916 nt DNA.

The more rapid migration and diffuse character of the interstrand-crosslinked forms of DNA (Forms II & III), apparent at much lower concentrations of 1,1/t,t than for cisplatin, can be explained in terms of the large size of this DNA, 2961 bp (Figure 3.35). Using this DNA, when an interstrand crosslink first occurred in a detectable amount, a very small number of interstrand crosslinks were present. The two DNA strands, though

DNA with a small number of interstrand crosslinks (Form II)

DNA with an intermediate number of interstrand crosslinks

DNA with a large number of interstrand crosslinks (Form III)

Figure 3.35 Schematic representing the affects of a small, intermediate and large number of interstrand crosslinks on the size and shape of a DNA molecule.

linked together, were able to move away from each other, forming a molecule with an extended shape that moved very slowly through the gel and at a rate consistent with that of a single 5916 nt strand. As the number of interstrand crosslinks per DNA helix increased, the two DNA strands began to tie together at multiple sites along the strands, subject to the appropriate sequences being present and statistical distribution of binding. The formation of additional crosslinks kept the two strands closer together, making them more compact after being subjected to the denaturing conditions. This led to the observed increase in the DNA migration through the gel as the number of crosslinks increased. At the same time, however, the number of interstrand crosslinks occurred in a variety of locations along the DNA helix. The result was that all DNA molecules with interstrand crosslinks had an overall extended shape, being varied according to the exact locations of the crosslinks on the helix. The migration of such a molecule through an agarose denaturing gel was at a rate approximately consistent with that of a single 5916 nt strand, with a degree of variance due to the variety of shapes that one would expect to observe. This led to a more diffuse band observed at intermediate levels of interstrand crosslinking. As the number of interstrand crosslinks was further increased by further decreasing the bp: mc ratio, the two strands were held together at a large number of sites in a manner that gives a more uniform and compact structure (Form III).

The results of the denaturing gel analysis of the binding of $[(bpy)_2Ru(dpq)PtCl_2](CF_3SO_3)_2$ and $[(bpy)_2Ru(dpb)PtCl_2](CF_3SO_3)_2$ to linearized plasmid DNA are shown in Figure 3.36. At high bp: mc ratios both complexes exhibited behavior that was somewhat similar to cisplatin. For $[(bpy)_2Ru(dpq)PtCl_2](CF_3SO_3)_2$, only one form of DNA was observed at ratios ≥ 200:1, and this form migrated through the gel at a rate that was similar to the untreated control (Form I). Similar behavior was observed for the dpb analog, however a small amount of the second form, migrating just ahead of the 6557 nt standard, appeared in the 200 and 300: 1 samples (Form II). As the bp: mc ratio was decreased to 100: 1 for both complexes the second form of DNA appeared, again migrating slightly ahead of the 6557 nt standard (Form II). This second form migrated through the gel at a rate that increased as the bp: mc ratio was further decreased, and then leveled off (Form III). This occurred at a similar position in the gel as observed for

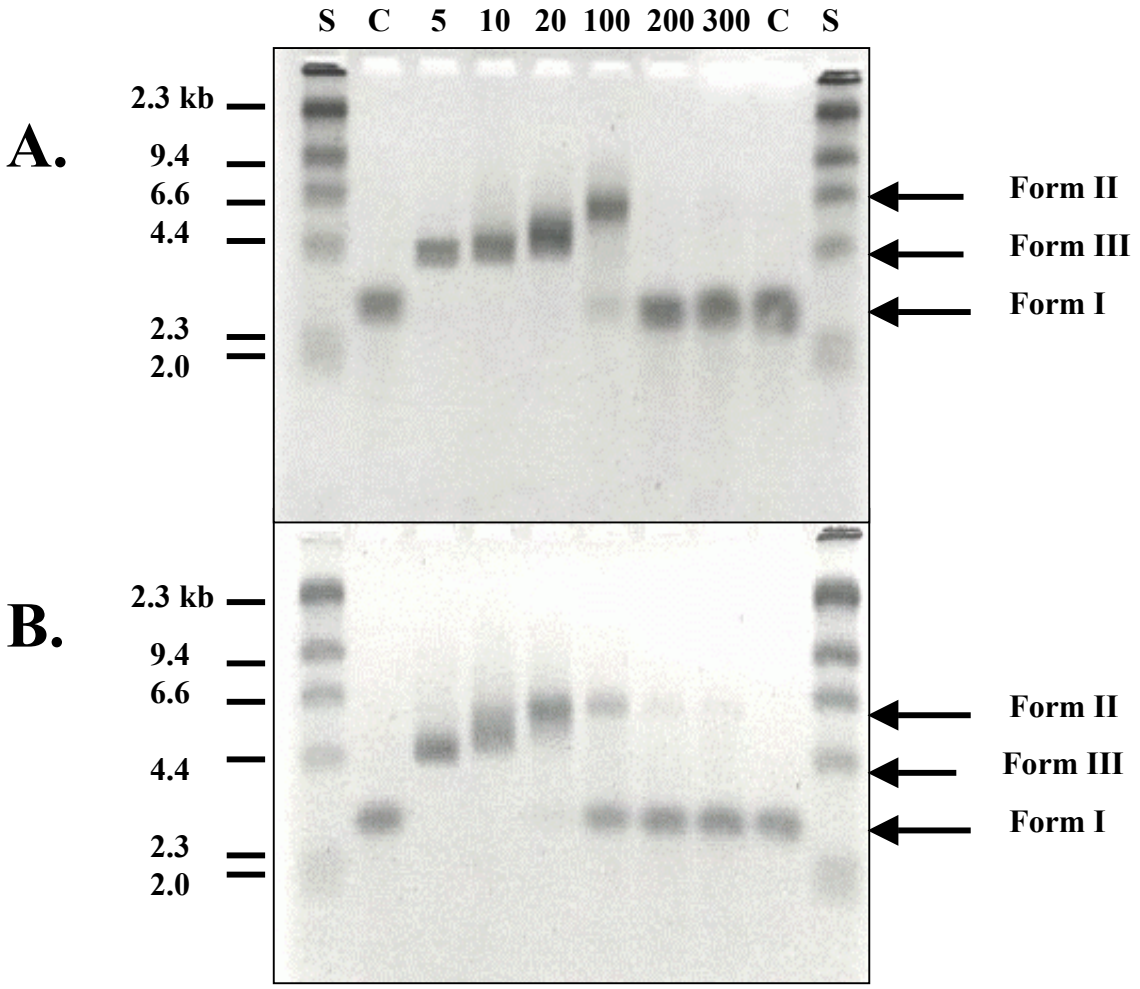

Figure 3.36 Denaturing agarose gel electrophoresis of the interaction of $[(bpy)_2Ru(dpq)PtCl_2](CF_3SO_3)_2$ **(A)** and $[(bpy)_2Ru(dpb)PtCl_2](CF_3SO_3)_2$ **(B)** (where bpy = 2,2′-bipyridine, dpq = 2,3-bis(2-pyridyl)quinoxaline, dpb = 2,3-bis(2-pyridyl) benzoquinoxaline) with linearized plasmid DNA. One μg of linearized plasmid DNA was incubated with metal complexes at a ratio of 5, 10, 20, 100, 200, or 300 base pairs to 1 metal complex at 37 °C for 4 h. A control sample (C) containing only linearized plasmid DNA (no metal added) was incubated under identical conditions. Samples containing 100 ng of DNA were analyzed on denaturing agarose gels, which were then stained with 0.5 mg/ml ethidium bromide and photographed under UV illumination. A molecular weight standard (S) was included for reference.

the 1,1/t,t study, migrating at approximately the same rate as the 4361nt standard. Interestingly, at bp: mc ratios of ≤ 20:1, only the more slowly migrating form of DNA was observed for both metal complexes (Forms II & III).

The results of the denaturing gel analysis of the binding of $[(phen)_2Ru(dpq)PtCl_2](CF_3SO_3)_2$ and $[(phen)_2Ru(dpb)PtCl_2](CF_3SO_3)_2$ to linearized plasmid DNA are shown in Figure 3.37. The results for these two compounds were similar to the previously shown Ru-Pt bimetallics and with cisplatin at high DNA bp: mc ratios. At the highest DNA bp: mc ratios, ≥ 200: 1, both forms of DNA were observed, with the majority migrating at approximately the same rate as the untreated control (2958 nt) (Form I). However, a small amount of the second form (Form II) did appear, migrating at approximately the same rate as the 6557 nt standard. As the DNA bp: mc ratio was decreased, the DNA form migrating at an equivalent rate as the untreated control (Form I) diminished in quantity and disappeared at the 20: 1 DNA bp: mc ratio. At this point, the majority of the DNA was the form migrating at the rate of the 6557 nt standard (Form II). As the DNA bp: mc ratio was further decreased, the migratory rate of this second DNA form increased and migrated at a rate similar to that of the 4361 nt standard (Form III). This occurred at a similar position in the gel as observed for the 1,1/t,t standard and the other Ru-Pt bimetallics. Again, as with the bpy-analogs, only the more slowly migrating form of DNA was observed at bp: mc ratios ≤ 20:1 for both metal complexes (Forms II & III).

Comparison of the results of the denaturing gel analysis of the Ru-Pt bimetallics with that for the two standards, cisplatin and 1,1/t,t, afforded the opportunity to further probe the mode of interaction of the new complexes with DNA. Overall, all four Ru-Pt complexes displayed behavior that was very similar to cisplatin at high DNA bp: mc ratios, and very similar to 1,1/t,t at low DNA bp: mc ratios. At DNA bp: mc ratios of 200 and 300: 1, only one form of DNA was present in the gel, which migrated at a rate very similar to the untreated control (Form I). This behavior was very similar to that observed for cisplatin, and has suggested that the Ru-Pt complexes primarily display intrastrand crosslinking at low concentration. As the bp: mc ratio was decreased the second form of

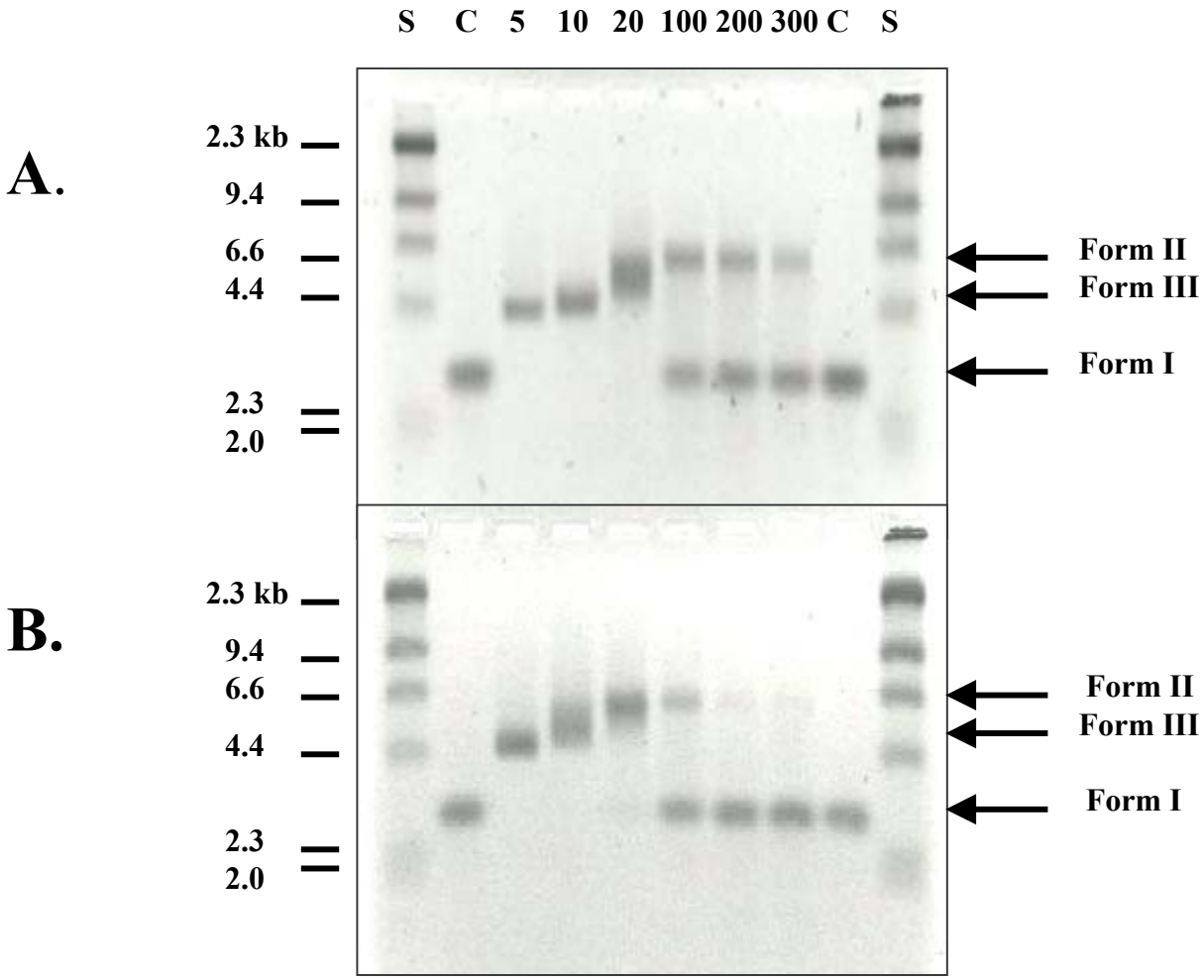

Figure 3.37 Denaturing agarose gel electrophoresis of the interaction of $[(phen)_2Ru(dpq)PtCl_2](CF_3SO_3)_2$ **(A)** and $[(phen)_2Ru(dpb)PtCl_2](CF_3SO_3)_2$ **(B)** (where phen = 1,10-phenanthroline, dpq = 2,3-bis(2-pyridyl)quinoxaline and dpb = 2,3-bis(2-pyridyl)benzoquinoxaline) with linearized plasmid DNA. One μg of linearized plasmid DNA was incubated with metal complexes at a ratio of 5, 10, 20, 100, 200, or 300 base pairs to 1 metal complex at 37 °C for 4 h. A control sample (C) containing only linearized plasmid DNA (no metal added) was incubated under identical conditions. Samples containing 100 ng of DNA were analyzed on denaturing agarose gels, which were then stained with 0.5 mg/ml ethidium bromide and photographed under UV illumination. A molecular weight standard (S) was included for reference.

DNA, which was interstrand crosslinked, appeared (Form II). This form appeared at the 100:1 bp: mc ratio for the $[(bpy)_2Ru(dpq)PtCl_2](CF_3SO_3)_2$ system, and appeared at 20: 1 for cisplatin. This behavior at low DNA bp: mc ratios has suggested a slightly higher tendency of the Ru-Pt complexes to form interstrand crosslinks than cisplatin. In addition, this Ru-Pt system displayed a much more pronounced change in the migration of the interstrand crosslinked form as the bp: mc ratio was decreased from 100 to 5: 1 to generate Form III. This was more similar to the effects seen for 1,1/t,t and has provided further evidence that the Ru-Pt complex forms a higher percentage of interstrand crosslinks than cisplatin. Additional evidence for increased incidence of interstrand crosslinking by the Ru-Pt systems was the fact that at bp: mc ratios ≤ 20: 1 only the interstrand crosslinked form of DNA was observed. This is significantly different from cisplatin, which at these ratios still exhibits small amounts of DNA that does not have any significant interstrand crosslinking.

Analysis by denaturing gel electrophoresis is a powerful technique that can provide much information on DNA binding detection and differentiation between compounds that display different DNA crosslinking modes. However, this technique can also provide some qualitative insight into the efficiency of interstrand crosslinking, through consideration of the location at which interstrand crosslinking is first detected (Form II DNA). Form II DNA is the point in which the two complementary DNA strands are held together by a small number of interstrand crosslinks (see Figure 3.35). For the $[(bpy)_2Ru(BL)PtCl_2]^{2+}$ systems, Form II DNA appears at 100: 1 bp: mc ratio, while for the $[(phen)_2Ru(BL)PtCl_2]^{2+}$ systems Form II DNA appears at the 300: 1 bp: mc ratio (albeit low concentration). For cisplatin, Form II DNA appears at the 20:1 bp:mc ratio, whereas for 1,1/t,t Form II DNA appears at the 300: 1 bp: mc ratio (high concentration). The fact that Form II DNA appears at a 5 to 15-fold higher metal concentration for both bpy- and phen-based Ru-Pt systems suggests that these systems are dramatically more efficient at forming interstrand crosslinks than cisplatin but not as efficient as 1,1/t.t.

The onset of Form II DNA also points to some interesting differences between the bpy- and phen- series of the Ru-Pt complexes. Since Form II DNA appears at the 100: 1

bp: mc ratio for the bpy-based complexes and the 300: 1 bp: mc ratio for the phen-based complexes, the phen-based complexes appear to form interstrand crosslinks at a higher efficiency than their bpy-based counterparts. In addition, a comparison within each series (bpy- or phen-based) shows an another trend. For those Ru-Pt complexes with the dpq bridging ligand, the amount of Form II DNA is greater (DNA band is denser on the gel) than those Ru-Pt complexes with the dpb ligand. Therefore, it appears that while the identity of the terminal ligand plays a major role in the formation of interstrand crosslinks, the identity of the bridging ligand is also a factor. A comparison of the terminal ligands bpy and phen along with the bridging ligands dpq and dpb shows that these ligands differ in size and extent of aromaticity within each of their respective groups. These differences may play a role in the ability of each specific complex to properly orient with respect to the DNA helix and form interstrand crosslinks.

Our Ru-Pt complexes were designed to be potentially bifunctional, binding DNA through intercalation of the bridging ligand and/or crosslinking through the $PtCl_2$ site. It has been shown previously that ruthenium bimetallic complexes utilizing the dpb bridging ligand bind to DNA by intercalation.[149] It is therefore reasonable to suggest that all the Ru-Pt complexes (the dpb complexes being most favored) bind to DNA in a bifunctional manner, in which intercalation of the bridging ligand may orient the complex to covalently bind DNA via intrastrand crosslinking, with some propensity for interstrand crosslinking. As shown previously, the efficiency of interstrand crosslinking varies between the bpy- and phen-series of Ru-Pt complexes, and within each series as the bridging ligand is changed from dpq to dpb. The exact factor that gives rise to the difference in interstrand crosslinking efficiency has not been determined, and is the subject of future investigations. However, it is clear that the overall shape of the metal complex is vitally important, dictating the level of preassociation of the complex to the DNA helix, leading to interstrand crosslinking of varying efficiency.

Chapter 4: Conclusions and Future Work

Conclusions

The purpose of this work was to design, develop synthetic methodologies for, and prepare a new class of supermolecules that would display covalent binding to DNA. These supermolecules consist of building blocks that chemically couple ruthenium (II) light absorbers to reactive metals. In this case, ruthenium (II) polyazine light absorbers were coupled to a *cis*-$Pt^{II}Cl_2$ unit through the bridging ligands dpq and dpb. The rationale behind placing a known DNA binding site (*cis*-$Pt^{II}Cl_2$) into a supermolecule was to provide for DNA binding while also allowing attachment of other parts each aimed at performing a particular function. These additional building blocks may enhance/change the DNA binding characteristics of the supermolecule. The use of coordination chemistry to construct these molecules makes synthetic variation relatively straightforward and facilitates study of how portions of the supermolecule affect spectroscopic and redox properties as well as DNA binding.

The successful synthesis and characterization of the new bimetallic complexes $[(bpy)_2Ru(BL)PtCl_2](CF_3SO_3)_2$, and $[(phen)_2Ru(BL)PtCl_2](CF_3SO_3)_2$ (where bpy = 2,2′-bipyridine, phen = 1,10-phenanthroline, dpq = 2,3-bis(2-pyridyl)quinoxaline and dpb = 2,3-bis(2-pyridyl)benzoquinoxaline) represents the first and essential step toward the accomplishment of this goal. The uniqueness of this molecular architecture made this a formidable task. All four complexes display intense bands in their electronic absorption spectrum attributed to bpy- and phen-based $n \rightarrow \pi^*$ and $\pi \rightarrow \pi^*$ transitions with dpq- and dpb-based $\pi \rightarrow \pi^*$ transitions appearing at lower energy. All four complexes also display MLCT transitions to each acceptor ligand in the visible region, with the Ru→BL CT based transitions occurring at lower energy. The Ru→BL CT transitions are red-shifted in comparison to the ruthenium monometallic synthetic precursors, $[(bpy)_2Ru(BL)]^{2+}$ and $[(phen)_2Ru(BL)]^{2+}$. The electrochemistry of these complexes shows reversible Ru-based oxidations and two reversible, BL-based couples that occur prior to reductions of the terminal ligands. In addition, an overlapping irreversible Pt oxidation is observed just prior to the $Ru^{II/III}$ couple. The presence of two

reversible BL-based couples at low potential, a red shift in the MLCT band in comparison to the monometallic synthons, and the presence of a Pt oxidation is consistent with Ru-Pt bimetallic formation. In addition, the complexes $[(bpy)_2Ru(BL)PtCl_2](CF_3SO_3)_2$ and $[(phen)_2Ru(BL)PtCl_2](CF_3SO_3)_2$ are all water-soluble.

The demonstration that the Ru-Pt complexes bind DNA represents the second step toward the accomplishment of this goal. The DNA-binding of the Ru-Pt complexes was probed by reaction with linearized plasmid DNA followed by analysis by native agarose gel electrophoresis. The results of these studies indicate that the Ru-Pt complexes strongly bind DNA in a concentration dependent fashion and imply that this technique is useful for detecting metal complex-DNA adducts. The comparison between the results obtained for cisplatin, 1,1/t,t and the Ru-Pt complexes displays marked differences, indicating that synthetic modification by changing BL can impact DNA migration trends and leads to changes in DNA binding characteristics. The lack of change in DNA migration obtained for DNA treated with the ruthenium monometallic synthons supports covalent binding through the Pt^{II} site.

The calculation of R_f values for the denaturing gels has made it relatively straightforward to compare the inhibition of DNA migration produced by the Ru-Pt complexes, cisplatin and 1,1/t,t. This data indicates that the Ru-Pt complexes reduce the migration of DNA to a much greater extent than cisplatin or 1,1/t,t. This data also shows that all Ru-Pt complexes reduce DNA migration by approximately the same extent under the nondenaturing conditions. Also, the low %RSDs indicate that the technique of gel electrophoresis is highly reproducible.

Theoretical modeling of DNA migration according to molecular weight affects has provided vital information on the validity of the experimental results. A comparison between theoretical and experimental migration distances establishes that the inhibition of DNA migration caused by the Ru-Pt complexes is not solely due to molecular weight.

Changes in charge and/or DNA shape occur in concert with the MW gain, further impacting DNA migration.

Analysis of the native gel results by gel densitometry has characterized a secondary effect observed in the native gel studies and provided another method of metal-DNA adduct detection. The binding of the Ru-Pt complexes significantly affected the emission of ethidium bromide stained DNA. The binding of the cisplatin and 1,1/t,t did not lead to this effect. This phenomenon has been quantitated by gel densitometry and found to be dependent on the concentration of Ru-Pt complex. Inhibition of ethidium bromide intercalation, caused by metal-complex binding distorting the shape of the DNA helix, could be the cause. This is unlikely as the results from cisplatin and 1,1/t,t dramatically differ from those observed with the Ru-Pt complexes. Intercalation of the Ru-Pt complexes into the DNA helix, thereby inhibiting ethidium bromide intercalation, could also account for these results. Native gel electrophoresis analysis of the interaction of the monometallic ruthenium synthons with linearized plasmid DNA appears to point away from this as the major cause as these monometallic synthons do not give inhibition of ethidium bromide emission nor affect the migration of the DNA. Precipitation studies have ruled out the possibility of DNA precipitation as the cause of decreased ethidium bromide emission. However, it was found that the Ru-Pt complexes quench the emission of ethidium bromide in aqueous fluid solution. It is clear that this emission inhibition is dependent on the binding of the Ru-Pt complexes. All above data suggest that the Ru-Pt complexes quench the emission of ethidium bromide. This effect would be greatly enhanced within a DNA helix due to an increased local concentration relative to a fluid solution.

Further analysis of the DNA-Ru-Pt complex interaction by denaturing gel electrophoresis has shown the utility of this technique for examining the type of binding exhibited by these complexes. The results of these studies indicate that the Ru-Pt complexes, like cisplatin, predominantly form intrastrand crosslinks. Our Ru-Pt complexes from interstrand crosslinks at a significantly higher percentage than cisplatin and the percentage varies as our BL is substituted. A comparison of the point at which

the diffuse DNA bands first appear for the 1,1/t,t and Ru-Pt systems indicates that the Ru-Pt systems are much less efficient at forming interstrand crosslinks than 1,1/t,t. In addition, since the location of the diffuse bands for the Ru-Pt complexes is dependent on the identity of the terminal & bridging ligand, some ligand based interaction contributes to the efficiency of interstrand crosslinking. A preassociation by intercalation may be operating by possibly serving to direct the subsequent covalent attachment of the Ru-Pt complexes.

Future Work

This work represents a major accomplishment toward the development of supermolecules constructed from ruthenium polyazine and *cis*-$PtCl_2$ building blocks that display DNA binding. These molecules therefore form the basis of a new series of bioactive metal complexes. Due to their DNA binding ability, these complexes may find applications in medicine, chemistry, and molecular biology. However, like any scientific research, more studies need to be accomplished.

One of the major attractive features of this molecular design is that synthetic variation of the supermolecule can be facilitated by the correct choice of building blocks. The inclusion of building blocks of a variety of shape and functionality would expand this series of bioactive molecules. This expansion would may result in a diversity of molecules with DNA binding and or interaction abilities.

As stated previously, the supermolecules developed in this study are potentially bifunctional, with the *cis*-$PtCl_2$ site providing for covalent attachment to DNA and the ruthenium bridging ligand site providing for possible intercalation. The inclusion of an intercalation site on this molecule may serve to direct the covalent binding of these complexes to DNA. The results presented in this manuscript suggest that this idea is feasible. To further test this concept, additional work could be focused on developing additional complexes with ligands highly predisposed for intercalation. An example would be to incorporate the dppz ligand (where dppz = dipyrido[3,2-*a*: 2′, 3′-*c*]phenazine,

(see Figure 1.13 for $[Ru(bpy)_2(dppz)]^{2+}$ and $[Ru(phen)_2(dppz)]^{2+}$) into the design of these supermolecules. Through the correct sequence of synthetic steps, the dppz ligand could be attached to a Ru-BL monometallic complex. The resulting complex, $[(TL)(dppz)Ru(BL)PtCl_2](CF_3SO_3)_2$ (where TL = bpy or phen, BL = dpp (2,3-bis(2-pyridyl)pyrazine), dpq, dpb) would not only be highly predisposed for DNA intercalation, but the luminescent behavior of Ru-dppz complexes may provide an additional spectroscopic handle for probing its DNA interaction.

Another candidate for this type of analysis would be to incoporate the tpy ligand into the supramolecular framework (where tpy = 2, 2′, 2′′-terpyridine). Platinum complexes of this tridentate ligand have been shown to bind to DNA by intercalation. However, inclusion of this moiety on the Ru(II) center would only occupy three coordination sites, leaving three more for substitution by a bridging and/or other ligands. This idea is presently being developed by our research group. In this case, complexes of the type $[(tpy)(X)Ru(BL)PtCl_2](PF_6)_2$ (where X = a monodentate phosphine or a Cl^-, and BL = bpm (2,2′-bipyrimidine), dpp, dpq) have been synthesized and are undergoing DNA binding studies. The inclusion of a phosphine on the Ru(II) center should provide a convienent handle for NMR analysis of the interaction of these complexes with DNA. In addition to providing an NMR handle, phosphines enriched with ^{32}P could be incorporated onto the Ru(II) center. ^{32}P is radioactive, and may open the door to additional means by which DNA binding could be monitored (scintillation counting being an example).

The additional coordination site on complexes of the type $[(tpy)(Cl)Ru(BL)](PF_6)$ may provide for a host of other possibilities. Other ligands/compounds could be tethered to the Ru(II) center and introduce a totally new class of supermolecules. Examples of such compounds would be amino and nucleotides. The inclusion of these moieties may provide for enhanced DNA-reactivity due to biological recognition. Living cells require amino and nucleic acids as building blocks for proteins and nucleic acids. Placing these on the Ru(II) center may increase the possibility of transport across cell membranes and hence may influence DNA binding activity. Another idea would be to tether known

drugs to these positions. Antitumor drugs like cyclophosphoamide and the nitrogen mustards might be candidates. This would also produce a potentially bifunctional molecule. Tethering drugs which have different modes of action than cisplatin could also produce some interesting results. An possible candidate would be a vinca alkaloid such as vincristine, which produces its antitumor effects by interfering with microtubule assembly.[3,7.8]

The Ru(II) unit incorporated into the supermolecules developed in this study all have polyzine terminal ligands. Another idea worth pursuing would be to move away from Ru(II)-polyazine terminal ligand complexes to those containing simpler ligands such as ammines. These complexes are worth studying because the ammine ligands around the Ru(II) center would decrease the size of the Ru(II) unit, perhaps reducing any hinderance to DNA intercalation associated with the terminal ligands. Also, hydrogen bonding of coordinated NH_3 ligands to the DNA double helix is known and might greatly impact subsequent covalent binding.

One of the most important features of new class of supermolecules is the bridging ligand. The bridging ligand allows the ruthenium(II) light absorber to be coupled to the reactive Pt center. In addition, they provide the possible DNA intercalation site. However, the incorporation of additional bridging ligands into this supermolecule could allow larger molecular arrays to be constructed. These larger metal systems could then incorporate multiple platinum centers, thereby producing supermolecules which could covalently bind DNA via multiple platinum sites. An example of such a supermolecule could be $[(bpy)Ru\{(dpb)PtCl_2\}_2]^{2+}$. Further extension to even more platinum centers would be possible through the use of ruthenium tris-bridging ligand complexes, such as $[Ru(dpp)_3]^{2+}$.

As stated previously, the Ru(II) center can function as a chromophore, leading to efficient light absorption by the Ru-Pt systems throughout the ultraviolet and visible region of the electromagnetic spectrum. The light-absorbing properties of the ruthenium center may thus allow the complex to become photoactivated, leading to enhanced

reactivity of the complex with DNA. This enhanced reactivity may take the form of more efficient crosslinking, or perhaps a more dramatic effect such as DNA strand scission. These supermolecules would then become prime candidates as agents for photodynamic therapy. Photodynamic therapy is a therapeutic method by which light-sensitive agents are administered to patients. Normally unreactive, these agents can be excited by light to produce a reactive (cytotoxic) form. This reactive form would subsequently react with cancer cells (by some mechanism, such as DNA crosslinking or strand scission) eventually producing cell death. In this regard, the ability to tune the light-absorbing properties of these supermolecules is highly advantageous. By simple synthetic modification, the light absorbing properties of these supermolecules could be modified such that they could absorb virtually anywhere within the UV or visible region. At present, these complexes have not been studied in this regard and these studies remain for future work.

In addition to synthetic variation, new methods could be developed to probe the interaction of these supermolecules with DNA. The possible bifunctional DNA-binding nature of these complexes suggests the need for a rigorous examination of the intercalative binding of these complexes. This could be accomplished through an electronic absorption spectroscopy study of the Ru-Pt complex – DNA interaction. In addition, ^{195}Pt NMR could be utilized to examine the DNA interaction of these complexes, in which changes of the Pt resonance upon DNA binding could be monitored. Studies to quantitate platinum binding are also of considerable interest. If the amount of platinum binding was known, the gel electrophoresis studies could be better understood in terms of how each effect (molecular weight, charge, shape distortion) contributes to the inhibition of DNA migration. Platinum-DNA binding has been previously quantitated by atomic absorption spectroscopy (for cisplatin) and this method could be applied to these systems
as well.[182-184]

References

1) Whitehouse, M., Slevin, M., *Cancer: The Facts*, 2nd ed.; Oxford University Press: Oxford, 1996.

2) McAllister, R.M., Horowitz, S.T., Gilden, R.V., *Cancer*, BasicBooks: New York, 1993.

3) Haskell, C.M., *Cancer Treatment*, Haskell, C.M., Ed.; W.B. Saunders Company: Philadephia, 1995.

4) Prescott, D.M., Flexer, A.S. *Cancer: The Misguided Cell*; Sinauer Associates, Inc.: Sunderland, 1986.

5) Cooper, G.M. *The Cancer Book*; Jones and Bartlett: Boston, 1993.

6) Ward, D.E. *The Cancer Handbook*; Ohio State University Press: Columbus, 1995.

7) Pratt, W.B., Ruddon, R.W. *The Anticancer Drugs*, Oxford University Press: New York, 1979.

8) Oppenheimer, S.B. *Cancer: A Biological and Clinical Introduction*, Allyn and Bacon: Boston, 1982.

9) Weiss, R.B., Christian, M.C. *Drugs* **1993**, *3*, 360.

10) Peyrone, M. *Ann. Chem. Pharm.* **1845**, *51*, 1.

11) Rosenberg, B., Van Camp, L., Krigas, T. *Nature* **1965**, *205*, 698.

12) Rosenberg, B. *Cancer* **1985**, *55*, 2303.

13) Rosenberg, B., Van Camp, L., Grimley, E.B., Thomson, A.J. *J. Biol.Chem.* **1967**, *242*, 1347.

14) Higby, D.J., Wallace, H.J., Albert, D., Holland, J.F. *J. Urol.* **1974**, *112*, 100.

15) Wiltshaw, E., Carr, T. *Rec. Res. Cancer Res.* **1974**, *48*, 178.

16) Hayes, D.M., Cvitkovic, E., Golbey, R.B. *Cancer* **1977**, *39*, 1372.

17) Fricker, S.P., *Metal Compounds in Cancer Therapy*; Fricker, S.P., Ed.; Chapman & Hall: London, 1994.

18) Sigel, A., Sigel, H. *Metal Ions in Biological Systems*, Sigel A., Sigel, H., Ed.; Marcel Dekker: New York 1996.

19) Sherman, S.E., Lippard, S.J. *Chem. Rev.* **1987**, *87*, 1153.

20) Boyd, R.F., Hoerl, B.G., *Basic Medical Microbiology*, Little, Brown and Company: Boston, 1991.

21) Alberts, B., Bray, D., Lewis, J., Raff, M., Roberts, K., Watson, J.D. *Molecular Biology of the Cell*, Garland Publishing: New York, 1994.

22) Carter, P.J., Ciflan, S.A., Sistare, M.F., Thorp, H.H. *J. Chem. Ed.* **1997**, *74*, 641.

23) Fictinger-Schepman, A.M.J., Lohman, P.H.M., Reedijk, J. *Nuc. Acids. Res.* **1982**, *10*, 5345.

24) Freifelder, D. *Physical Biochemistry*, W.H. Freeman and Company: San Francisco, 1976.

25) Sambrook, J., Fritsche, E.F., Maniatis, T. *Molecular Cloning: A Laboratory Manual*; Cold Spring Harbor Laboratory Press: Cold Spring Harbor, 1989.

26) Van Holde, K.E., *Physical Biochemistry*; Prentice-Hall, Inc.: Edgewood Cliffs, 1971.

27) Ushay, H.M., Tullius, T.D., Lippard, S.J. *Biochemistry*, **1981**, *20,* 3744.

28) Cohen, G.L., Bauer, W.R., Barton, J.K., Lippard, S.J. *Science*, **1979**, *203*, 1014.

29) Farrell, N.P., de Almedia, S.G., Skov, K.A. *J. Am. Chem. Soc.* **1988**, *110*, 5018.

30) Roberts, J.D., Van Houten, B., Qu, Y., Farrell, N.P. *Nuc. Acids. Res.* **1989**, *17*, 9719.

31) Zou, Y., Van Houten, B., Farrell, N.P. *Biochem*. **1993**, *32*, 9632.

32) Hongo, A., Seki, S., Akiyama, K., Kudo, T. *Int. J. Biochem.* **1994**, *26*, 1009.

33) Bellon, S.F., Colman, J.H., Lippard, S.J. *Biochemistry* **1991**, *30*, 8026.

34) Bellon, S.F., Lippard, S.J. *Biophys. Chem.* **1990**, *35*, 179.

35) Rice, J.A., Crothers, D.M., Pinto, A.L., Lippard, S.J. *Proc. Natl. Acad. Sci. USA* **1988**, *85*, 4158.

36) Yohannes, P.G., Zon, G., Doetsch, P.W., Marzilli, L.G. *J. Am. Chem. Soc.* **1993**, *115*, 5105.

37) Villani, G., Hubscher, U., Butour, J.L. *Nuc. Acids. Res.* **1988**, *16*, 4407.

38) Donahue, B.A., Augot, M., Bellon, S.F., Trieber, D.K., Toney, J.H., Lippard, S.J., Essigman, J.M. *Biochemistry*, **1990**, *29*, 5872.

39) Andrews, P.A. *Can. Treat. Res.* **1994**, *73*, 217.

40) Scanlon, J.K., Sabet-Kashani, M., Tone, T., Funato, T. *Pharm. Ther.* **1992**, *52*, 385.

41) Andrews, P.A., Howell, S.B. *Cancer Cells* **1990**, *2*, 35.

42) Akiyama, S., Chem, Z-S., Sumizawa, T., Furukawa, T. *Anti Can. Drug. Des.* **1999**, *14*, 143.

43) Chao, C.C.K. *J. Formos. Med. Assoc.* **1996**, *95*, 893.

44) Kelland, L.R., Sharp, S.Y., O'Neill, C.F., Raynaud, F.I., Beale, P.J., Judson, I.R. *J. Inorg. Biochem.* **1999**, *77*, 111.

45) Harrap, K.R. *Cancer Res.* **1995**, *55*, 2761.

46) Kelland, L.F. *J. Inorg. Biochem.* **1999**, *77*, 121.

47) Zou, Y., Van Houten, B., Farrell, N.P. *Biochemistry*, **1994**, *33*, 5404.

48) Farell, N.P., Qu, Y., Feng, L., Van Houten, B. *Biochemistry* **1990**, *29*, 9522.

49) Sigel, A., Sigel, H. *Metal Ions in Biological Systems*; Sigel, A., Sigel, H., Eds; Marcel Dekker: New York, 1996.

50) Farell, N.P. *Cancer Invest.* **1993**, *11*, 578.

51) Roberts, J.D., Peroutka, J., Beggioilin, G., Manzotti, C., Piazzoni, L., Farrell, N.P. *J. Inorg. Biochem.* **1999**, *77*, 47.

52) MacGregor, T.D., Balcarova, A., Qu, Y., Tran, M-C., Zaludova, R., Brabec, V., Farrell, N.P. *J. Inorg. Biochem.* **1999**, *77*, 47.

53) Perego, P., Gatti, L., Caserini, C., Supino, R., Colangelo, D., Leone, R., Spinelli, S., Farrell, N.P., Zunino, F. *J. Inorg. Biochem.* **1999**, *77*, 59.

54) Fricker, S.P., *Metal Compounds in Cancer Therapy*; Fricker, S.P., Ed.; Chapman and Hall: London, 1994, pp 109.

55) Fricker, S.P., *Metal Compounds in Cancer Therapy*; Fricker, S.P., Ed.; Chapman and Hall: London, 1994, pp 147.

56) Fricker, S.P., *Metal Compounds in Cancer Therapy*; Fricker, S.P., Ed.; Chapman and Hall: London, 1994, pp 180.

57) Fricker, S.P., *Metal Compounds in Cancer Therapy*; Fricker, S.P., Ed.; Chapman and Hall: London, 1994, pp 46.

58) Fricker, S.P., *Metal Compounds in Cancer Therapy*; Fricker, S.P., Ed.; Chapman and Hall: London, 1994, pp 92.

59) Sava, G., Pacor, S., Bregant, F., Ceschia., V., Mestroni, G. *Anti-Cancer Drugs* **1990**, *1*, 99.

60) Fricker, S.P., *Metal Compounds in Cancer Therapy*; Fricker, S.P., Ed.; Chapman and Hall: London, 1994, pp 65.

61) Lehman, L.S., *J. Mol. Biol.* **1961**, *3*, 18.

62) Neville, D.M., Davies, D.R., *J. Mol. Biol.* **1966**, *17*, 805.

63) Waring, M. *J. Mol. Biol.* **1970**, *54*, 247.

64) Long, E.C., Barton, J.K. *Acc. Chem. Res.*, **1990**, *23*, 273.

65) Saenger, W. *Principles of Nucleic Acid Structure*, Springer-Verlag: New York, 1984.

66) Wolfe, A., Shimer, G.H., Meechan, T. *Biochemistry*, **1987**, *26*, 6392.

67) Heidelberger, C. *Annu. Rev. Biochem.* **1975**, *44*, 79.

68) Berman, H.M., Young, B.R. *Annu. Rev. Biophys. Bioeng.* **1981**, *10*, 87.

69) Dougherty, G., Pilbrow, J.R. *Int. J. Biochem.* **1984**, *12*, 1179.

70) Neide, S. *Prog. Med. Chem.* **1979**, *16*, 151.

71) Jeanette, K.W., Lippard, S.J., Vassiliades, G.A., Bauer, W.R. *Proc. Natl. Acad. Sci. USA*, **1974**, *71*, 4825.

72) Bond, P.J., Langridge, R., Jeanette, K.W., Lippard, S.J. *Proc. Natl. Acad. Sci. USA*, **1975**, *12,* 4825.

73) Howe-Grant, M., Wu, K.C., Bauer, W.R., Lippard, S.J. *Biochemistry* **1976**, *15*, 4339.

74) Jeanette, K.W., Gill, J.T., Sadownick, J.A., Lippard, S.J. *J. Am. Chem. Soc.* **1976**, *98*, 6159.

75) Barton, J.K., Lippard, S.J. *Biochemistry*, **1979**, *18*, 2661.

76) Howe-Grant, M., Lippard, S.J. *Biochemistry*, **1979,** 1563**.**

77) Wakelin, L.P.G., McFadyen, W.D. Walpole, A., Roos, I.A.G. *Biochem. J.* **1984**, *222*, 203.

78) McFayden, W.D., Wakelin, L.PG., Roos, I.A.G., Hillcoat, B.L. *Biochem. J.* **1986**, *238*, 757.

79) McFayden, W.D., Wakelin, L.P.G., Roos, I.A.G., Hillcoat, B.L. *Biochem. J.* **1987**, *242*, 177.

80) Wong, Y., Lippard, S.J. *J. Am. Chem. Soc.* **1977**, 824.

81) Wang, A.H., Nathans, J., van der Marcel, G., van Boom, J.H., Rich, A. *Nature*, **1978**, *276*, 471.

82) Lippard, S.J., Berg, J.M. *Principles of Bioinorganic Chemistry*; University Science Books: Mill Valley, 1994.

83) Pasternack, R.F., Gibbs, E.J. *Metal-DNA Chemistry*; American Chemical Society: Washington, D.C., 1989.

84) Jenkins, Y., Friedman, A.E., Turro, N.J., Barton, J.K. *Biochemistry*, **1992**, *31*, 10809.

85) Kalyanasundaram, K. *Photochemistry of Polypyridine and Porphyrin Complexes*; St. Edmundsbury Press: Bury St. Edmonds, 1992.

86) Juris, A., Balzani, V., Campagna, S., Belser, P., Von Zelewsky, A. *Coord. Chem. Rev.* **1988**, *84*, 85.

87) Carter, R.L. *Molecular Symmetry and Group Theory*, Wiley: New York, 1998.

88) Roundhill, D.M. *Photochemistry and Photophysics of Metal Complexes*; Plenum Press: New York, 1994.

89) Kalyanasundaram, K. *Coord. Chem. Rev.* **1982, *46***, 159 incl. references cited therein.

90) Balzani, V., Moggi, L., Manfrin, M.F., Bolletta, F., Gleria, M. *Science*, **1975**, 852.

91) Braunstein, C.H., Baker, A.D., Strekas, T.C., Gafney, H.D. *Inorg. Chem.* **1984**, *23*, 857.

92) Fuchs, Y., Lofters, S., Dieter, T., Shi, W., Morgan, R., Strekas, T., Gafney, H., Baker, D.J. *J. Am. Chem. Soc.* **1987**, *109*, 2691.

93) Rillema, D.P., Mack, K.B. *Inorg. Chem.* **1982**, *21*, 3849.

94) Rillema, D.P., Callahan, R.W., Mack, K.B. *Inorg. Chem.*, **1982**, *21*, 2589.

95) Richter, M.M., Brewer, K.J. *Inorg. Chim. Acta.* **1991**, *180*, 125.

96) Richter, M.M., Brewer, K.J. *Inorg. Chem.* **1992**, *31*, 1594.

97) Richter, M.M., Brewer, K.J. *Inorg. Chem.* **1993**, *32*, 2827.

98) Richter, M.M., Brewer, K.J., *Inorg. Chem.* **1993**, *32*, 5762.

99) Richter, M.M., Jensen, G.E., Brewer, K.J. *Inorg. Chim. Acta.* **1995**, *230*, 35.

100) Molnar, S.M., Neville, K.R., Jensen, G.E., Brewer, K.J. *Inorg. Chem Acta.* **1993**, *206*, 69.

101) Kalyanasundaram, K., Nazeruddin, Md. K. *Chem. Phys. Lett.* **1989**, *158*, 45.

102) Yamagishi, A. *J. Chem. Soc. Chem. Commun.* **1983**.

103) Kumar, C.V., Barton, J.K., Turro, N.J. *J. Am. Chem. Soc.* **1985**, *107*, 5518.

104) Barton, J.K., Danishefsky, A.T., Goldberg, J.M. *J. Am. Chem. Soc.* **1984**, *106*, 2172.

105) Kelly, J.M., Tossi, A.B., McConnell, D.J., Ohuigin, C. *Nuc. Acids. Res.* **1985**, *13*, 6017.

106) Rehmann, J.P., Barton, J.K. *Biochemistry*, **1990**, *29*, 1701.

107) Barton, J.K. *Science*, **1986**, *233*, 727.

108) Haworth, I.S., Elcock, A.H., Freeman, J., Rodger, A., Richards, W.G. *J. Biomol. Struc. Dyn.* **1991**, *9*, 23.

109) Hiort, C., Norden, B., Rodger, A. *J. Am. Chem. Soc.* **1990**, *112*, 1971.

110) Eriksson, M., Leijon, M., Hiort, C., Norden, B., Graslund, A. *J. Am. Chem. Soc.* **1992**, *114*, 4933.

111) Satyanarayana, S., Dabrowiak, J.C., Chaires, J.B. *Biochemistry*, **1993**, *32*, 2573.

112) Pyle, A.M., Rehmann, J.P., Meshoyrer, R., Kumar, C.V., Turro, N.J., Barton, J.K. *J. Am. Chem. Soc.* **1989**, *111*, 3051.

113) Chambron, , J-C., Sauvage, J-P., Amouyal, E., Koffi, P. *New J. Chem.* **1985**, *9*, 527.

114) Amouyal, E., Homsl, A., Chambron, J-C., Sauvage, J-P. *J. Chem. Soc. Dalton. Trans.* **1990**, 1841.

115) Murphy, C.J., Barton, J.K. *Meth. Enzymol*. **1993**, *226*, 576.

116) Freidman, C., Chambron, J-C., Sauvage, J-P., Turro, N.J., Barton, J.K. *J. Am. Chem. Soc.* **1990**, *112*, 4960.

117) Hartshorn, R.M., Barton, J.K. *J. Am. Chem. Soc.* **1992**, *114*, 5919.

118) Dupureur, C.M., Barton, J.K. *J. Am. Chem. Soc.* **1994**, *116*, 10286.

119) Hiort, C., Lincoln, P., Norden, B. *J. Am. Chem. Soc.* **1993**, *115*, 3448.

120) Freidman, A.E., Kumar, C.V., Turro, N.J., Barton, J.K. *Nuc. Acids. Res.* **1991**, *19*, 2595.

121) Coates, C.G., Jacquet, L., McGarvey, J.J., Bell, S.E.J., Al-Obaidi, A.H.R., Kelly, J.M. *J. Am. Chem. Soc.* **1997**, *119*, 7130.

122) Fees, J., Kaim, W., Moscherosch, M., Matheis, W., Klima, J., Krejcik, M., Zalis, S. *Inorg. Chem.* **1993**, *32*, 166.

123) Gupta, N., Grover, N., Neyhart, G.A., Liang, W., Singh, P., Thorp, H. *Angew. Chem. Int. Engl. Ed.* **1992**, *31*, 1048.

124) Xiong, Y., He., X-F., Zou, H-M., Wu, J-Z., Chen, X-M., Ji, L-N., Li, R-H., Zhou, J-Y., Yu, K-B. *J. Am. Chem. Soc. Dalton Trans.* **1999**, 19.

125) Naing, K., Takahashi, M., Taniguchi, M., Yamagishi, A. *Inorg. Chem.* **1995**, *34*, 350.

126) Morgan, R.J., Chatterjee, A., Baker, D., Strekas, T.C. *Inorg. Chem.* **1991**, *30*, 2687.

127) Moucheron, C., Kirsche-De Mesmaeker, A., Choua, S. *Inorg. Chem*. **1997**, *36*, 584.

128) Holmlin, R.E., Barton, J.K. *Inorg. Chem.* **1995**, *34*, 7.

129) Holmlin, R.E., Stemp, E.D.A., Barton, J.K. *J. Am. Chem. Soc.* **1996**, *118*, 5236.

130) Holmlin, R.E., Yao, J.A., Barton, J.K. *Inorg. Chem.* **1999**, *38*, 174.

131) Brewer, K.J., Murphy, R.W. Jr., Spurlin, S.R., Petersen, J.D. *Inorg. Chem.* **1986**, *25*, 882.

132) Murphy, R.W. Jr., Brewer, K.J., Getiffe, G., Petersen, J.D. *Inorg. Chem.* **1989**, *28*, 81.

133) Petersen, J.D., Murphy, R.W. Jr., Brewer, K.J., Ruminski, K.R. *Coord. Chem. Rev.* **1985**, *61*, 261.

134) Berger, R.M. *Inorg. Chem.* **1990**, *29*, 1920.

135) Biano, A.J., Carlson, D.L., Wolosh, G.M., DeJesus, D.E., Knowles, C.F., Szabo, E.G., Murphy, R.W. Jr. *Inorg. Chem.* **1990**, *29*, 2327.

136) Molnar, S.M., Jensen, G.E., Vogler, L.M., Jones, S.W., Laverman, L., Bridgewater, J.S., Richter, M.M., Brewer, K.J. *J. Photochem. Photobiol. A.: Chem.* **1994**, *80*, 315.

137) Molnar, S.M., Nallas, G., Bridgewater, J.S., Brewer, K.J. *J. Am. Chem. Soc.* **1994**, *116*, 5206.

138) Dose, E.V., Wilson, L.J. *Inorg. Chem.* **1978**, *17*, 2660.

139) Rillema, D.P., Taghdiri, D.G., Jones, D.S., Keller, C.D., Worl, L.A., Meyer, T.J., Levy, H.A. *Inorg. Chem.* **1987**, *26*, 578.

140) Denti, G., Campagna, S., Sabatino, L., Ciano, M., Balzani, V. *Inorg. Chem.* **1990**, *29*, 4750.

141) Barligelletti, F., De Cola, L., Balzani, V., Hage, R., Haasnoot, J., Reeddikl, J., Vos., J.G. *Inorg. Chem.* **1989**, *28*, 4344.

142) Balzani, V., Moggi, L. *Coord. Chem. Rev.* **1990**, *917*, 313.

143) Balzani, V. *J. Photochem. Photobiol. A.: Chem.* **1990**, *51*, 55.

144) Balzani, V. *Supramolecular Photochemistry*; Reidel: Dordrecht, 1987.

145) MacQueen, D.B., Petersen, J.D. *Inorg. Chem.* **1990**, *29*, 2313.

146) Kalyanasundaram, K.G., Nazeeruddin, Md.K. *J. Phys. Chem.* **1992**, *96*, 5865.

147) Vogler, L.M., Scott, B., Brewer, K.J. *Inorg. Chem.* **1993**, *32*, 898.

148) Bridgewater, J.S., Vogler, L.M., Molnar, S.M., Brewer, K.J. *Inorg. Chim. Acta.* **1993**, *208*, 179.

149) Carlson, D.L., Huchital, D.H., Mantilla, S.J., Sheardy, R.D., Murphy, R.W. Jr. *J. Am. Chem. Soc.* **1993**, *115*, 6424.

150) Lincoln, P., Norden, B. *J. Chem. Soc. Chem. Commun.* **1996**, 2145.

151) Sullivan, B.P., Salmon, D.J., Meyer, T.J. *Inorg. Chem.* **1978**, *17*, 3334.

152) Bard, A.J., Faulkner, L.R. *Electrochemical Methods, Fundamentals and Applications*; Wiley: New York, 1980, pp. 701.

153) Goodwin, H.A., Lions, F. *J. Am. Chem. Soc.* **1959**, *81*, 6415.

154) Sahai, R., Rillema, D.P. *Inorg. Chim. Acta.* **1986**, *118*, L35.

155) Sahai, R., Rillema, D.P. *J. Chem. Soc. Chem. Commun.* **1986**, 1133.

156) Rillema, D.P., Allen, G., Meyer, T.J., Conrad, D. *Inorg. Chem.* **1983**, *22*, 1617.

157) Ish-Horowitz, D., Burke, J.F. *Nuc. Acids. Res.* **1981**, *9*, 2989.

158) Milkevitch, M., Brauns, E.B., Storrie, H., Shirley, B.W., Brewer, K.J. *Inorg. Chem.* **1997**, *36*, 4534.

159) Ausubel, F., Brent, R., Kingston, R.E., Moore, D.D., Seidman, J.G., Smith, J.A., Struhl, K. *Short Protocols in Molecular Biology;* Wiley: New York, 1995.

160) Milkevitch, M., Shirley, B.W., Brewer, K.J. *Inorg. Chim. Acta.* **1997**, *264*, 249.

161) Milkevitch, M., Brauns, E.B., Brewer, K.J. *Inorg. Chem.* **1996**, *35*, 1737.

162) Yam, V.W., Lee, W.M., Cheug, K. *J. Chem. Soc. Chem. Commun.* **1994**, 2075.

163) Campagna, S., Denti, G., Sabatino, L., Serroni, S., Ciano, M., Balzani, V. *J. Chem. Soc. Chem. Commun.* **1989**, 1500.

164) Roffia, S., Marcacciio, M., Paradisi, C., Paolucci, F., Balzani, V., Denti, G., Serroni, S., Campagna, S. *Inorg. Chem.* **1993**, *32*, 3003.

165) Serroni, S., Juris, A., Campagna, S., Venturi, M., Denti, G., Balzani, V. *J. Am. Chem. Soc.*, **1994**, *116*, 9086.

166) Balzani, V., Campagna, S., Denti, G., Juris, A., Serroni, S., Venturi, M. *Coord. Chem. Rev.* **1994**, *132*, 1.

167) Carlson, D.L., Murphy, W.R. *Inorg. Chim. Acta.*, **1991**, *181*, 61.

168) Kober, E.B., Sullivan, B.P., Dressick, W.J., Caspar, J.V., Meyer, T.J. *J. Am. Chem. Soc.* **1980**, *102*, 7385.

169) Juris, A., Besler, P., Barigelletti, F., Von Zewelsky, A., Balzani, V. *Inorg. Chem.*, **1986**, *25*, 256.

170) Kober, E.B., Marshall, J.L., Dressick, W.J., Sullivan, B.P., Caspar, J.V., Meyer, T.J. *Inorg. Chem.,* **1985**, *24*, 2755.

171) Johnson, S.R., Westmoreland, T.D., Caspar, J.K., Barqawi, K.R., Meyer, T.J. *Inorg. Chem.* **1987**, *27*, 3195.

172) Allen, G.H., Sullivan, B.P., Meyer, T.J. *J. Chem. Soc. Chem. Commun.* **1981**, 793.

173) Sullivan, B.P., Calvert, J.M., Meyer, T.J. *Inorg. Chem.* **1980**, *19*, 1404.

174) Dodsworth, E.S., Lever, A.B.P. *Chem. Phys. Lett.* **1986**, *124*, 152.

175) Pulleyblank, D.E., Shure, M., Vinograd, J. *Nuc. Acids. Res.* **1977**, *4*, 1409.

176) Projan, S.J., Carleton, S., Novick, R.P. *Plasmid*, **1983**, *9*, 182.

177) Moore, S.P., Sutherland, B.M. *Anal. Biochem.* **1985**, *144*, 15.

178) Baguley, B.C., Le Bret, M. *Biochemistry*, **1984**, *23*, 937.

179) Al-Hakeem, M., Sommer, S.S. *Anal. Biochem.* **1987**, *163*, 433.

180) Jin, W.J., Wei, Y.S., Liu, C.S., Shen, G.L., Yu, R.Q. *Spectrochim. Acta. Part A.* **1997**, *53*, 2701.

181) Wallace, A.W., Murphy, W.R., Petersen, J.D. *Inorg.Chim. Acta.* **1989**, *166*, 47.

182) Reed, E., Sauerhoff, S., Poirer, M.C. *Atomic Spectroscopy*, **1988**, *9*, 93.

183) Pera, M.F., Harder, H.C. *Clin. Chem.* **1977**, *23*, 1245.

184) LeRoy, A.F., Wehling, M.L., Sponseller, H.L., Friauf, W.S., Solomon, R.E., Dedrick, R.L., Litterst, C.L., Gram, T.E., Guarino, A.M., Becker, D.A. *Biochem. Med.* **1977**, *18*, 184.